NMR STUDIES AND COMPUTER SIMULATIONS OF SOLUTES IN NEMATIC LIQUID CRYSTALS

By

James Munro Polson

B.Sc., The University of Guelph, 1988
M.Sc., The University of Guelph, 1990

A THESIS SUBMITTED IN PARTIAL FULFILLMENT OF

THE REQUIREMENTS FOR THE DEGREE OF

DOCTOR OF PHILOSOPHY

in

THE FACULTY OF GRADUATE STUDIES

DEPARTMENT OF PHYSICS AND ASTRONOMY

We accept this thesis as conforming

to the required standard

THE UNIVERSITY OF BRITISH COLUMBIA

May 1996

In presenting this thesis in partial fulfilment of the requirements for an advanced degree at the University of British Columbia, I agree that the Library shall make it freely available for reference and study. I further agree that permission for extensive copying of this thesis for scholarly purposes may be granted by the head of my department or by his or her representatives. It is understood that copying or publication of this thesis for financial gain shall not be allowed without my written permission.

Department of _Physics_

The University of British Columbia
Vancouver, Canada

Date _May 31, 1996_

Abstract

This thesis is concerned with the orientational and conformational behaviour of molecules partially oriented in a nematic liquid crystal. We have studied these systems experimentally using Multiple-Quantum NMR spectroscopy, and computationally using the Monte Carlo simulation method.

An important goal of the experimental component of this thesis was the investigation of the usefulness of applying Multiple-Quantum NMR spectroscopy as an aid for the analysis of complex one-quantum NMR spectra of oriented solutes. The technique was applied to biphenylene and butane. For the eight-spin molecule biphenylene, the analysis of the six-quantum and seven-quantum spectra was shown to be sufficient to provide a simple solution of the one-quantum spectrum. However, it was necessary to reduce the number of fitting parameters by fitting the proton geometrical coordinates and molecular order order parameters instead of the dipolar coupling constants. An analysis of the dipolar coupling constants was used to determine the vibrationally averaged molecular structure. An analysis of the seven-quantum and eight-quantum spectra of the ten-spin molecule butane provided an excellent prediction of the one-quantum spectrum, which could then be solved trivially. The dipolar coupling constants were analyzed to study the conformational behaviour of butane. The *trans-gauche* energy difference was determined to be in the range of 2.1–3.0 kJ/mol. This is significantly less than the gas phase value and indicates that the condensed environment enhances the *gauche*-conformer probability. Further, the conformational biasing was primarily a result of the isotropic component of the solute-solvent interaction; the anisotropy of the nematic solvent has only minor effects. Finally, the analysis of the couplings involved the use of mean-field models to

describe orientational ordering for each conformer. Several models were able to provide an adequate description of orientational ordering as determined by the ability to fit the dipolar coupling constants.

Monte Carlo computer simulations were used to investigate the mechanisms for orientational ordering of solutes in nematics and test several empirical and theoretical mean-field models of ordering. The importance of shape anisotropy and electrostatic interactions were studied. Solute and solvent molecular shapes were approximated by hard ellipsoids. Some simulations incorporated the interaction between point quadrupoles placed at the centres of the ellipsoids. In the purely hard-core systems, orientational order parameters and orientational distribution functions were calculated for a collection of different solutes under under a variety of conditions. Several empirical models were used to analyze the data. Fitting parameter values were quantitatively very similar to values obtained from previous fits to experimental data. This result clearly demonstrates the importance of anisotropic short-range repulsive forces for orientational ordering in nematics and firmly establishes the connection between these various molecular-shape models with these interactions. The quadrupolar systems were used to investigate a mean-field model in which an interaction between the solute molecular quadrupole moment with an average electric-field gradient provides an orientational ordering mechanism. Simulations indicate that the electric-field gradient is highly dependent on the properties of the solute, contrary to some experimental evidence. Further, a mean-field theory developed to describe this model was found to provide a qualitatively correct but quantitatively imprecise prediction of orientational ordering.

Table of Contents

List of Tables

List of Figures

Acknowledgement

I would like to thank my supervisor Prof. Elliott Burnell for his guidance, encouragement and generousity over the past five years. It has been a great pleasure to work together.

I am also grateful to my other supervisor Prof. Myer Bloom, who has been a great inspiration to me, for his insight and generousity.

I would like to thank Prof. Gren Patey for numerous stimulating discussions and very helpful advice that helped to shape a large part of this thesis.

Thanks to Leon ter Beek, Chandrakumar and Ray Syvitski for stimulating discussions and for making the lab an enjoyable place to work.

Finally, I want to thank my wife Beth for her love, encouragement and understanding which helped make it all possible.

Chapter 1

Introduction

1.1 Liquid Crystals

1.1.1 Nematic Liquid Crystals

In natural light, a nematic liquid crystal has the appearance of a cloudy fluid with thread-like structures floating within. Upon closer examination under a cross polarizing microscope, the fluid takes on a marbled texture that is indicative of an underlying structural complexity. When heated above some unique temperature, it changes to a clear liquid, while cooling will eventually freeze the sample into a solid. Thus, on a macroscopic scale it is already apparent that this substance can assume a state intermediate between that of an isotropic liquid and a crystalline solid.

The liquid-crystalline state of matter was first reported by Reinitzer in 1888 who observed this macroscopic phase behaviour in cholesterol benzoate [1]. A year later, Lehman demonstrated that it displayed birefringence, a property of anisotropic systems [2]. The label "liquid crystal" was introduced to describe this compound which displayed properties of two very different states: the fluidity of an isotropic liquid and the optical properties of an anisotropic crystal.

Some understanding of the properties of a nematic liquid crystal can be obtained by examining it on a microscopic scale. Typically, each of the constituent molecules is elongated, with a length to width ratio greater than 3:1. As well, a nematogen generally is comprised of a semi-rigid core with flexible alkyl "tails" attached at either or both

Figure 1.1: Molecular Structure of N–(4–ethoxybenzylidene)–4′–n–butylaniline
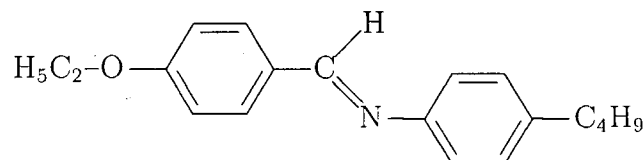
ends. An illustrative example is given in Figure 1.1 which shows the molecular structure of the nematogen N–(4–ethoxybenzylidene)–4′–n–butylaniline (EBBA).

The organization of molecules in a nematic phase is illustrated by the microscopic "snapshot" in Figure 1.2, which is a planar projection of a three-dimensional system where each of the line segments represents a nematogen. The centers of mass of the individual molecules are arranged so that there are no long-range positional correlations. The lack of long-range positional order is also a property of isotropic liquids. Unlike the latter, however, molecules in a nematic phase do display long-range orientational order; that is, the direction of the long axis of any one nematogen is correlated with that of another that is far from it on a length scale defined by the dimensions of the molecules. The result is an arrangement where the molecules are partially aligned along some average direction, which is referred to as the nematic director.

The nematic phase is labeled *uniaxial* since the director is the only unique axis characterizing the phase. As a consequence, it is cylindrically symmetric: all measured properties are invariant to rotations about the director. Further, the nematic phase is apolar in the sense that measured properties are invariant to reflections in a plane perpendicular to the director. Thus, the director vector, strictly speaking, is not uniquely defined for it may point in either of two opposite directions along the symmetry axis of the phase. It is important to note that the symmetry properties of the nematic phase are not also

Figure 1.2: Molecular Organization in a Nematic Phase.
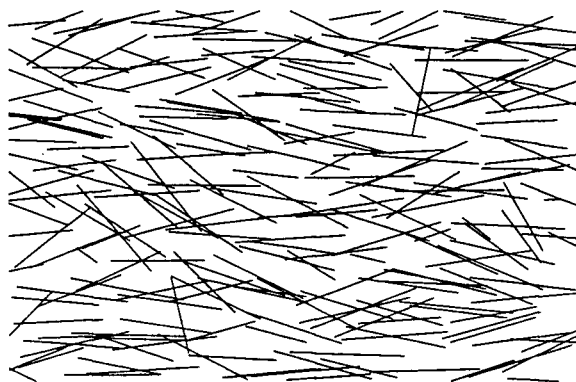
properties of the individual molecules. Generally, nematogens possess neither cylindrical nor reflection symmetry.

In the absence of external fields, the nematic director varies throughout the sample in an irregular manner. Note that the the length scale over which there is an appreciable variation in the direction of the director is large ($\sim$1 μm) compared to the dimensions of the molecules ($\sim$20 Å) [3]. The cloudy appearance of a macroscopic sample of a nematic liquid crystal arises from the scattering of light as it propagates through the sample between regions characterized by different directors. The spatial variation of the nematic director may be continuous or discontinuous. The boundaries marking the discontinuities are called disclinations and are manifested in a macroscopic sample as the floating thread-like structures. Thus, the visible macroscopic features of nematics are closely related to the microscopic phenomenon of molecular orientational ordering.

1.1.2 Other Liquid Crystalline Phases

The nematic phase is one example among many of a *mesophase* (from the Greek word *mesos* = middle) which has properties intermediate between those of crystalline solids and isotropic liquids. This phase is classified as a *thermotropic* mesophase because a transition to this phase may be brought about by purely thermal processes. Thermotropic liquid crystals are not at all uncommon: approximately 0.5% of all organic compounds possess a thermotropic mesophase. The other main category of thermotropic phases is the *smectic* phase, which has, in addition to orientational order, some degree of positional order in at least one dimension. In this case, the molecules are arranged on average in equidistant planes, although there may be considerable positional fluctuations about this configuration. Further, this class is divided into many types, each classified according to several criteria, including the preferred direction of the molecules relative to the layer normal and the spatial organization of the molecules within the layers.

The third main category of thermotropic liquid crystals is the *cholesteric* phase, labeled thus because many derivatives of cholesterol belong to this class. This phase is composed of chiral molecules which form a type of nematic phase in which there is a regular twist to the director along some helical axis; that is, the director twists at a fixed angle per unit length along the axis. The pitch of the twist may vary from 200 nm to ∞ [4] . Today cholesteric liquid crystals are described as *chiral* nematics and are categorized as a subclass of nematic liquid crystals.

More recently, thermotropic liquid crystalline phases composed of disc-shaped molecules have also been discovered. These "exotic" phases include the optically isotropic *cubic* phase, and the *columnar* phase in which molecules are stacked in regular columns with spatial disorder present in only one dimension along the column axis.

While thermotropic liquid crystal phases are induced by thermal processes alone,

lyotropic liquid crystalline phases are formed as a result of mixing compounds with amphiphilic properties with a solvent. Between the extremes of pure amphiphile and its isotropic solution in an excess of the solvent, there exist at intermediate concentrations a wide variety of structured phases consisting of ordered arrangements of amphiphile and solvent which possess anisotropic properties characteristic of liquid crystalline phases. Lyotropic phases occur abundantly in nature, most notably in biological cell membranes, an example which underscores the importance of understanding the properties of liquid crystals generally.

1.2 Orientational Order and Intermolecular Forces in Nematic Liquid Crystals

The properties common to all of the mesophases described above are the presence of orientational order combined with some degree of positional disorder. An important component in the study of liquid crystals is the understanding of the relationship between the long-range orientational order and the anisotropic intermolecular forces which give rise to this property. Since the nematic phase is the mesophase possessing the highest degree of symmetry, it is ideal for studying to give insight into this relationship. It is perhaps surprising that, more than a century after Reinitzer's discovery, a detailed understanding of the mechanisms responsible for the ordering in this "simple" phase is still lacking. Nevertheless, great progress has been achieved due to a combination of experimental, theoretical and, more recently, computational techniques.

There are several molecular properties which contribute to, or in some way affect, the orientational ordering of molecules in a nematic liquid crystal. It is now recognized that the essential feature is the anisotropy in molecular shape. Just as the short-range repulsive forces dominate and determine the structure of a fluid at high densities for

many isotropic liquids, these forces couple to the molecular shape anisotropy to produce a strong contribution to molecular alignment in anisotropic liquid crystals. Results of recent computer simulations show that at sufficiently high densities, a system of elongated hard particles can form a stable nematic phase [5, 6]. Other related and important factors include molecular biaxiality and flexibility. Each of these properties, present in all nematogens, will play a major role in the local packing arrangement of molecules in this dense phase and therefore influence substantially the degree of orientational order and the stability of the nematic phase.

Nematogens generally have electric dipole and quadrupole moments and molecular polarizabilities of significant magnitude. Thus, electrostatic interactions are expected to contribute to some degree to orientational ordering. In addition, the anisotropic component of attractive dispersion forces, which arise from correlated electrostatic fluctuations between polarizable molecules, will also play a role. All of these interactions are generally believed to have a perturbative effect on the structure of the fluid which is mainly determined by the anisotropic short-range forces.

There is a great variety of theories developed to explain the phenomenon of orientational ordering in nematic liquid crystals, and it is beyond the scope of this thesis to describe any of them in detail. However, there are two influential and contrasting theories which have some relation to the material which will follow later. These approaches are due to Onsager [7], who showed that a nematic phase could arise in a system of infinitely long hard rods, and to Maier and Saupe [8, 9, 10], who showed that long-range orientational order may arise in a system where only attractive, anisotropic long-range forces are present. The main features relevant to the present work are described below. First, however, a quantitative description of orientational order is presented.

1.2.1 Orientational Distribution Function and Order Parameters

For a uniaxial phase, the orientational ordering of a single rigid molecule is described completely by the orientational distribution function (ODF), $f(\theta, \phi)$, defined so that $f(\theta, \phi) \sin \theta d\theta d\phi$ is the probability that nematic director assumes polar angles in the molecular frame in the range $[\theta, \theta + d\theta]$ and $[\phi, \phi + d\phi]$. The ODF may be expanded in terms of spherical harmonics:

$$f(\theta, \phi) = \sum_{l \ even} \sum_m \frac{2l + 1}{4\pi} \bar{Y}_{lm}^* Y_{lm}(\theta, \phi), \tag{1.1}$$

where

$$\bar{Y}_{lm}^* = \int_0^{2\pi} d\phi \int_0^\pi d\theta \sin \theta Y_{lm}^*(\theta, \phi) f(\theta, \phi), \tag{1.2}$$

and where $\bar{Y}_{lm}^* = \bar{Y}_{l,-m}$. The summation is restricted to even values of l as a result of the apolarity of the nematic phase.

In many theories of liquid crystals, the nematogens are modeled in a highly simplified manner, and the shape is often approximated by introducing cylindrical symmetry. In this case the ϕ-dependence of the ODF vanishes and the above expansion reduces to the following:

$$f(\theta) = \sum_{l \ even} \frac{2l + 1}{2} \bar{P}_l P_l(\cos \theta), \tag{1.3}$$

where θ is the angle between the molecular symmetry axis and the nematic director, and where

$$\bar{P}_l = \int_0^\pi d\theta \sin \theta P_l(\cos \theta) f(\theta) \tag{1.4}$$

are called orientational order parameters.

For molecules without cylindrical symmetry, it is useful to describe the ODF in Cartesian coordinates. The leading terms in an expansion analogous to that of Eq. (1.1) are

$$f(\theta, \phi) = \frac{1}{4\pi} \left[1 + 5 \sum_{\alpha, \beta} S_{\alpha\beta} \cos \theta_\alpha \cos \theta_\beta + ... \right] \tag{1.5}$$

where

$$S_{\alpha\beta} = \left\langle \frac{3\cos\theta_\alpha \cos\theta_\beta - \delta_{\alpha\beta}}{2} \right\rangle \qquad (1.6)$$

is a symmetric traceless matrix known as the Saupe order matrix, and where θ_α is the angle between the α-molecular axis and the nematic director. For the case of molecules with cylindrical symmetry, the Saupe order matrix has only one independent element, $S_{zz} = \bar{P}_2$.

It is important to remember that the ODF described above is applicable in principle to rigid molecules only. Thus, the flexibility inherent to nematogens introduces a complication to this simple description of orientational order of single molecules. Generally, nematogen order parameters obtained experimentally are defined with respect to a rigid subunit such as a phenyl ring which comprises the core of the molecule. The problem of describing the orientational ordering of flexible molecules in a uniaxial medium will be returned to at a later stage.

1.2.2 Molecular-Statistical Theories of Nematic Liquid Crystals

The present work is concerned with the relationship between intermolecular forces and orientational order in nematic liquid crystals. A molecular-statistical theory is one which seeks to elucidate the nature of this connection. Generally, such a theory begins with some necessarily idealized form of the intermolecular potential, which nevertheless incorporates its most important features. These potentials are used to calculate in some approximate way the configurational partition function which is then used to calculate the free energy and the related thermodynamic properties. For mean-field theories of nematic liquid crystals, the free energy is expressed as a functional of the ODF, minimization with respect to which yields a self-consistent expression for the ODF which

can be solved numerically, or possibly analytically with further approximations. Thermodynamic stability of the solutions is tested by examining the related free energy. The approach of this type of theory contrasts with that of the phenomenological variety, including most notably the Landau-de Gennes theory [11], which makes no attempt to calculate the partition function and thus has nothing to say about the underlying mechanisms responsible for orientational ordering.

Described below are very brief descriptions of the Onsager and Maier-Saupe theories, including only those aspects which have some relevance to the present study.

1.2.2.1   Onsager Theory

In 1949 Onsager presented a theory for orientationally ordered fluids in which the molecules are modeled as long hard rods and attractive forces are neglected entirely [7]. The approach involves the application of imperfect gas theory using a virial expansion of the configurational partition function. The partition function was calculated for a mixture of particles for which the components of the mixture were interpreted as identical particles with different orientations. It was shown that the leading terms in the calculated free energy, A, are given by:

$$\frac{\beta[A - A^\circ]}{N} = \int d\omega f(\omega) ln(4\pi f(\omega)) + (ln\rho - 1) + B_2\rho + B_3\rho^2 + ... \qquad (1.7)$$

where A° is the ideal free energy related to integrations over translational and rotational momenta associated with the contributions of these degrees of freedom to the total energy of the system. As well, $\beta \equiv (k_BT)^{-1}$ where k_B is the Boltzmann constant, N is the number of particles in the system, $\omega \equiv (\theta, \phi)$, ρ is the number density and B_2, B_3,..., are the virial coefficients. The latter quantities may be written as functionals of the ODF, $f(\omega)$. For example,

$$B_2 = \frac{1}{2} \int d\omega d\omega' f(\omega) f(\omega') V_{ex}(\omega, \omega'), \qquad (1.8)$$

where $V_{ex}(\omega, \omega')$ is the excluded volume between particles with orientations ω and ω'. In the limit of very long rods, Onsager showed that the contributions from the higher order terms beyond that containing B_2 were negligible. This contrasts with the other extreme case, that of hard spheres, where the higher order terms contribute significantly and cannot be neglected. Minimization of the free energy with respect to $f(\omega)$ using the expression in Eq. (1.7) and neglecting the higher order terms yields

$$f(\omega) \sim exp \left[-\rho \int d\omega' V_{ex}(\omega, \omega') f(\omega') \right] \qquad (1.9)$$

a self-consistent expression which can be solved to obtain $f(\omega)$. It may be shown that an orientationally ordered phase is thermodynamically stable for this system at sufficiently high densities.

The important aspect of this theory is that it emphasizes the importance of orientation-dependent excluded-volume interactions. For elongated rods, the excluded volume is smaller for parallel than for perpendicular orientations, and thus is a more favoured arrangement. Further, the existence of a stable orientationally ordered phase in a system with constant energy, and thus where entropy should be at a maximum, may be understood by noting that there are two competing contributions to the total entropy, each associated with translational and orientational degrees of freedom. For increasing elongation and density, the translational entropy becomes the dominant term, and orientational entropy is "sacrificed" to maximize the total entropy.

While this theory provides a simple qualitative understanding of the importance of short-range anisotropic forces to the phenomenon of orientational ordering, it is of limited relevance for real nematogens. In this case, the molecular elongation is not sufficiently large to neglect higher order terms in the expansion; thus, correlations between three and more particles will play a role in influencing the orientational behaviour. Significant improvement of the theory may be obtained with the (very difficult) evaluation of higher

order virial coefficients. For example, it was found that the orientational behaviour of systems of hard particles with more realistic dimension ratios can be adequately described by the including the B_3 term into the theory [12].

1.2.2.2 Maier-Saupe Theory

In the Maier-Saupe theory of nematic liquid crystals [8, 9, 10], the principal ordering mechanism is taken to be the anisotropic component of a long-range attractive interaction, originally proposed to be the London dispersion force. The pair potential is then used to derive a mean-field pseudopotential which is used to describe the ODF. The mean-field potential for one particle is obtained by averaging the pair potential over the rotational coordinates of one of the molecules, and the magnitude and orientation of the intermolecular displacement vector. For a pair potential between two particles, $u(\vec{r}, \omega, \omega')$, the following ODF relation may be derived:

$$f(\omega) \sim \exp\left[-\beta\rho \int d\vec{r}d\omega' u(\vec{r}, \omega, \omega') f(\omega') g(\vec{r})\right],\qquad(1.10)$$

where $\vec{r}$ is the intermolecular vector and $g(\vec{r})$ is the pair correlation function. The relation above may be derived by several different procedures. The key approximation that all of these approaches use is to neglect short-range correlations. In particular, the dependence on the orientational coordinates of the pair correlation function is neglected, and $g(\vec{r}, \omega, \omega')$ is replaced by $g(\vec{r})$. The expression in Eq. (1.10) is a self-consistent relation which must be solved to obtain the ODF.

As a further approximation, the constituent molecules are assumed to be rigid and possess $D_{\infty h}$ symmetry. The leading term in an expansion of the anisotropic pair potential can be written as

$$u(r, \theta_{12}) = -\epsilon(r) P_2(\cos\theta_{12}),\qquad(1.11)$$

where θ_{12} is the relative orientation between the molecules, and where $\epsilon(r) > 0$. Finally,

the distribution of intermolecular vectors is taken to be spherically symmetric, i.e. $g(\vec{r}) \approx g(r)/4\pi$. Under these approximations, and upon substitution of Eq. (1.11) into Eq. (1.10), it may be shown that there is a stable nematic phase with molecular orientational ordering described by the following ODF:

$$f(\theta) \sim \exp\left[-\beta\epsilon\bar{P}_2 P_2(\cos\theta)\right], \qquad (1.12)$$

where

$$\epsilon = \rho \int dr 4\pi r^2 \epsilon(r) g(r), \qquad (1.13)$$

for $T < 0.2203\epsilon/k_B = T_{NI}$, and where T_{NI} is the nematic–isotropic phase transition temperature.

That the Maier-Saupe theory of nematic liquid crystals and its derivatives has been such a successful theory for describing orientational order seems surprising considering the severity of the approximations. For example, there clearly will be significant short-range orientational correlations between real nematogens arising from short-range repulsive forces which are entirely neglected in the theory. As well, the assumption of a spherical distribution of intermolecular vectors is difficult to rationalize given the highly anisotropic nature of the system.

1.3 Solutes as Probes of Intermolecular Forces

1.3.1 NMR and Orientationally Ordered Solutes

There are a variety of experimental techniques which in principle can provide quantitative information about orientational ordering in nematic liquid crystals. For example, X-ray diffraction can be used to measure the full ODF, $f(\theta)$, while polarized Raman scattering can yield estimates of the order parameters $\bar{P}_2$ and $\bar{P}_4$ [4]. In practice, such information is often difficult to obtain using these methods. Nuclear Magnetic Resonance (NMR),

by contrast, is an excellent technique for studying order in anisotropic systems. Its principal limitation, however, is that it is capable of measuring order parameters of only the second rank, and therefore yields only a modest amount of information relative to that contained in the complete ODF. Nevertheless, it has been shown to be an extremely effective tool for elucidating the details of orientational behaviour in liquid crystals and is highly relevant, both directly and indirectly, to the present work. We shall not provide a detailed description of the basic theory of NMR, but only a brief outline of its relation to the determination of orientational order parameters.

An analysis of the NMR spectra of orientationally ordered molecules can yield a variety of different intramolecular coupling constants which are parameters of the nuclear spin Hamiltonian. An important example of this is the direct dipole-dipole coupling constant, which for a pair of like spins may be written as

$$D_{ij} = -\frac{\gamma^2 \hbar \mu_0}{8\pi^2} \left\langle \frac{\frac{3}{2}\cos^2 \theta_{ij}^Z - \frac{1}{2}}{r_{ij}^3} \right\rangle, \tag{1.14}$$

where γ is the gyromagnetic ratio of the spin, $\hbar$ is Planck's constant, μ_0 is the magnetic permeability of free space, and θ_{ij}^Z is the angle between the internuclear vector and the external magnetic field which is defined to be along the Z-axis. The ensemble average includes both averaging over the internuclear distance and over the direction of the internuclear vector. For rigid molecules, and neglecting vibrations, r_{ij} is fixed, and the expression can be written as

$$D_{ij} = -\frac{\gamma^2 \hbar \mu_0}{8\pi^2 r_{ij}^3} S_{\alpha\beta} \cos \theta_\alpha \cos \theta_\beta, \tag{1.15}$$

where $S_{\alpha\beta}$ is the Saupe order matrix defined in Eq. (1.6), and where θ_α is the angle between the internuclear vector and the molecular α-axis.

The measurement of dipolar coupling constants for nematogens is complicated for two reasons. First, the spectra are often impossible to analyze. Generally, this is the case for

proton NMR, since individual nematogens may have ~20 proton spins. The result is an extremely complex spectrum composed of many overlapping, unresolvable lines. Second, the nematogens are flexible molecules which sample a large number of conformations. This conformational freedom greatly complicates the analysis of the coupling constants even if they can be measured. In this case, Eq. (1.15) is not a valid expression for the dipolar coupling constant.

A very useful alternative for studying orientational order in nematic liquid crystals is to employ solutes as probes of orientational order. Generally, a rigid molecule with lower than T_d symmetry will be partially oriented when dissolved in an anisotropic nematic environment as it samples the same intermolecular forces which align the nematogens themselves. The solute will be characterized by its own ODF and orientational order parameters. Solutes may be chosen to simplify the spectral analysis and interpretation of the coupling constants: symmetric, rigid solutes with sufficiently few spins are often ideal.

There are other important reasons why this approach can be highly useful for studying orientational ordering. The principle objective of many studies is to gain some insight into the underlying mechanisms responsible for the ordering. By studying the behaviour of the nematogens alone, it is difficult to disentangle the many factors and to understand the relative importance and effect of the various intermolecular forces. In contrast, it is often possible to choose a specific solute or collection of solutes for which a specific interaction is the principal orienting mechanism. An analysis of the orientational order parameters may then provide some understanding of the role of this interaction in the nematic phase generally.

In the following sections, we review some important results of several NMR studies which employ solutes as probes in nematic liquid crystals. We emphasize those which focus on understanding the role of electrostatic and short-range repulsive interactions

and molecular flexibility in nematic liquid crystals.

1.3.2 Electrostatic Interactions

1.3.2.1 The Average Electric-Field Gradient

An important study that provided direct evidence for identifying a specific intermolecular interaction as an orienting mechanism employed molecular hydrogen and its deuterated analogues as probe solutes in a nematic solvent [13, 14]. Since a deuteron is a quadrupolar nucleus, the nuclear spin Hamiltonian for partially oriented D_2 and HD is parameterized by a quadrupolar coupling constant, B_Q, as well as the dipole-dipole and scalar coupling constants, D_{12} and J_{12}, between the two spins. Analysis of the spectra for D_2 and HD is trivial and yields directly the values of the couplings. In the absence of external fields, the ratio of B_Q/D_{12} should be a solvent-independent molecular property. The fact that this ratio was observed to be strongly solvent-dependent and deviate significantly from its gas-phase value can be explained by proposing that the probe solute experiences a non-zero average external electric-field gradient (EFG). This external EFG arises from the contributions from the solvent molecule charge distributions to the electrostatic potential sampled on average by the solute. The EFG interacts with the nuclear quadrupole moment and makes an additional contribution to the quadrupole coupling constant:

$$B_Q = -\frac{3}{4}\frac{eQ_D}{h}(\bar{F}_{ZZ} - eq\bar{P}_2),\tag{1.16}$$

where Q_D is the principal component of the deuteron nuclear quadrupole moment, $\bar{F}_{ZZ}$ is the principal component of the average external EFG, and $\bar{P}_2 = S_{zz}$ is the solute order parameter. The z-axis is the molecular symmetry axis while the Z-axis defines the direction of both the external magnetic field and the nematic director which aligns along it. Note that the EFG is a traceless, symmetric second-rank tensor. As a result of the cylindrical symmetry and apolarity of the uniaxial phase, however, the form of the EFG

tensor is simplified further: the off-diagonal terms vanish, $\bar{F}_{XX} = \bar{F}_{YY} = -\frac{1}{2}\bar{F}_{ZZ}$, and the tensor is characterized by only one independent element, $\bar{F}_{ZZ}$. In the mean-field limit, the molecular quadrupole moment interacts with the average electric-field gradient according to a mean-field potential given by

$$U(\theta) = -\frac{1}{2}\bar{F}_{ZZ}Q_{zz}P_2(\cos\theta), \tag{1.17}$$

where Q_{zz} is the principal molecular quadrupole moment and θ is the angle between the molecular symmetry axis and the nematic director. Application of this potential using values for $\bar{F}_{ZZ}$ obtained from the spectral analysis was found to provide excellent estimates of the measured order parameters for D_2 and HD [13, 14]. These calculations carefully incorporated both the presence of intramolecular vibrations and the quantum-rotor nature of these small molecules.

It is very likely that the average EFG-molecular quadrupole interaction is a valid model for other probe solutes as well. The most straightforward hypothesis is to take the average EFG as a solvent-dependent property which interacts with the probe in a manner independent of the molecular properties of the solute. In studies of other oriented solutes, this hypothesis cannot be tested directly. The situation is complicated by the inability to measure $\bar{F}_{ZZ}$ directly from spectral analysis and the importance of additional intermolecular forces as orienting mechanisms, most notably the anisotropic short-range repulsive forces. Considering this latter point, it is not surprising that predictions of orientational order parameters for a variety of other molecules, employing Eq. (1.17), and using known values of the molecular quadrupole moments and the values of the EFG measured using molecular hydrogen, are very poor [15, 16]. However, some qualitative agreement is provided by the orientational behaviour of specific solutes. For example, acetylene, like D_2, orients with a negative order parameter in the nematic solvent EBBA. While it is difficult to rationalize this behaviour by invoking other orienting mechanisms,

it is entirely consistent for a molecule with a positive quadrupole moment which interacts with a negative EFG, as was measured for this solvent using D_2. Similarly, the behaviour of the order parameters for benzene and hexafluorobenzene, molecules with very similar shape but with opposite signs of quadrupole moments, follow the pattern predicted by this mechanism using values of the EFG obtained from D_2 for various nematic solvents [16]. Finally, the presence of non-vanishing dipolar and quadrupolar coupling constants for deuterated methanes in a nematic solvent can be understood as arising from a vibration-rotation coupling that results from a second-rank tensorial interaction between the solute and a solvent mean-field [17]. A study of the quadrupolar coupling constants gives consistent results for theoretically solvent-independent quantities in different nematic solvents when an external EFG with values determined in the studies of D_2 and HD was incorporated into the analysis [18].

1.3.2.2 The Emsley-Luckhurst Potential of Mean Torque and the Average EFG

Emsley, Luckhurst, and coworkers have developed a theory for describing orientational ordering of solutes in uniaxial liquid crystals which is closely related to the Maier-Saupe theory [19]. A potential of mean torque is derived by integrating the solute-solvent pair potential over the solvent coordinates. In analogy with the expression for the ODF relation in Eq. (1.10), the solute ODF, $f(\omega)$, in the mean-field approximation is given by

$$f(\omega) \sim \exp\left[-\beta U(\omega)\right] \qquad (1.18)$$

where

$$U(\omega) = \rho \int d\vec{r}\, d\omega'\, u(\vec{r}, \omega, \omega') \tilde{f}(\omega') g(\vec{r}), \qquad (1.19)$$

where $u(\vec{r}, \omega, \omega')$ is the solute-solvent pair potential, and where we henceforth adopt the convention of labeling the solvent ODF as $\tilde{f}(\omega)$ to differentiate it from that of the solute.

Note that $f(\omega)$ is not determined self-consistently in this method, but is expressed in terms of the solvent ODF. As in the Maier-Saupe theory, the pair potential in the present theory is expanded and truncated to second rank; however, in this case, the biaxiality of both the solute and solvent molecules is included, in analogy to an extended version of the Maier-Saupe theory [20]. Further, as in the original formulation of the present theory, the distribution of the intermolecular vector was taken to be spherically symmetric: $g(\vec{r}) \approx g(r)/4\pi$. With the approximations described above, and in the limit of negligible biaxiality for the solvent orientational ordering, the following mean-field potential is obtained:

$$U(\theta, \phi) = -\bar{u}_{200}\bar{P}_2^{(nem)}P_2(\cos\theta) - \sqrt{\frac{3}{2}}\bar{u}_{202}\bar{P}_2^{(nem)}\sin^2\theta\cos 2\phi, \qquad (1.20)$$

where $\bar{P}_2^{(nem)}$ is the nematogen order parameter. The coefficient $\bar{u}_{200}$ is analogous to the parameter ϵ defined in Eq. (1.13), i.e. an average over the radial component of the axially symmetric second-rank term of the expansion of the pair potential, while $\bar{u}_{202}$ is a similar term which accounts for the biaxiality of the molecules in the pair potential. Orientational order parameters may be calculated using the following relation:

$$S_{\alpha\beta} = \frac{\int \left(\frac{3}{2}\cos\theta_\alpha\cos\theta_\beta - \frac{1}{2}\delta_{\alpha\beta}\right)\exp[-\beta U(\theta,\phi)]\sin\theta d\theta d\phi}{\int \exp[-\beta U(\theta,\phi)]\sin\theta d\theta d\phi}, \qquad (1.21)$$

where θ_α, the orientations of the molecular axes with respect to the nematic director, are functions of the polar angles, θ and ϕ.

Applying this model to fit experimental orientational order parameters, the linear dependence of the fitted potential on the solvent order parameter $\bar{P}_2^{(nem)}$ is generally satisfied. It is also generally observed that the ratio $\lambda \equiv \bar{u}_{200}/\bar{u}_{202}$ is strongly dependent on both temperature and solvent [19, 21, 22, 23]. By contrast, the theory predicts that the temperature dependence should be determined solely by $\bar{P}_2^{(nem)}$. As well, for the case of second-rank tensorial solute-solvent interactions, λ is predicted to be solvent-independent.

There are a number of possibilities to explain this deficiency in the theory, including the presence of multiple contributions to the pair potential. This has been investigated by Emsley *et al.* with special emphasis on electrostatic interactions, its relation to the observed non-zero average EFG in nematic solvents, and the consequence to the dispersion-force contribution to the potential of mean torque [22, 23, 24]. In the context of the theory, it can be shown that the observation of a finite EFG indicates that the distribution of intermolecular vectors cannot be spherically symmetric, in contrast to the assumption of the Maier-Saupe theory and its derivatives. Further, the quadrupole-quadrupole interaction is found to be the lowest order multipole expansion term which can contribute to the mean potential in the case where the distribution possesses only cylindrical symmetry. For an axially symmetric molecule, for example, the following mean-field potential is obtained [24]:

$$U_Q(\theta) \sim \overline{r^{-5}} Q_{zz}^{(v)} Q_{zz}^{(u)} \bar{P}_4^+ \bar{P}_2^{(nem)} P_2(\cos\theta) \tag{1.22}$$

According to Eq. (1.17), this corresponds to an EFG given by

$$\bar{F}_{ZZ} \sim \overline{r^{-5}} Q_{zz}^{(v)} \bar{P}_4^+ \bar{P}_2^{(nem)}, \tag{1.23}$$

where $Q_{zz}^{(v)}$ and $Q_{zz}^{(u)}$ are the quadrupole moments of the solvent and solute, respectively. Further, the average over r is performed as in Eq. (1.13), and $\bar{P}_4^+$ is a fourth-rank order parameter describing the orientational distribution of intermolecular vectors. The lack of spherical symmetry of the intermolecular vector distribution also modifies the form of the mean-field potential arising from dispersion interactions.

The orientational order of anthracene and anthraquinone, molecules with similar molecular shapes and polarizabilities but with significantly different quadrupole moments, was studied and analyzed using the modified theory above [25]. It was concluded that the observed behaviour of S_{zz} and λ could only be explained by a dependence of

$\bar{P}_2^+$ and $\bar{P}_4^+$ on both solvent *and* solute properties. This contrasts with the proposal by Burnell *et al.* that the average EFG is a property of the nematic solvent alone. However, it is important to note that the analysis considered contributions only from electrostatic and dispersion forces, neglecting entirely contributions from the probably very important short-range repulsive forces. This latter interaction cannot be easily incorporated into the framework of the Emsley-Luckhurst theory which, like the Maier-Saupe theory, is valid for the case of long-range forces and neglects the effects of short-range correlations.

A further complication of the theory was discovered by Luckhurst *et al.* in a Molecular Dynamics study of a system of Gay-Berne nematogens and the validity of the Maier-Saupe theory to this system [26]. In particular it was found that the orientational distribution of solute-solvent intermolecular vectors is highly dependent on the intermolecular distance r. This implies that separately averaging over the magnitude and direction of the inter-molecular displacement $\vec{r}$ is invalid and that the theory must be reformulated to account for this feature. It may be shown that the expression for the EFG must be rewritten in the following form:

$$\bar{F}_{ZZ} \sim \rho Q_{zz}^{(v)} \left[\int \frac{\bar{P}_4^+(r)g(r)dr}{r^3} \right] \bar{P}_2^{(nem)}. \tag{1.24}$$

The consequence of this result will be discussed at a later stage in this thesis.

1.3.2.3 Further Comments on Electrostatic Interactions

In the application of the Emsley-Luckhurst theory to electrostatic interactions above, it is found that the lowest order non-vanishing multipole-multipole term is that for the quadrupole-quadrupole interaction, which results in a mean EFG with which the solute interacts. It is easy to understand why, for example, the dipole-dipole term does not contribute within the context of the theory. In this case, a solute dipole moment interacts with a mean electric field, which is necessarily zero for an apolar nematic phase.

However, Photinos *et al.* have demonstrated the importance of intramolecular dipole-dipole interactions in their studies of the orientational ordering of α-bromonated alkanes [27, 28]. The observed bias on the segmental orientational order relative to the case of regular alkanes was shown to result from interaction of the local dipole moment at the bromine position with the local dipoles on the nematogens. The effect was explained qualitatively by the asymmetric arrangement which results from off-centered local dipoles on molecules with short-range repulsive cores. This results in strong short-range correlations which contributes significantly to the orientational ordering. In principle, these interactions should then contribute to the ordering of solutes with dipole moments in a zero-EFG liquid crystal where it has been assumed, in the mean-field limit, that electrostatic interactions are insignificant.

There is further evidence that the mean-field approach to electrostatic interactions is too simplistic. Terzis *et al.* have derived an alternative theory to describe orientational ordering of solutes in nematic solvents which incorporates explicitly both the anisotropic excluded volume interaction and interactions between electrostatic multipole moments [29]. The effects of molecular polarizability were also included, though they were generally found to be relatively insignificant. The theory derives hard-core (HC) and electrostatic (ES) contributions to a mean-field potential. The derivation involves a reduction of the full many-particle distribution function and incorporates many approximations, including neglecting correlations between solvent molecules and truncating the effective range of the electrostatic energy to a local region. The latter choice necessarily excludes the validity of the theory for dealing with long range dipole-dipole interactions. The following contributions to the mean-field potential are obtained:

$$\frac{U_{HC}(\omega)}{k_B T} = \rho \int V_{ex}(\omega, \omega') \tilde{f}(\omega') d\omega' \qquad (1.25)$$

and

$$\frac{U_{ES}(\omega)}{k_B T} = \rho \int d\vec{r} d\omega' \tilde{f}(\omega') \left[1 - \exp\left(-u_{ES}(\vec{r}, \omega, \omega')/k_B T\right)\right] g_{HC}(\vec{r}, \omega, \omega'), \qquad (1.26)$$

where $g_{HC}(\vec{r}, \omega, \omega') = 0$, for overlapping configurations, or 1, for non-overlapping configurations, and $u_{ES}(\vec{r}, \omega, \omega')$ is the electrostatic contribution to the pair potential. The potentials were expanded to fourth-rank and used to analyze experimental order parameters for a small collection of solutes by adjusting the solvent dimensions and nematic order parameters. The values of these were used to measure the strength of HC interaction and the various ES interactions including dipole-quadrupole, quadrupole-quadrupole terms. The main conclusions from this study were as follows: the effects of the ES interactions were of comparable magnitude to those of the HC interactions; they are highly sensitive to the shapes and electrostatic properties of the solvent and solute molecules; they cannot be described consistently by means of a coupling between the solute quadrupole moment and an external average EFG.

However, there may be flaws in both the theory and its application to the analysis of the experimental data. The relation for the HC mean-field potential above has exactly the same form as the self-consistent expression for the ODF in Onsager's theory. In that case, the neglect of correlations between three and more molecules is a severe approximation for particles with dimensions of typical nematogens. This may be even more severe for approximating the HC contribution to the ODF for solutes which have considerably less shape anisotropy than the nematogens, and may significantly underestimate its contribution to orientational ordering. In light of this, the conclusions drawn by the study are arguable, and an alternative approach to studying the combined effects of HC and ES interactions on solute orientational order must be found.

1.3.3 Short-Range Repulsive Forces and Mean-Field Models

It is generally accepted today that short-range anisotropic forces provide the principle orienting mechanism for nemotogens in their nematic phase. It is highly probable that this mechanism should also dominate for other molecules dissolved in an oriented phase. The fact that this is not the case for molecular hydrogen is probably due to its small size and nearly spherical shape. However, for molecules with dimensions closer to those of the nemotogens and with greater shape anisotropy, it is very likely to be true.

In previous experiments with deuterated molecular hydrogen, it was found possible to combine nematic solvents with measured values of the EFG of opposite signs to form a mixture that has a vanishing EFG. Specifically, the following two mixtures were observed to have this property: (1) 55 wt% Merck ZLI 1132[1] / EBBA at a temperature of T=301.4 K [31]; (2) 30 wt% 5CB[2] / EBBA at 316 K [32]. If the EFG is a property of solvent alone, then it should vanish for any other solute as well, along with its associated contribution to orientational ordering. Under this assumption, these zero-EFG mixtures are ideal for studying the other interactions contributing to orientational ordering of the solute.

The orientational order parameters of a wide collection of solutes have been measured in the different zero-EFG mixtures and analyzed to test the importance of short-range repulsive forces as an ordering mechanism. The basic approach of the analysis is to construct a model pseudopotential, $U_{SR}(\omega)$, which is highly sensitive to the molecular size and shape, to describe the orientational behaviour of an arbitrary solute. Molecules are modeled using van der Waals spheres to represent the atoms. Orientation-dependent projections of the molecules parallel and perpendicular to the nematic director are used

---

[1]A eutectic mixture of alkylcyclohexylcyanobiphenyls and cyclohexylcyanobiphenyls. See Ref. [30] for composition.
[2]4-n-pentyl-4'-cyanobiphenyl

to define the potential in a way designed to have a lower energy, and therefore a higher probability, for elongated molecules aligned along the director, and, for oblate molecules, perpendicular to the director. The potential may be characterized by one or two solvent-dependent model parameters which describe the strength of the interaction between the solute and the nematic solvent. Molecular order parameters may be calculated using Eq. (1.21). Several of these models shall be used and examined extensively in subsequent chapters, and we choose not to describe the details until then.

The essential idea of this approach is that a model which incorporates the details of the molecular shape should be able to provide an adequate description of orientational order for arbitrary solutes if the principal ordering interaction is short-range and repulsive in nature. Long-range attractive forces, by contrast, should be relatively insensitive to molecular shape. Several different models have been developed to analyze the large collection of order parameters which have been measured for solutes in zero-EFG liquid crystals. Of particular interest are the models developed by Burnell and coworkers [33, 34, 35, 36], and a model due to Ferrarini *et al.* [37] which is closely related to that proposed by Zimmerman *et al.* [36]. The most important result of these studies is that the models which incorporate in the most detailed manner the molecular shape generally provide the best predictions of orientational behaviour and are able to predict the principal order parameters to within 10% of their measured values.

1.3.4 Flexibility

With few exceptions, the molecules which form nematic liquid-crystalline phases are highly flexible and sample a wide variety of conformations. The near-universal presence of this property is a result of the fact that it increases the entropy and therefore decreases the free energy of the nematic mesophase relative to that of the crystalline-solid phase; thus, the system will not freeze before it passes into a liquid crystalline phase. Since molecular

shape anisotropy is the dominant factor contributing to the orientational ordering in these systems, the ordering behaviour is strongly influenced by the packing structure of the fluid. Molecular flexibility is expected to strongly affect the organization in the fluid via the complex relationship between translational, orientational and internal entropy, and therefore will alter significantly the orientational behaviour relative to that expected for systems of rigid molecules.

Important examples of internal motion include the the following: rotation about one or more bonds that bridge the rigid units that form the core of the molecule, and the rapid exchange between conformations of alkyl chains which are often connected to the rigid cores.

The incorporation of molecular flexibility into molecular-statistical theories of liquid crystals is a challenging task. These theories generally choose to ignore this factor and derive results in terms of interactions between rigid molecules, which may be thought of loosely as the average over all conformational states. Some Molecular Dynamics computer simulations have successfully simulated nematic systems composed of molecules which are modeled in detail and include internal flexibility together with an accurate molecular structure [38, 39]. However, such calculations are extremely time-consuming and can only be run over short times for relatively small systems.

Experimental NMR measurements can provide some insight into the conformational behaviour of flexible mesogens. Deuterium NMR of isotopically substituted species directly yields order parameters of individual rigid molecular subunits. Proton NMR spectra of nematogens are highly complex and cannot be analyzed without using additional techniques such as partial deuteration with deuterium decoupling. Nevertheless, the dipole-dipole spin couplings that may be obtained contain considerably more information than the deuterium quadrupole coupling constants. In either case, the analysis requires a suitable quantitative measure of the orientational ordering. The Saupe matrix

in Eq. (1.6) is designed for rigid molecules; the use of an average $S_{\alpha\beta}$ appropriate for an average molecular structure has been considered before and shown to be inappropriate for large molecules with large amplitude internal motions between conformations not related by symmetry [40], conditions which certainly describe typical nematogens. The necessary alternative approach requires a separate $S_{\alpha\beta}$ to describe the orientational ordering of each conformer, and is valid provided that the rate of molecular reorientation is rapid compared to the rate of exchange between conformers [41, 42]. Thus, a very large number of independent order parameters is required to characterize the orientational behaviour of most nematogens.

As in the case of investigating the intermolecular forces which contribute to orientational ordering of nematic liquid crystals, probe solutes may be used to provide some insight into the role of molecular flexibility for such systems. The principal advantage is that specific solutes may be chosen for convenience. The spectra of relatively simple solutes can be analyzed in a straightforward manner, either directly or with the help of some additional tool like that of Multiple-Quantum NMR spectroscopy which we shall presently describe. The orientational ordering and conformational behaviour of flexible solutes may reflect that of similar flexible components of nematogens. For example, studies of the behaviour of alkanes oriented in a nematic liquid crystal may provide some understanding of the role of nematogen alkyl tails. An important question about the conformational behaviour of flexible molecules which can be investigated concerns the role of the solvent in biasing the conformational equilibrium from that for isolated molecules.

Although a large number of independent order parameters are in principal required to describe the ordering of nematogens, this problem can be circumvented by employing model potentials described in Section 1.3.3. The models are characterized by only one or two parameters and can be used to calculate the order parameters for each conformer. A related advantage of studying flexible solutes is that the success that a particular model

has in fitting a set of NMR data provides an additional test of the overall ability of a model to adequately describe molecular orientational order. This approach has been used to study the conformational behaviour and orientational ordering of alkanes of various lengths in several recent NMR studies [43, 44, 45, 46, 47, 48, 49].

1.4 Multiple-Quantum NMR

1.4.1 Application to the Analysis of NMR Spectra

In NMR studies of solutes ordered in liquid crystals, information about orientational ordering is obtained from an analysis of coupling constants, which, in turn, are obtained from an analysis of NMR spectra. In the case of deuterium NMR, the spectra are relatively simple, even for complex molecules such as typical nematogens. They consist of a set of of doublets, each corresponding to a unique deuteron on the molecule, whose splitting is related to the order matrix of the corresponding rigid molecular subunit. This is a consequence of the large magnitude of the quadrupole coupling constant associated with the spin which interacts with a *local* electric-field gradient, which dominates the spin Hamiltonian. In the case of proton-NMR, however, it is the dipolar coupling constants which are the principal determinant of the fine structure in the spectrum. This leads to far more complex spectra that require sophisticated numerical methods for analysis.

The general procedure for fitting a spectrum requires detailed information about the molecular structure, estimates of $S_{\alpha\beta}$, and, in the case of flexible molecules, some knowledge about the geometry and relative weighting of each of the conformations sampled, in order to calculate initial estimates of the D_{ij}. These may be be used, together with literature values of isotropic chemical shifts, to generate an initial spectrum. If the parameters are sufficiently accurate, then individual lines between experimental and calculated spectra may be assigned and fit using very well-established numerical techniques.

Many solute molecules with ≥ 8 spins have a complex spin-Hamiltonian that gives rise to a correspondingly complex spectrum which may be very difficult to solve, even in the case of very symmetric molecules. The number of measurable transitions increases rapidly with the number of spins, eventually resulting in a quasi-continuous spectrum of overlapping, unresolvable lines. The case for spin systems of intermediate complexity, where the spectrum consists of lines which are generally resolvable but is still highly complex, deserves some attention. For these systems, extremely accurate initial estimates of the spin-Hamiltonian parameters are required. Small deviations may scramble positions of the numerous, densely packed lines to the point where adequate assignment becomes virtually impossible. However, such spectra in principle can be analyzed if a method were available with which to provide sufficiently accurate estimates of the NMR spin-Hamiltonian parameters.

Multiple-Quantum (MQ) NMR spectroscopy is one possible method. The structure of higher orders of MQ spectra can be very simple, yet contain the same information that is available from the analysis of the corresponding, conventional NMR spectrum. Thus, the solution of MQ spectra does not pose the same severe demands as that of the conventional spectrum. Estimates of the coupling constants and chemical shifts obtained from the MQ spectra may then be used to solve the one-quantum spectrum with much less difficulty than would otherwise be the case. Yet the technique has generally been ignored as a basic tool for studying such systems.

It is interesting to note that the phenomenon of continuous wave (CW) MQ-NMR was observed over thirty years ago. In this case the usual NMR selection rules forbidding most MQ transitions was circumvented by increasing the strength of the perturbing RF field. An unwelcome consequence of this technique, however, is that the spectral line positions and intensities depend not only of the unperturbed internal spin Hamiltonian, but on the magnitude of the perturbing field as well. Thus, it was not until the introduction of

the two-dimensional Fourier Transform NMR technique that MQ NMR could become a truly useful method. This is due to the fact that the frequencies of MQ transitions are obtained from the indirect observation of associated MQ coherences which evolve during a time in which the system is free from any external RF field.

Although this approach was first suggested in the landmark 2D-NMR paper by Aue *et al.* in 1976 [50], MQ-NMR methodology was developed mainly by Pines and coworkers at Berkeley in years shortly afterward. There is an enormous variety of MQ experiments that were developed during that time, and it is far beyond the scope of this thesis to describe most of these; an excellent review of this subject may be found in the review by Weitekamp [51]. However, a brief description of the basic method and underlying theory for measuring standard MQ spectra is presented below.

1.4.2 Theoretical Background

In the absence of an external RF field, the Hamiltonian for a collection of like spins of $I = \frac{1}{2}$ (i.e. non-quadrupolar nuclei) is composed of the Zeeman, dipolar and scalar coupling terms:

$$H = H_Z + H_D + H_J \tag{1.27}$$

The Zeeman Hamiltonian, H_Z, is given by

$$H_Z = -\sum_{i=1}^{N} h\nu_i I_{Zi} \tag{1.28}$$

where the chemically shifted frequencies, ν_i, are given by

$$\nu_i = \frac{\gamma H_0}{2\pi}(1 - \sigma_{ZZ,i}), \tag{1.29}$$

where γ is the gyromagnetic ratio of the nucleus, H_0 is the static external magnetic field, defined to be along the Z-axis, and $I_{Z,i}$ is the Z-component of the spin operator for the ith spin of a system of N spins. The quantity $\sigma_{ZZ,i}$, is the component of the chemical-shift

tensor projected onto the external field and is related to the molecular-frame components $\sigma_{\alpha\beta,i}$ by the following relation:

$$\sigma_{ZZ,i} = \frac{1}{3}\sum_{\alpha}\sigma_{\alpha\alpha,i} + \frac{2}{3}\sum_{\alpha,\beta}S_{\alpha\beta}\sigma_{\alpha\beta,i}, \tag{1.30}$$

where $S_{\alpha\beta}$ is the Saupe order matrix defined in Eq. (1.6). Note that the second term vanishes for isotropic systems.

The direct dipolar Hamiltonian is given by

$$H_D = \sum_{i<j}hD_{ij}(3I_{Z,i}I_{Z,j} - \vec{I}_i\cdot\vec{I}_j), \tag{1.31}$$

where the dipolar coupling constant D_{ij} between spins i and j, was defined previously for the general case in Eq. (1.14) and, for rigid molecules, described by Eq. (1.15).

The indirect dipolar or scalar Hamiltonian is approximately given by

$$H_J = \sum_{i<j}hJ_{ij}\vec{I}_i\cdot\vec{I}_j \tag{1.32}$$

Note that the general form of this Hamiltonian includes an anisotropic component which has exactly the same form as the direct dipolar Hamiltonian. However, for most couplings involving protons, the anisotropy is small and may be ignored.

The expressions written above are valid in the high field limit, where the chemical shift, and the direct and indirect dipolar interactions are small compared to the principal Zeeman interaction of the bare nucleus with the external magnetic field. The eigenstates and eigenvalues are obtained from a diagonalization of the Hamiltonian and are parameterized by $\sigma_{ZZ,i}$, D_{ij} and J_{ij}. Thus, the associated spectral transition frequencies and intensities are also a function of the coupling constants.

The total Hamiltonian commutes with the Z-component of the total angular momentum operator, $I_Z \equiv \sum_i I_{Z,i}$:

$$[H, I_Z] = 0 \tag{1.33}$$

Thus, I_Z is also diagonal in the Hamiltonian eigenbasis and its eigenvalue, M_i, given by

$$I_Z|i\rangle = M_i|i\rangle \tag{1.34}$$

for an eigenstate $|i\rangle$, is a "good" quantum number, and thus, each eigenstate can be labeled with a unique value of M_i. The spectra measured using either CW NMR employing weak RF fields, or through fourier transformation of the Free Induction Decay (FID) following a "hard" RF pulse yield a spectrum characterized by transitions between eigenstates $|i\rangle$ and $|j\rangle$ which, in the case of infinitely sharp lines, is given by

$$F(\omega) = \sum_{i<j} |\langle i|I_\pm|j\rangle|^2 \, \delta(\omega - \omega_{ij}), \tag{1.35}$$

where $\omega_{ij} \equiv E_i - E_j$ for eigenvalue energies E_i and E_j. This gives rise to the main NMR selection rule: $n_{ij} \equiv \Delta M_{ij} \equiv M_i - M_j = \pm 1$. The *order* of a particular transition is given by the value of n_{ij}. Thus, a standard NMR spectrum is characterized by transitions of order ± 1.

Before describing how this selection rule may be overcome to permit effectively transitions between all orders, it is useful to examine the number of transitions associated with each particular MQ order. It can easily be shown that for an N-spin system, which has 2^N distinct eigenstates and energy levels, the number of n-order transitions is given by $Z_n = (2N)!/((N+n)!(N-n)!)$ for $n \leq N$. For a general ten-spin system, $Z_{10}=1$, $Z_9=20$, $Z_8=190$,..., $Z_1=167960$, $Z_0=184756$. Thus, the number of transitions increases rapidly for decreasing MQ order. The higher order spectra, those for $n = N - 1$, $N - 2$, $N - 3$, contain the same information about the NMR coupling constants as does the one-quantum spectrum, yet contain far fewer transitions. This means that there is a vast redundancy in the conventional NMR spectrum. Note that for many molecules which have some degree of symmetry, many energy levels within each manifold are degenerate. Further, it may be shown that all transitions between states belonging to the different

irreducible representations of the permutation group (i.e. permutation of spin indices in the eigenstates) are forbidden. These factors can reduce considerably the number of observable transitions of all orders for molecules with some degree of symmetry.

A basic pulse sequence that may be used for the generation and observation of MQ coherences is given by the following:

$$\left(\frac{\pi}{2}\right) - \tau - \left(\frac{\pi}{2}\right) - t_1 - \left(\frac{\pi}{2}\right) - \tau' - t_2(acquire) \tag{1.36}$$

An understanding of how MQ transitions are observed in a two-dimensional NMR experiment requires an understanding of the time evolution of the spin density operator over the course of the experiment. This may be calculated using the Liouville equation:

$$\frac{\partial \rho}{\partial t} = \frac{i}{\hbar}[\rho, H] \tag{1.37}$$

Prior to the application of the RF pulses, the equilibrium density operator, in the high-temperature limit, is given by:

$$\rho_{eq} \approx \mathbf{1} - \left(\frac{\gamma \hbar H_0}{k_B T (2I + 1)^N}\right) I_Z \tag{1.38}$$

The identity operator $\mathbf{1}$ plays no role under time evolution of ρ and may be ignored. Application of a strong 90° Y-pulse converts I_Z into I_X. The density operator evolves under the internal Hamiltonian according to the Liouville equation above. For the Hamiltonian described above, it can be shown that $I_X = (I_+ + I_-)/2$, a ±one-quantum operator, evolves into other one-quantum coherence operators during the preparation time τ. Following the application of a second RF pulse, these one-quantum coherences are transformed into all possible MQ coherences. The magnitude of the MQ coherences depends strongly on τ and the NMR coupling constants that characterize the spin Hamiltonian. The MQ coherences evolve for the evolution time t_1, again under the internal spin Hamiltonian alone. The third pulse partially converts the spin order back into one-quantum

coherences which evolve into the observable I_X, which may be recorded as a function of t_2. Two-dimensional fourier transformation and projection onto the f_1 axis yields a spectrum of MQ transitions which corresponds to the time evolution of MQ coherences during the evolution time t_1.

The basic pulse sequence may be modified further to accomplish specific goals. Application of particular phase cycles can be used to selectively detect particular orders of MQ spectra in order to reduce the spectral width and improve the digital resolution [52]. Offsetting the RF frequency from resonance can be used for the separation of individual orders. If necessary, 180° pulses can be incorporated to refocus the effects of static magnetic field inhomogeneities.

1.4.3 Limitations

The primary interest in MQ spectroscopy in this thesis is in its application to simplify spectral analysis of one-quantum spectra. While this method is potentially very useful for such problems, it is also clear that there are factors which can limit its range of applicability.

As the size N of the spin system increases, the number of MQ coherences increases considerably. Consequently, the initial order manifested in the equilibrium magnetization is distributed over an increasingly large number of coherences during the evolution period of the MQ experiment. The effective signal-to-noise therefore is reduced substantially for larger molecules. Elaborate methods designed to transfer the order to a particular order of coherence, and thus to reduce this "thinning out", have been devised [53, 54, 55]; however, these are non-trivial experiments and still may be of limited use for larger molecules. For typical nematogens with ≈20 proton spins, even specific high MQ orders will contain a prohibitively large number of coherences. The inefficiency of using a single pulse for converting the MQ coherences back into one-quantum coherences is also a severe

limitation of the basic pulse sequence. Time reversal pulse sequences which are intimately related to the sequences designed for selective excitation of particular MQ orders have been developed to circumvent this problem [56].

As stated previously, the magnitudes of the MQ coherences evolving during t_1 are a complex function of the preparation time τ and the NMR coupling constants. A problem associated with this fact is that it can be very difficult to choose a particular τ such that all coherences of a particular order of interest are appreciably populated. One may employ several values of τ and sum the individual spectra. Further, a search procedure for optimizing τ has been described [57], but this is suitable for maximizing the integrated intensity of an entire MQ order and not for individual coherences.

Finally, there is the usual problem of truncation in the t_1 domain common to all two-dimensional NMR experiments. In typical experiments, it may take an unrealistically large number of t_1 increments for wide spectra to avoid this problem. This truncation results in a widening of the experimental lines, reducing the signal-to-noise ratio and increasing the uncertainty of the estimated line frequency. Note that natural line broadening is magnified n-fold for n-quantum coherences in the absence of refocusing pulses and may contribute significantly to the broadening of lines of higher MQ orders.

Clearly, these problems are not insurmountable. Many variations of the basic experiment have been devised to deal with them. However, most of these techniques utilize complex pulse trains which require near-ideal pulses. Loss of coherence due to RF inhomogeneity for example, a problem inherent to high resolution NMR systems, can be a serious impediment. Even the application of single 180° refocusing pulses can produce troublesome artifacts under such conditions. Thus, the limits of the basic pulse sequence deserved to be explored. As demonstrated in this thesis, this simple and undeservedly ignored technique can be very useful.

1.5 Monte-Carlo Simulations

A principal goal of many studies of orientational ordering in liquid crystals is an understanding of the relationship of molecular properties to the long-range correlations. Unfortunately, it is often the case that experimental data are very difficult to interpret unambiguously: the effects and relative importance of different molecular properties are difficult to determine. The use of specific solutes to enhance the effects of specific intermolecular forces on the molecular alignment is a helpful, but limited method.

Computer simulations provide an effective complementary approach to study such systems in that they can aid in the interpretation of experimental data, as well as supply a means to test specific theories. There are two main types of simulation techniques: the Molecular Dynamics (MD) and Monte Carlo (MC) methods. MD simulations follow the real time development of a system of interacting particles by starting from some initial configuration and integrating Newton's equations of motion over a time interval as long as is computationally convenient. Periodic boundary conditions are employed to accommodate the finite size of the model system. Equilibrium properties of the system, including various order parameters and distribution functions, are determined by averaging over the sequence of states generated by the time evolution of the particles. An advantage of the MD method is that quantities related to the dynamics of the system, such as diffusion constants, may be measured.

The MC method, in contrast to the MD method, makes no attempt to simulate the true dynamics of the system. Instead, a sequence of micro-states is generated by a stochastic process such that the probability of the occurrence of a particular state in the chain is given by the appropriate ensemble (microcanonical, canonical or grand canonical). This can be achieved by using a *Markov process* to generate the sequence. In this process, a system which is initially in some state i undergoes a transition to

another state j with some probability P_{ji} that is independent of the previous history of the system. The transition probability is chosen to satisfy the principal of detailed balance characteristic of systems in equilibrium,

$$P_{ji}\pi_i = P_{ij}\pi_j, \tag{1.39}$$

where π_i is the equilibrium probability that the system in the ith state. For the canonical ensemble, this leads to the following relation:

$$\frac{P_{ji}}{P_{ij}} = \frac{\pi_j}{\pi_i} = \exp[-\beta(E_j - E_i)], \tag{1.40}$$

where E_i is the energy of the ith state.

One possibility for choosing the transition probabilities is that given by the *Metropolis* algorithm [58]. In this method, the system is arranged in some initial configuration for a finite collection of particles. One of the particles is chosen randomly, and a move (e.g. translation, rotation) is attempted and the energy difference between the initial and final states, $\Delta E = E_j - E_i$, is calculated. If $\Delta E > 0$, then the move is accepted, i.e. $P_{ji} = 1$; if $\Delta E < 0$, then the move is accepted with the probability given by $P_{ij} = e^{-\beta \Delta E}$. It is trivial to show that this algorithm is consistent with the relations above.

The sequence of states generated by this Markov process is governed by the appropriate probability distribution, and is independent of the initial configuration under the assumption that it is possible to reach a particular configuration from any other in a finite number of steps. The configurations generated in the early stage of the sequence prior to the establishment of equilibrium are not counted in the calculation of expectation values of quantities of interest. There is no general, quantitatively precise method for determining whether or not the system has attained equilibrium. A simple approach is to monitor block averages, measured over a specific number of steps, of a quantity of interest. Generally, after a short-lived transient effect, the quantity settles to some

average value with some degree of statistical fluctuation. Further, the rate with which equilibrium is attained is highly dependent on the success ratio of individual moves. The translations and rotations which may characterize the move are chosen randomly within some maximum range of values relative to the current ones. Generally, it is found that the maximum values should be chosen to yield a success ratio of about 50% in order to attain equilibrium most rapidly.

MC simulations have been used to study a wide variety of systems, including liquid crystals. We make no attempt to review the many studies which use the MC method to investigate orientational ordering in these anisotropic systems. It should be pointed out, however, that the models employed in many of these theories fix the particles to points on a lattice, thereby eliminating the translational degrees of freedom. Particles interact through some highly simplified anisotropic interaction that drives the transition from a disordered to an ordered phase. A notable example of this is the Lebwohl-Lasher model in which lattice-fixed particles interact with a potential that has an orientation-dependence of $P_2(\cos\theta)$, where θ is the angle between the orientations of a pair of cylindrically symmetric particles [59]. Despite the highly simplistic nature of these models, they have provided an invaluable tool for studying the details of liquid-crystal phase transitions and providing a test for various theories of liquid crystals.

A significant development in the understanding of liquid crystals was made by Frenkel and coworkers over a decade ago using MC simulations. It was discovered that systems composed of hard convex bodies such as ellipsoids and spherocylinders could form stable orientationally ordered liquid crystalline phases for sufficiently high densities in the absence of any soft or long-range anisotropic interactions [5, 60]. Note that these systems are characterized by constant energy since it is infinite in the case of overlap between any of the particles, a situation which is therefore forbidden, but is otherwise unaffected by the configuration of the system. Thus, these systems undergo phase transitions due solely

to the maximization of entropy. This work underscored the importance of short-range repulsive forces, whose anisotropy is closely related to the anisotropy in the molecular shape, as an ordering mechanism in liquid crystals. More recently, Weis *et al.* investigated the perturbative effects of electrostatic interactions on the orientational order and phase stability in such systems by including local dipoles on the hard particles [61, 62, 63].

The use of MC simulations which use similar models to study orientational ordering of solutes in nematic liquid crystals may provide insight into the importance of ordering mechanisms that are difficult to determine by experiment alone. In the present work, we are concerned with the influence of shape and electrostatic interactions on molecular ordering. Specifically, we focus on the interpretation of NMR experimental data of Burnell and coworkers for solutes ordered in nematic solvents [33, 64]. For example, the relationship of various model potentials related to the size and shape of the molecule and the short-range repulsive forces which the model is assumed to describe deserves attention, as well as the EFG-quadrupole moment orienting mechanism described earlier. These properties may be easily examined using solutes modeled as hard particles of various shapes incorporated into a bath of orientationally oriented hard ellipsoids and including specific electrostatic multipoles on the individual particles. To date, the only computer simulations of solutes in liquid crystals have focused on two specific solutes, benzene [65] and hexane [66], with attention given to dynamical and conformational properties specific to these solutes. Our aim is to gain a more general understanding of solute ordering by studying a wide range of solutes without attempting to realistically model any particular molecule.

1.6   Outline of Thesis

This thesis is concerned with both experimental NMR and MC methods to study orientational order of solutes in nematic liquid crystals in order to gain an understanding of the anisotropic intermolecular forces which induce orientational order.

The experimental work presented here focuses on the use of MQ spectroscopy as a tool for the analysis of spectra of solutes with spin systems of intermediate complexity. Chapter 2 presents a study of biphenylene as an illustrative example. This eight-spin molecule is highly symmetric yet gives rise to a complex spectrum which only through an analysis of the six- and seven-quantum spectra can be solved to determine the dipolar couplings. These are then used for a determination of its molecular structure.

In Chapter 3, we apply the same MQ methods to study butane as a solute in a nematic liquid crystal. This molecule is of significant interest since it is the simplest alkane which undergoes the large amplitude conformational changes between *trans* and *gauche* states. This ten-spin molecule gives rise to a particularly complex and feature-less spectrum which, nevertheless, is comprised of well-resolved lines. An analysis of the readily acquired seven- and eight-quantum spectra are found to give excellent estimates of the coupling constants and render trivial an analysis of the one-quantum spectrum. The dipolar coupling constants are analyzed to provide an estimate of the effective *trans-gauche* energy difference and the individual internal and external contributions, the latter including both isotropic and anisotropic components. Further, the analysis of the couplings requires the use of a mean-field model to describe the orientational ordering in order to calculate the order parameters for each conformation. We employ several different models to this end, comparing the results obtained for each, and comment on their relative effectiveness.

In Chapter 4, we use MC simulations to investigate the influence of molecular shape

on the orientational ordering of solutes in a nematic solvent. Both solvent and solute molecules are modeled as hard prolate ellipsoids whose only intermolecular interaction is determined by the requirement that they cannot overlap. The orientational order parameters and distribution functions of solutes of a wide variety of sizes and shapes are studied in detail. The results are analyzed in terms of the same mean-field models used in Chapter 3. The results of the analysis are compared to analogous results of the analysis of experimental NMR data. This comparison gives significant insight into the relationship between the mean-field models and short-range repulsive forces, as well as the general importance of short-range repulsive forces as a molecular ordering mechanism in nematic liquid crystals.

In Chapter 5, we present results from a further study employing MC simulations to study ordering in nematics. In this case, a point quadrupole placed at the centre of each particle; both solvent-solute and solvent-solvent quadrupole-quadrupole interactions are considered, in addition to the hard-core interactions. This system is used to study the additional effects of electrostatic interactions on solute orientational ordering and its importance relative to that of short-range repulsive forces. Further, this model system is used to investigate the hypothesis that the interaction of the solute quadrupole moment with a solute-independent average EFG is a generally valid and significant ordering mechanism. Finally, the results are analyzed in terms of the theories developed by Luckhurst and Emsley (Section 1.3.2.2) and Photinos (Section 1.3.2.3).

In Chapter 6, we summarize the important results of the thesis and present our final comments on this material.

Chapter 2

Multiple-Quantum NMR of Oriented Solutes (I): Biphenylene as an Illustrative Example

The material presented in this chapter has been published in ref. [67].

2.1   Introduction

The use of NMR spectroscopy to determine the geometry of small rigid molecules aligned in liquid crystal solvents is well established and has proven to be very useful [68, 69, 70]. In such systems, the dipolar coupling constants, which are only partially averaged by the anisotropic molecular reorientation, contain direct information about internuclear distances and ordering which may be disentangled to yield the nuclear spin geometry and molecular order parameters. The ability to obtain the dipolar coupling constants is clearly contingent on the complexity of the spin system. In cases where the number of spins in the molecule is large (≥ 8), or where there is little or no molecular symmetry, the NMR spectrum becomes very complex and often impossible to solve using conventional line assignment techniques.

Multiple-quantum (MQ) NMR has long been recognized as a valuable tool in the study of oriented systems [71, 72, 73, 74]. MQ spectra contain far fewer lines than the conventional one-quantum spectrum, a feature that greatly simplifies the assignment of lines in the fitting process. In a system of n coupled spin-1/2 nuclei, the spectra of order $n-1$ and n-2 often contain a sufficient number of lines to obtain the dipolar coupling constants and chemical shifts. Despite this attractive feature, MQ-NMR spectroscopy

has not been widely employed in such studies. One exception is the recent study by Field *et al.* where MQ-NMR was used to determine the proton geometry of the seven-spin system 1-bromonaphthalene [75]. In this case the one-quantum spectrum was too difficult to solve, even with the aid of MQ spectra. A major limitation of MQ techniques in such cases is the inability to obtain linewidths of the order that may be obtained for conventional one-quantum NMR spectra. As in many 2-D NMR experiments, significant line broadening results from signal truncation due to limitations in the number of evolution time increments achievable under practical conditions. Consequently, the accuracy with which the frequencies of transitions, and therefore the dipolar coupling constants, may be determined suffers greatly. The logical solution is to use the information obtained from the MQ spectra as a starting point in the solution of the one-quantum spectrum, where linewidths of the order of 1 Hz are easily achievable. Far more accurate values for the dipolar coupling constants may be then obtained. Surprisingly, few studies have been reported in which MQ spectral information has been utilized to solve one-quantum spectra. Yet, the study by Rendell *et al.* in which MQ information was used (and required) to solve the one-quantum spectrum of the six-spin system 1,3-dichloro-2-ethenylbenzene [76] clearly demonstrates that it is possible under practical conditions. It must be noted, however, that in the limit of increasing complexity of a spin system the one-quantum spectrum degenerates into a broad mass of unresolvable, overlapping lines, rendering analysis impossible. Even when the spectral lines are resolvable but very numerous, small inaccuracies in the dipolar coupling constants obtained from MQ spectra may significantly alter line order and intensity in the calculated one-quantum spectrum, providing little additional advantage in assignment of lines to the experimental spectrum.

In this chapter, we present a study of oriented biphenylene. The molecular structure of biphenylene is shown in Figure 2.3. The NMR spectrum of this eight-spin system, shown in Figure 2.4, is very complex, despite the high degree of molecular symmetry

Figure 2.3: Atomic Labeling and Axis System for Biphenylene.
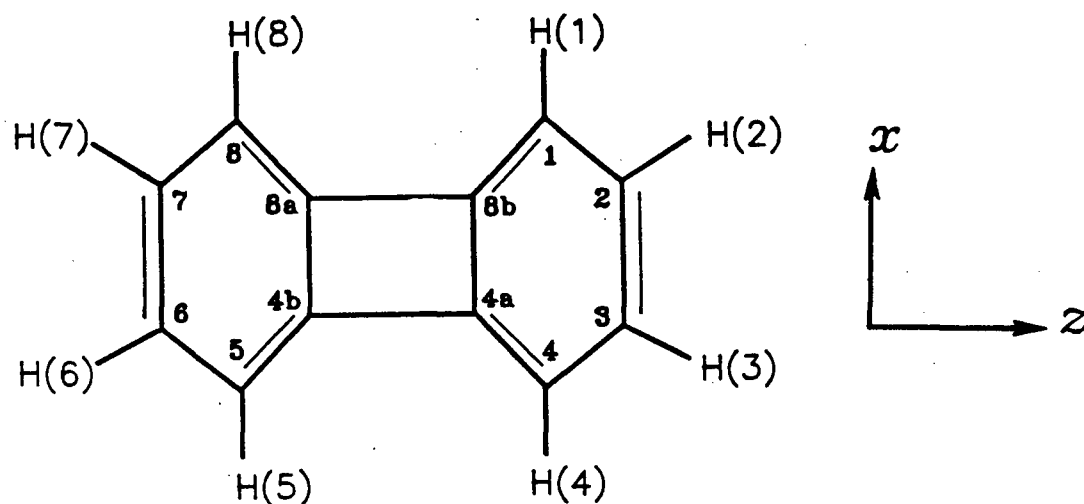
of this planar molecule. An approximate geometry determined by an early electron-diffraction experiment was available and provided a useful starting point in the solution of the spectrum [77]. Yet initial attempts to solve the spectrum without any additional information were unsuccessful. A solution of the one-quantum spectrum alone may be possible with sufficient patience. However, this seemed an ideal spin system of medium complexity to probe the usefulness and drawbacks of MQ techniques for such problems.

A simple pulse sequence commonly used to generate and detect MQ coherences is given by

$$(\frac{\pi}{2})_\phi - \tau - (\frac{\pi}{2})_\phi - t_1 - (\frac{\pi}{2}) - \tau - t_2(acquire). \qquad (2.41)$$

Various one-quantum coherences evolve during the preparation time τ. The second RF pulse converts them to coherences of all orders. These range from $-n$ to n for an n spin-1/2 system. The coherences evolve during the evolution time t_1. The third pulse partially converts the MQ coherences back into one-quantum coherences which then

Figure 2.4: Calculated and Observed NMR Spectra of Partially Oriented Biphenylene.

Frequency (Hz)
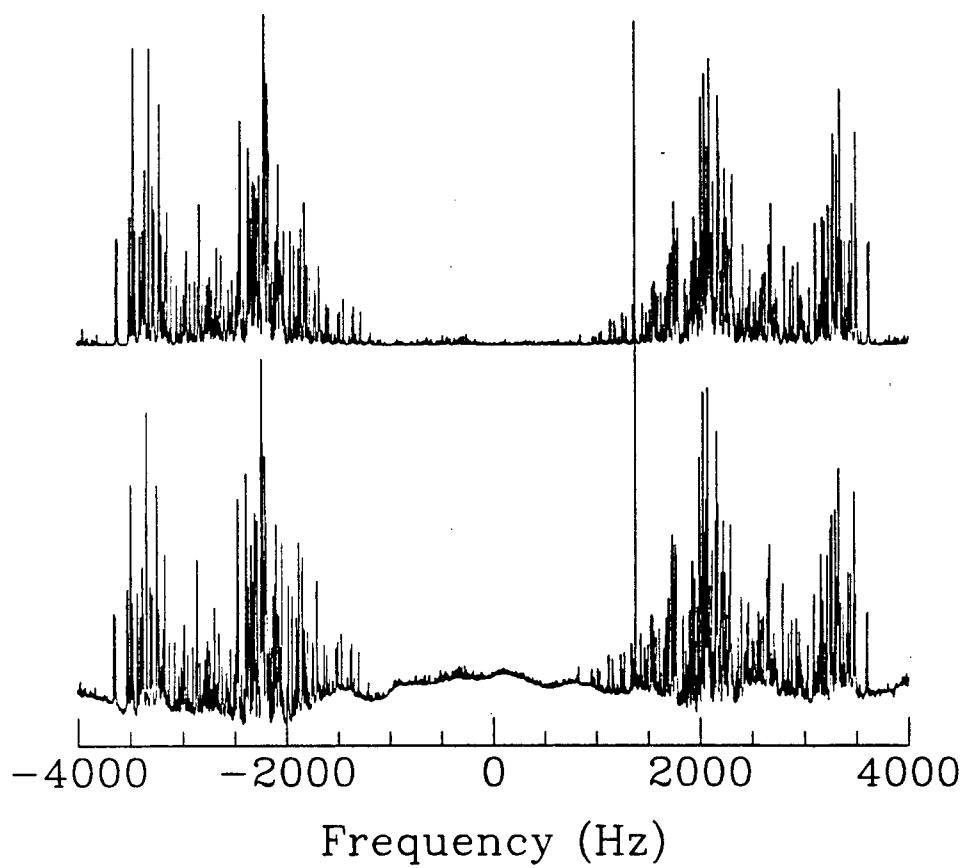
evolve into the I_x or I_y coherences detected directly during the detection time t_2. A 2-D fourier transform of the resulting interferogram followed by a projection onto the f_1 axis yields a MQ spectrum with lines corresponding in principle to transitions of all orders permitted by symmetry selection rules. In practice, intensities of coherences of all orders are modulated in a very complex way by τ and it is often necessary to coadd spectra obtained with several preparation times to ensure that all predicted lines are observed with sufficient intensity.

Selective detection of $\pm p$-order coherences is accomplished by the repeated application of pulse sequence (2.41), where the phase ϕ of the first and second pulses is incremented $2p$ times by an amount $\Delta\phi = \pi/p$ [52]. Alternate addition and subtraction of the resulting signals cancels all but those contributions resulting from evolution of $\pm p$-order coherences during t_1. While in principle this phase-cycle filter also permits the detection of $\pm kp$-order coherences where $k=1,2,3,...$, in practice this is rarely a problem since for an n spin-1/2 system, n is the highest attainable order, and it is the $n-1$, $n-2$ and $n-3$ spectra that are of most interest. A longer phase-cycle of $4p$ steps in increments of $\pi/(2p)$ steps with the receiver phase incremented in steps of $\pi/2$ permits quadrature detection of p-order coherences [78]. Refocusing π pulses may be inserted mid-way in the evolution time t_1 to reverse the effects of magnetic field inhomogeneities, to which a p-quantum coherence is p times as sensitive compared to a one-quantum coherence. However, this will also refocus the effects of chemical shifts—information that may be very important when ultimately attempting to solve the one-quantum spectrum. In addition, unless a technique such as Time Proportional Phase Incrementation (TPPI) [71] is implemented, the frequency offset typically used to separate the detected orders in the MQ spectrum will also be destroyed. Consequently, refocusing pulses were not used in this study.

2.2 Experimental

The sample was prepared as a 5 mol% solution of biphenylene in a liquid crystal mixture of 55 wt% Merck ZLI 1132 and EBBA. This liquid crystal mixture has been the subject of an ongoing investigation in our lab as it has been shown to possess a vanishing average electric-field-gradient at 301.4K [31], although this feature is of no importance for the material in this chapter. The 5mm o.d. sample tube was fitted with a capillary tube containing acetone-d_6, used to provide the lock signal. Experiments were carried out on a Bruker AMX-500 spectrometer at 500 MHz at a temperature of 301.4K.

The six- and seven-quantum spectra were acquired using pulse sequence (2.41) with preparation times of 6, 7and 8 ms and a recycle delay of 3 s. There were 256 data points acquired in t_2 and 1024 increments in t_1. Selective-detection phase cycles employing 12 steps of 30° increments for the six-quantum spectra and 14 steps of 25.75° increments for the seven-quantum spectra were used. The f_1 dimension was zero-filled to 4096 prior to the 2-D magnitude fourier transform. The MQ spectrum was obtained by using a summed projection of the 2-D spectrum onto the f_1 axis. The summed projection has been demonstrated to give a significantly better signal-to-noise ratio than the application of the "skyline" projection [75] or use of a $t_2=0$ cross section of the time-domain interferogram [79]. Peak positions were calculated using the standard Bruker UXNMR peak-picking routine.

2.3 Results and Discussion

The one-quantum spectrum of oriented biphenylene is shown in Figure 2.4. A linewidth of just under 3 Hz at half-maximum was achieved. The lines are clustered in two dense regions spaced roughly 5000 Hz apart, each subdivided into two slightly overlapping

regions about 1000 Hz apart. The presence of this overall feature proved useful in obtaining first order estimates of the two independent, non-vanishing order parameters S_{zz} and S_{xx}, both defined in the coordinate system of Figure 2.3. An estimate of the proton geometry of biphenylene was used based on a gas phase electron-diffraction study [77]. While the calculated carbon geometry was accurately determined in this study, the C-H bond lengths and C-C-H bond angles were far less precisely measured, and are the key structural parameters sought in the present study. Trial guesses of the molecular order parameters were used to calculate sets of dipolar coupling constants and therefore spectral simulations. A chemical shift difference between the two chemically distinct proton sites of 50 Hz was used initially, based on an isotropic chemical shift difference of 0.10 ppm reported for biphenylene [80]. Similarly, the indirect spin-spin coupling constants were assigned their isotropic values and are not expected to deviate significantly. The overall structure of the spectrum was fairly insensitive to variation of the chemical shift difference by up to ±300 Hz, and was therefore mainly determined by the (larger) dipolar coupling constants. The values of S_{zz} and S_{xx} were varied until the simulated spectra roughly mirrored the experimental spectra. Of particular use in this "fit" were the two doublets (not clearly resolvable as such in Figure 2.4) at the outer edges of the spectrum, each with about a 10 Hz splitting and clearly separated from any other lines of significant intensity. In fact, these were the only lines that could be unambiguously assigned from the initial calculated spectrum which was otherwise able only to reproduce the gross spectral structure. All efforts to assign other individual lines failed to yield a satisfactory convergence. Clearly, both the line positions and intensities are extremely sensitive to slight deviations in molecular geometry, the chemical shift difference and the molecular order parameters.

Typical six- and seven-quantum spectra are shown in Figures 2.5 and 2.6, respectively. The seven-quantum spectrum is particularly simple, having only four predicted lines

Figure 2.5: Six-Quantum ^{1}H NMR Spectrum of Biphenylene
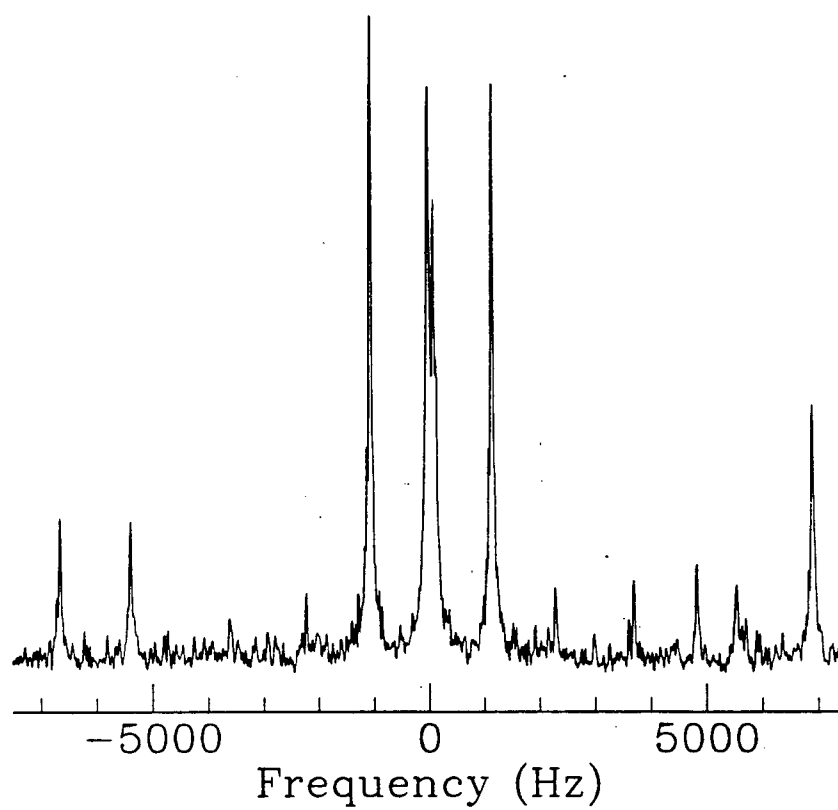
Acquired with a preparation time of τ=6 ms.

Figure 2.6: Seven-Quantum ^{1}H NMR Spectrum of Biphenylene
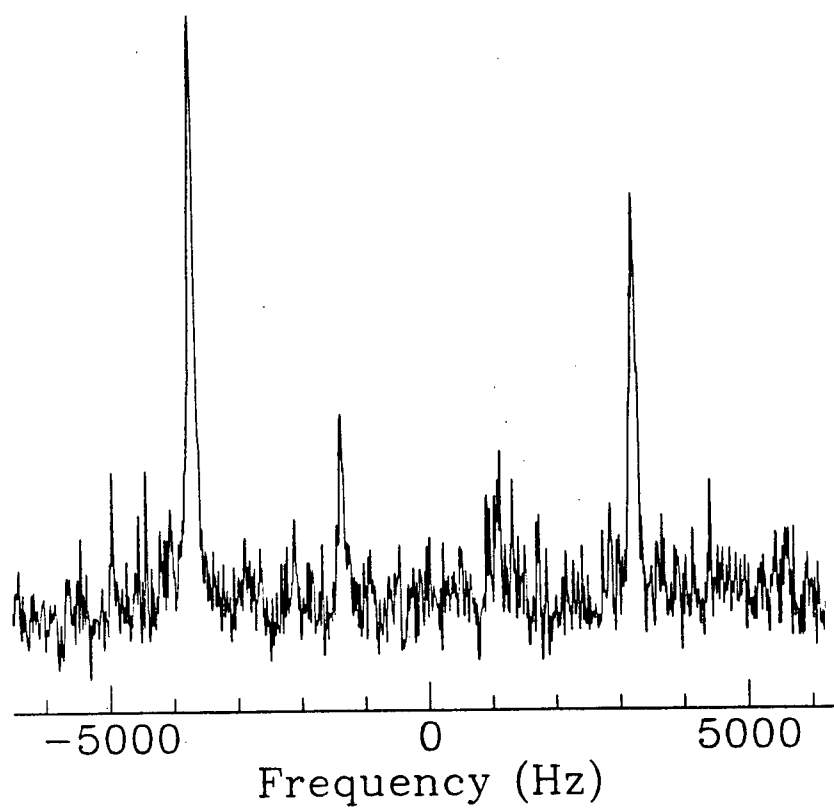
Acquired with a preparation time of τ=7 ms.

due to the D_{2h} spin symmetry, one doublet for each magnetically inequivalent proton. While the outer doublet has a very strong intensity, the inner doublet is less clearly visible with one peak dipping into the noise. Other seven-quantum spectra acquired with other preparation times (6 and 8 ms) unambiguously fix the position of this elusive peak. This situation is fairly typical of MQ spectra where it is often impossible to clearly observe all predicted peaks with a single preparation time. While there are only 11 lines clearly visible in the six-quantum spectrum of Figure 2.5, a total of 15 different lines were observed in all of the acquired six-quantum spectra. Since the MQ spectra were acquired at different times under potentially slightly different experimental conditions (e.g. temperature), the spectra were not actually coadded. The linewidths were typically 50–60 Hz, determined mainly by magnetic field inhomogeneities and signal truncation in the t_1 domain.

The frequencies of the six- and seven-quantum spectral lines are presented in Table 2.1, each centered about the product of the MQ order and the average chemical shift. These values are the averaged frequencies of spectra obtained with the three different preparation times. The variations of the frequencies of the lines that were observable in different spectra were small, roughly 2–3 Hz for the more intense lines and 5–10 Hz for the weaker lines. The fact that these variations are considerably smaller than the average linewidth indicates that the Bruker UXNMR peak-picking routine was able to adequately determine peak positions in these experiments. The six- and seven-quantum averaged spectral frequencies were fit simultaneously using a version of the program LEQUOR [81] modified for use with MQ spectra. Initial MQ spectra were simulated using the dipolar coupling constant parameters estimated from the earlier "fit" of the one-quantum spectrum. These calculated spectra were remarkably similar to the experimental spectra with line positions deviating by only about 100 Hz or less from their measured values. Since the average line spacings are of the order of kHz here, this presents few problems with

Table 2.1: Experimental and Calculated Frequencies (Hz) of Observed MQ Transitions.

MQ Order	Experimental	Calculated (1)[a,b]	Calculated (2)[c]
6-Q	−6854.1	−6852.2	−6853.4
	−5504.8	−5499.6	−5494.7
	−4792.3	−4793.0	−4790.9
	−3660.1	−3663.5	−3658.7
	−2252.9	−2251.3	−2253.9
	−1101.2	−1101.5	−1097.3
	−78.7	−84.8	−86.1
	79.7	82.6	85.5
	1101.2	1099.6	1097.6
	2245.2	2249.2	2253.9
	3646.7	3646.0	3642.7
	4823.8	4820.1	4820.8
	5421.9	5423.9	5418.9
	5617.5	5618.5	5618.2
	6681.4	6682.9	6681.9
7-Q	−3500.7	−3502.5	−3501.8
	−1165.4	−1168.5	−1161.8
	1250.2	1249.7	1247.9
	3414.0	3416.3	3415.7

[a]Fit directly from MQ line frequencies by varying the proton coordinates (x_i, z_i) and S_{xx}/S_{zz} with S_{zz} fixed.
[b]RMS=2.8 Hz.
[c]Calculated from the fitting parameters obtained from the fit of the one-quantum spectrum.

spectral line assignment.

In the initial attempt to fit the six- and seven-quantum spectra, the 10 independent dipolar coupling constants and two chemical shifts were varied. The indirect spin-spin coupling constants were fixed at their isotropic values. The spectra were easily fit, and the coupling constants and chemical shift values obtained were used to simulate a one-quantum spectrum. Upon close comparison, however, lines could not be unambiguously assigned, and it did not appear to be a significant improvement over the initial calculated one-quantum spectrum. Again, all attempts to assign lines from this starting point failed. At this point, five-quantum spectra were acquired and incorporated into the analysis in the hope that assignment of additional lines would improve the accuracy in the fitting process. Since the five-quantum spectrum is considerably more densely clustered with lines than the six- and seven-quantum spectra, most lines could not be unambiguously assigned. A total of 9 five-quantum lines, located mainly at the fringes of the spectrum, sufficiently well separated from any others, were included in the spectral fit. The fitting quickly converged, but again the values of the dipolar coupling constants and chemical shifts obtained were unable to assist in the assignment of lines in the one-quantum spectrum.

The difficulty in obtaining reliable estimates of the coupling constants and chemical shifts clearly stems from the low ratio of the number of assigned lines (19 from the six- and seven-quantum spectra alone, and 28 from the five-quantum spectrum as well) to the number of fitting parameters. To reduce the number of fitting parameters, 5 geometric and ordering parameters (the x and z coordinates of the two distinct proton sites and the ratio of S_{xx}/S_{zz}, with S_{zz} scaled to a realistic value) replaced the 10 independent dipolar coupling constants in the fit. The six- and seven-quantum spectra were again fit with an RMS=2.8 Hz. The positions of the fitted lines are shown in Table 2.1. The dipolar coupling constants calculated from these parameters, listed in Table 2.2, were then used

to simulate the one-quantum spectrum, and this time with considerable success. The lines in the simulated spectrum accurately matched those in the experimental spectrum, both in relative intensity and order. At this point the solution of the one-quantum spectrum was trivial. A total of 144 lines were assigned and fit with an RMS=0.13 Hz varying the *J*-couplings as well as the dipolar coupling constants and chemical shifts. While it might have been possible to assign more lines, care was taken not to assign lines that were overlapping, particularly in the denser portions of the spectrum. The fitted spectrum is shown in Figure 2.4, and the fitting parameters are listed in Table 2.2 and compared with the isotropic values. Although the fitted J-coupling constants do not significantly deviate from the isotropic values, the fitted chemical shift difference is over three times the measured isotropic value, clearly the result of a large chemical shift anisotropy. Frequencies of MQ spectral lines simulated with parameters obtained from the one-quantum fit are also presented in Table 2.1.

The dipolar coupling constants were used by the program SHAPE [82] to determine directly the molecular geometry and molecular order parameters. The C-H bond length and C-C-H bond angles (determined using the r_α geometry of the biphenylene carbon skeleton) were calculated and are listed in Table 2.3 along with the molecular order parameters. The scale was fixed by setting the C-H bond lengths of the two distinct protons to be equal. A second fit was performed using a version of the program SHAPE modified to correct for the non-negligible effects of molecular vibrations on the dipolar coupling constants [83, 84, 85]. A set of force constants calculated in the electron diffraction experiment by Yokozeki *et al.* [77] were used to calculate the mean-square amplitudes of vibration required for the correction [86, 87]. Vibrationally corrected fitted parameters are also shown in Table 2.3. One notable effect of the vibrational corrections is to decrease slightly the value of the C-H bond length by about 0.02 Å. In either case, the C-H bonds come within 2° of bisecting both C-C-C bond angles. The complete r_α

Table 2.2: Fitting Parameters (Hz) from the Multiple-Quantum and One-Quantum Spectral Fits.

Parameter	MQ	1-Q	Isotropic[a]
$D_{12}=D_{34}=D_{56}=D_{78}$	−1617.2	−1627.418(12)	—
$D_{18}=D_{45}$	−641.5	−645.505(40)	—
$D_{23}=D_{67}$	229.1	235.308(51)	—
$D_{17}=D_{28}=D_{35}=D_{46}$	−151.1	−153.094(14)	—
$D_{13}=D_{24}=D_{57}=D_{68}$	−81.5	−80.698(16)	—
$D_{16}=D_{25}=D_{38}=D_{47}$	−72.2	−73.101(16)	—
$D_{27}=D_{36}$	−68.5	−69.478(47)	—
$D_{26}=D_{37}$	−54.9	−55.523(47)	—
$D_{15}=D_{48}$	−44.0	−44.997(47)	—
$D_{14}=D_{58}$	25.0	24.986(47)	—
			—
$|\Delta\delta|$	163.824	168.916(54)	50.0
			—
$J_{12}=J_{34}=J_{56}=J_{78}$	—	6.77(7)	6.8
$J_{18}=J_{45}$	—	−0.08(14)	0.0
$J_{23}=J_{67}$	—	8.28(09)	8.24
$J_{17}=J_{28}=J_{35}=J_{46}$	—	0.08(06)	0.0
$J_{13}=J_{24}=J_{57}=J_{68}$	—	0.75(04)	0.74
$J_{16}=J_{25}=J_{38}=J_{47}$	—	0.15(03)	0.0
$J_{27}=J_{36}$	—	0.47(12)	0.0
$J_{26}=J_{37}$	—	−0.17(09)	0.0
$J_{15}=J_{48}$	—	−0.10(09)	0.0
$J_{14}=J_{58}$	—	1.07(09)	1.08

[a]From ref. [80] .

Table 2.3: Geometric Parameters from Fit of Dipolar Coupling Constants.

Parameter	Fitted Value(1)[a]	Fitted Value(2)[b]
C-H	1.1315(25) Å	1.11(1) Å
<C(8b)-C(1)-H(1)	124.54(8)°	123.9(4)°
<C(1)-C(2)-H(2)	119.41(3)°	117.5(2)°
S_{zz}	0.3236(8)	0.313(3)
S_{xx}	−0.02888(5)	−0.0224(2)

[a]From fit without vibrational corrections.
[b]From fit with vibrational corrections. The carbon skeleton was fixed to the r_α geometry given in ref. [77], and the C-H bond lengths were set equal.

structure is given in Table 2.4.

2.4 Conclusions

In this study, MQ spectra were used to assist in the solution of the one-quantum spectrum of partially oriented biphenylene. This eight-spin system produces a complex one-quantum spectrum, which despite the high degree of molecular symmetry, is very difficult to analyze using conventional line-assignment techniques. By contrast, the six- and seven-quantum spectra are very simple, and assignment of calculated to experimental line frequencies was trivial when an estimated proton geometry for this rigid molecule was used. Since the MQ spectral line frequencies were far less accurately measured than the one-quantum line frequencies, and, since there were many fewer lines in the MQ spectra than in the one-quantum spectrum, the initial fits of the MQ spectra could not yield sufficiently accurate estimates of the coupling constants to aid in the solution of the one-quantum spectrum. It was found necessary to reduce the number of fitting parameters by replacing the dipolar coupling constants with a lesser number of geometrical (proton positions) and molecular order parameters, thereby fully utilizing the molecular

Table 2.4: The r_α Geometric Parameters for Biphenylene.

Parameter	Value
C(1)-C(8b)[a]	1.365(12) Å
C(1)-C(2)[a]	1.415(12) Å
C(2)-C(3)[a]	1.359(15) Å
C(4a)-C(8b)[a]	1.427(18) Å
C(4a)-C(4b)[a]	1.518(6) Å
C-H[b]	1.108(10) Å
<C(4a)-C(8b)-C(1)[a]	122.5(6)°
<C(8b)-C(1)-C(2)[a]	115.0(2)°
<C(1)-C(2)-C(3)[a]	122.5(2)°
<C(8b)-C(1)-H(1)[b]	123.9(4)°
<C(1)-C(2)-H(2)[b]	117.5(2)°

[a] From ref. [77].
[b] From the present study.

symmetry of biphenylene, to obtain the required accuracy from the MQ fit. Dipolar coupling constants obtained from the fit of the one-quantum spectrum were used to obtain a vibrationally corrected proton geometry. This is one of the few studies in which analysis of MQ spectra was shown to simplify considerably the analysis of a complex one-quantum spectrum.

Chapter 3

Multiple-Quantum NMR of Oriented Solutes (II): Conformational and Orientational Behaviour of Butane

The material presented in this chapter has been published in ref. [88].

3.1 Introduction

With only one conformational degree of freedom, butane is the simplest flexible alkane. As such, it has attracted much interest and has been the subject of many studies, both experimental and theoretical/computational, concerned with the influence of condensed phases on the equilibrium conformational behaviour of non-rigid molecules. Early on, Flory had suggested that the average potential of hydrocarbon molecules should closely correspond to the unperturbed form with the configurational space populated according to the Boltzman distribution over intramolecular energy with intermolecular effects being ignored [89]. Later, this view was challenged by Chandler *et al.* whose rigorous statistical mechanical theory of hydrocarbon systems predicted an increase in the *gauche* conformer population as a result of short-range packing in the liquid [90, 91]. There is extensive experimental evidence to support the latter view. Gas phase studies typically report the *trans-gauche* energy, E_{tg}, to be 3.3–3.7 kJ/mol. [92, 93, 94, 95, 96], though a recent FTIR study has suggested that it may be as low as 2.9 kJ/mol [97]. Experimental studies of butane, both as liquid and dissolved in other isotropic liquid solvents, consistently report lower values for E_{tg}, generally in the range 2.1–2.5 kJ/mol [98, 99, 100].

The effect of a condensed phase environment on the conformational equilibrium of

butane has also been studied extensively using Molecular Dynamics (MD) and Monte Carlo (MC) computer simulations. These studies have generated less consistent and often confusing results over the last two decades. The earliest MD simulations of liquid butane [101, 102] and of butane in liquid carbon tetrachloride [103] appeared to indicate that there was a significant shift toward higher *gauche* populations. Another MD study of liquid butane found a negligible effect [104], as did the MC simulations of Jorgensen [105, 106, 107] who cited insufficient run time and inadequate convergence as explanations for the apparent MD shortcomings. Improved MD calculations suggested a significant solvent effect on conformer populations [108, 109, 110]. In this case it was argued that the MC calculations were in error since they had employed a strong attractive methyl-methyl potential which may neutralize the packing effects [110]. More recent MD and MC calculations have again concluded that there is no significant shift [111, 112]. Another recent study suggests that the conformational behaviour of butane is highly sensitive to minor details in the molecular structure and the intermolecular forces used in the calculations [113].

An understanding of the behaviour of flexible hydrocarbons in condensed phases is particularly important in the field of liquid crystals. Most molecules that form liquid crystal phases have hydrocarbon chains that are attached to rigid cores. These alkyl tails appear to be an important component of the orienting mechanism for the mesogens. Knowledge about the conformational and orientational behaviour of alkanes in nematic liquid crystals then should contribute to an understanding of the ordering of liquid crystals. The behaviour of longer alkanes in anisotropic fluids has been the subject of several recent NMR studies. While early NMR studies had relied on an analysis of quadrupolar coupling constants of deuterated alkanes [46, 114, 115], recent advances in two-dimensional NMR techniques combined with random deuteration of the chains have

made it possible to measure the dipolar couplings between proton pairs, greatly increasing the amount of information available about these systems [43, 44, 45, 116, 117]. A detailed analysis of the dipolar couplings for alkanes ranging from hexane to decane were used to study the effects of the nematic environment on their conformational equilibria [44, 45, 49]. These studies indicate that there is a shift towards higher populations of conformers with more *gauche* bonds, an effect corresponding to a lowering in E_{tg} relative to the gas phase values, similar to that observed for butane in isotropic liquids. Moreover, this effect appeared to result from the isotropic "solvent pressure" of the condensed phase: the anisotropic component of the solute-solvent interaction was found to influence only marginally the conformer probabilities by favouring elongated conformers slightly [45]. Similar results were found in a MD study of hexane incorporated as a solute in a model liquid-crystal solvent [66].

An essential component in the analyses for the NMR studies discussed above involves the use of mean-field models to describe the orientation of molecules in a nematic environment. These models are used to calculate the molecular order parameters for each conformer, which are, in turn, used to calculate the experimental dipolar coupling constants. Thus, the ability of each model to fit the experimental couplings may be used to provide a critical test of each model. One orientational model, developed by Burnell and co-workers, describes the interaction between solute and liquid crystal as arising from the size and shape anisotropy of the solute [32, 33, 34, 35, 36, 64]. The study by Rosen *et al.* [45] concluded that early versions of this model [33, 34] were inferior to the chord model, developed by Photinos *et al.* [47, 48, 49], in which C-C bond orientations relative to the director and correlations with orientations of neighbouring C-C bonds were the key factors in the molecular ordering. Another approximation used in the analyses of these studies was the three-state rotational isomeric state (RIS) model [89] to describe the accessible conformational states of each C-C torsion bond of the molecule. Though

its application permits a convenient analysis of the data, it was judged to be a severe approximation. Later, it was shown that the inclusion of torsion-angle fluctuations about the RIS *trans* and *gauche* states can significantly improve the quality of the fits [118].

In this chapter, we present a Multiple-Quantum (MQ) ^{1}H NMR study of butane in a nematic liquid crystal. We view this study as an extension of previous experimental and computational work on the effect of condensed phases on the conformational behaviour of butane, and as a continuation of the study of alkyl chain behaviour in a specifically anisotropic fluid. The simplicity of this alkane offers some advantages. First, the NMR spectrum of butane is sufficiently simple that, with the help of straightforward MQ experiments, its analysis is possible without the need to resort to either specific or random deuteration. In this way, one may measure the dipolar coupling constants much more precisely than was done for the longer alkanes. As well, certain assumptions used in studies of longer alkanes, such as the equivalence of the internal rotational potential for all C-C bonds along the chain, are unnecessary. One goal of this study is the determination of E_{tg} for butane in a condensed phase, and its dependence on both isotropic and anisotropic contributions from the solute-solvent interactions. However, since the use of mean-field models to describe the molecular orientation in a nematic liquid crystal is a key part of the analysis, an equally important aspect of this work is the investigation of the model-dependence of the results. The influence of both the mean-field model and the details of the geometry, including the *trans-gauche* dihedral angle and the RIS approximation, are discussed.

3.2 Theoretical Background

3.2.1 Dipolar Coupling Constants

NMR has proven to be an excellent technique to study the conformational behaviour and orientational ordering of molecules in anisotropic fluids. Most studies to date that have investigated the behaviour of hydrocarbons have used ^{2}H NMR spectroscopy to measure quadrupolar splittings, $\Delta\nu_Q$, of C–^{2}H bonds of deuterated molecules. The ^{2}H-NMR spectra consist of a set of doublets, each with a splitting given by

$$\Delta\nu_Q = \frac{3e^2qQ}{4h}S_{C-D} \tag{3.42}$$

where the order parameter S_{C-D} is given by

$$S_{C-D} = \left\langle \frac{3}{2}\cos^2\theta_{C-D} - \frac{1}{2} \right\rangle \tag{3.43}$$

and where θ_{C-D} is the angle that the C–^{2}H bond makes with the static magnetic field, along which the nematic phase director is aligned. Thus, the ^{2}H-NMR spectra readily provide information through S_{C-D} about orientational ordering of individual methylene segments along alkyl chains. On the other hand, the $\Delta\nu_Q$'s provide no direct information about inter-methylene correlations. Also, the number of distinct $\Delta\nu_Q$'s is limited to the number of independent carbon units along the chain. Thus, the information contained in quadrupolar couplings tends to be inadequate for studies in which detailed information about molecular orientational ordering and conformational behaviour is sought.

Dipolar coupling constants, by contrast, provide much more detailed information about flexible molecules. The dipolar coupling constant between protons i and j on a partially oriented molecule is given by

$$D_{ij} = -\frac{\gamma^2\hbar\mu_0}{8\pi^2}\left\langle \frac{\frac{3}{2}\cos^2\theta_{ij}^Z - \frac{1}{2}}{r_{ij}^3} \right\rangle \tag{3.44}$$

where r_{ij} is the internuclear distance and θ_{ij}^Z is the angle between the internuclear vector and the static magnetic field. The factor of r_{ij}^{-3} is significant because it provides information about the average distance between methylene groups on flexible alkyl chains. This feature, as well as information about the average orientation of internuclear vectors resulting from the dependence on θ_{ij}^Z, causes the D_{ij} to be highly sensitive to the molecular conformation and orientation. As well, there are many more independent dipolar coupling constants than quadrupolar coupling constants, a factor which greatly increases the information about molecular properties that may be extracted from the experimental data. In the case of butane, there are seven independent D_{ij}'s and only two $\Delta\nu_Q$'s.

Although there is a clear advantage in determining dipolar coupling constants, these are often difficult to obtain in all but the simplest molecules. The complexity of the ^{1}H one-quantum NMR spectrum of partially oriented molecules increases rapidly with the size and complexity of the corresponding molecular spin system. In large molecules, including the nematogens themselves which have ~ 20 ^{1}H spins, the large number of spectral lines results in severe overlap in which individual lines cannot be resolved, rendering any spectral analysis impossible. In molecules of intermediate complexity such as butane, this is not a major problem; however, the spectrum can still be sufficiently complex to hinder its analysis. In such cases, it is useful to analyze first high-order Multiple-Quantum (MQ) spectra. Such spectra have far fewer associated transitions, a feature that makes it much easier to assign lines of trial simulated spectra to those of the experimental spectra. The dipolar coupling constants obtained as fitted parameters may then be used as a starting point in the analysis of the one-quantum spectrum. The dipolar coupling constants obtained in the second stage of analysis are highly accurate. We have shown the usefulness of Multiple-Quantum spectroscopy as a tool in the analysis of one-quantum spectra for molecules of intermediate complexity in previous studies on the structural determination of the eight-spin molecule biphenylene [67], presented in

Chapter 2, and the six-spin molecule 1,3-dichloro-2-ethenylbenzene [76].

A significant alternative to this method that is suitable and necessary for molecules of greater complexity is the approach taken by Pines and coworkers [43, 44, 45, 116, 117]. In this case, random deuteration of the molecules, combined with MQ-filtered Correlated Spectroscopy (COSY) NMR experiments and ^{2}H double-quantum decoupling, were used to obtain spectra that are superpositions of subspectra comprised of a single splitting. These subspectra arise from isotopic species that have a single pair of protons and therefore yield directly the D_{ij} associated with each proton pair. This technique was used successfully to measure dipolar coupling constants for a series of oriented alkanes in a study [44, 45] that is highly relevant to the present work and on which we shall comment further.

3.2.2 Flexibility

A common approach to analyzing dipolar coupling constants of partially oriented flexible molecules is to assume that the molecule exists in several discrete conformations, each of which has its own distinct Saupe order matrix. This assumption is justified as long as the correlation time associated with the reorientation of the molecule, τ_R, and the rate of exchange, k, between the different conformations satisfy $k\tau_R \ll 1$ [41, 42]. An important model used for approximating the conformations of hydrocarbon chains is Flory's Rotational Isomeric State (RIS) model [89] in which each C–C torsion bond is assumed to exist in three states, *trans* and $\pm gauche$, with dihedral angles of 0° and $\pm\phi_g$, respectively, corresponding to the angles at the minima of the rotational potential profile. These two approximations form the basis for the analysis of the D_{ij}'s in the present study, as described below.

One can show that an experimentally measured dipolar coupling constant between protons i and j for a flexible molecule satisfying the condition described above is given

by

$$D_{ij} = \frac{2}{3} \sum_n p^n \sum_{\alpha\beta} S_{\alpha\beta}^n D_{ij,\alpha\beta}^n \qquad (3.45)$$

where p^n is the probability of the nth conformer, and where $S_{\alpha\beta}^n$, the Saupe order matrix for the nth conformer, is defined by

$$S_{\alpha\beta}^n = \left\langle \frac{3}{2} cos\theta_{\alpha,Z}^n cos\theta_{\beta,Z}^n - \frac{1}{2}\delta_{\alpha\beta} \right\rangle \qquad (3.46)$$

where $\theta_{\alpha,Z}^n$ is the angle between the α-molecular axis of the nth conformer and the nematic director, which, for many liquid crystals, is aligned with the static magnetic field along the Z-axis. $D_{ij,\alpha\beta}^n$ is a tensor defined by

$$D_{ij,\alpha\beta}^n = -\frac{\mu_0\gamma^2\hbar}{8\pi^2 r_{ij,n}^3} \left(\frac{3}{2} cos\theta_\alpha^{ij,n} cos\theta_\beta^{ij,n} - \frac{1}{2}\delta_{\alpha\beta} \right) \qquad (3.47)$$

where $\theta_\alpha^{ij,n}$ is the angle between the internuclear vector, $\vec{r}_{ij,n}$, and the nth α-molecular axis.

3.2.3 The Mean-Field Potential and E_{tg}

A useful approach to the analysis of the dipolar coupling constants is to model the solute energy with a mean-field potential, $U_n(\omega)$, which is a function of both the conformation and the orientation of the solute in the uniaxial nematic solvent. The potential can be divided into

$$U_n(\omega) = U_{int,n} + U_{ext,n}(\omega) \qquad (3.48)$$

where $U_{int,n}$ is the internal energy associated with the conformational state of an isolated molecule, and $U_{ext,n}(\omega)$ is the orientationally dependent energy of interaction between the solute and the external mean field. The latter term can written in terms of a spherical harmonic expansion which can be used to define the isotropic, $U_{ext,n}^{iso}$, and anisotropic,

$U_{ext,n}^{aniso}(\omega)$, components of the external field:

$$
\begin{aligned}
U_{ext,n}(\omega) &= c_{0,0}^n Y_{0,0} + \sum_{l=2}^{even} \sum_{m=-l}^{l} c_{l,m}^n Y_{l,m}(\theta, \phi) \\
&\equiv U_{ext,n}^{iso} + U_{ext,n}^{aniso}(\omega)
\end{aligned}
\tag{3.49}
$$

Note that the odd terms in the expansion for $U_{ext,n}^{aniso}(\omega)$ vanish as a result of the apolarity of the nematic phase. Also, since $U_{int,n}$ is purely isotropic, we shall omit the "*ext*" subscript on the anisotropic component of the external potential energy, $U_n^{aniso}(\omega)$, since it is only the external component of the solute energy which has an associated anisotropy. The isotropic component of the full solute potential energy, therefore, is the sum of internal and external contributions:

$$
U_n^{iso} = U_{int,n}^{iso} + U_{ext,n}^{iso}
\tag{3.50}
$$

We define the effective *trans-gauche* energy difference, E_{tg}, as the difference in the total isotropic potential energy for the *trans* and *gauche* states of the butane molecule:

$$
\begin{aligned}
E_{tg} &\equiv U_{gauche}^{iso} - U_{trans}^{iso} \\
&= E_{tg}^{int} + E_{tg}^{ext}
\end{aligned}
\tag{3.51}
$$

where E_{tg}^{int} is the internal energy difference between the *trans* and *gauche* states, and where

$$
E_{tg}^{ext} \equiv U_{ext,gauche}^{iso} - U_{ext,trans}^{iso}
\tag{3.52}
$$

is the external perturbation to the internal energy difference due to the condensed phase environment.

The anisotropic component of the mean field, $U_n^{aniso}(\omega)$, gives rise to the orientational ordering of the solute in the nematic environment. The elements for the Saupe order tensor for each conformer may be calculated by

$$
S_{\alpha\beta}^n = \frac{\int \left(\frac{3}{2}\cos\theta_{\alpha,Z}^n \cos\theta_{\beta,Z}^n - \frac{1}{2}\delta_{\alpha\beta}\right) \exp(-U_n^{aniso}(\omega)/kT)d\omega}{\int \exp(-U_n^{aniso}(\omega)/kT)d\omega}
\tag{3.53}
$$

One can show that the conformer probabilities can be written as

$$p^n = \frac{G^n \exp(-U_n^{iso}/kT) \int \exp(-U_n^{aniso}(\omega)/kT)d\omega}{\sum_n G^n \exp(-U_n^{iso}/kT) \int \exp(-U_n^{aniso}(\omega)/kT)d\omega} \tag{3.54}$$

where $G^n = \sqrt{I_{xx}^n I_{yy}^n I_{zz}^n}$ is a rotational kinetic energy factor, dependent on the principal values of the moment of inertia tensor for each conformer, $I_{\alpha\alpha}^n$, that arises from integrating out the molecular angular momenta from the full singlet probability distribution for flexible molecules. Eq. (3.54) clearly shows the dependence of the conformer probabilities on the anisotropic mean-field potential.

3.2.4 Modeling of $U_n^{aniso}(\omega)$

In order to extract conformational and orientational information from the experimental dipolar coupling constants using the relations described above, it is necessary to employ a suitable model for the anisotropic potential, $U_n^{aniso}(\omega)$. This is required since, in the limit of fast internal exchange between conformers, the conformer probabilities and molecular order parameters appear as products in the expression for D_{ij} in Eq. (3.45), and cannot be determined separately in a fit. Using a model for $U_n^{aniso}(\omega)$, however, the dipolar coupling constants may be calculated by optimizing the model parameters and E_{tg}, which generally are separately determinable, in the fit of the experimental D_{ij}. The p^n and $S_{\alpha\beta}^n$ are calculated using Eqs. (3.53) and (3.54). In the present study, we restrict the analysis to models that are characterized by a single parameter. We feel that this is a necessary restriction since we are limited to only seven independent ^{1}H dipolar coupling constants for butane. As well, by employing a wide variety of orientational models, we hope to bound E_{tg} to a limited range of values and thereby obtain a model-independent estimate of this quantity.

Below, we review briefly the important features of the models used in this study. More detailed descriptions may be found in the references cited.

3.2.4.1 Model A: Size and Shape Potentials

Burnell and coworkers have developed a series of related mean-field models for the orientational potential of solutes of arbitrary nature in a nematic liquid crystal [32, 33, 34, 35, 36, 64]. All of these models treat the solute as a collection of van der Waals spheres placed at the atomic sites in the molecule in order to approximate the molecular structure. It is the anisotropy in the shape of the solute interacting with the uniaxial nematic field that gives rise to the orientation dependence of the potential energy. There are six different varieties of this "Size and Shape" (SS) interaction that we describe below. First, however, there are two important considerations that we discuss.

(1) The general mean-field model developed by Burnell and coworkers consists of a contribution from the long-range interaction between the molecular electric-quadrupole moment (QM) with the average electric-field gradient (EFG) of the liquid crystal, in addition to the short-range SS interactions that we consider here. There is direct evidence of the QM-EFG interaction in the case of $^2H_2$, where it is the dominant orienting mechanism [13, 14, 119]. In addition, it was shown that one can construct liquid crystal mixtures in which the average EFG sampled by $^2H_2$ vanishes [31]. These zero-EFG mixtures were the nematic liquid crystals chosen for the experiments in which the SS potentials were developed, since the model predicts that the QM-EFG interaction vanishes in this case, leaving the short-range interaction as the sole mechanism responsible for solute orientation. While it is true that the average EFG experienced by an arbitrary solute will not be the same as that experienced by $^2H_2$ or any other solute, the high quality of the fits to experimental order parameters calculated under this assumption suggests that it is a reasonable approximation, though there has been some recent criticism of this claim [29]. Therefore, we use a zero-EFG nematic mixture in the present study, in keeping with these considerations. Previous studies of alkane behaviour in liquid crystals that

employed two of these models did not use a zero-EFG mixture nor comment at all on this matter [44, 45].

(2) It is very important to note that in all of the SS potentials developed by Burnell and coworkers, there a residual isotropic component; that is,

$$\langle U_{SS}^n \rangle = c_{0,0}^n Y_{0,0} = \frac{1}{4\pi} \int U_{SS}^n(\omega) d\omega \neq 0, \tag{3.55}$$

where $U_{SS}(\omega)$ represents any of the mean-field potentials discussed by Burnell and coworkers based on solute size and shape anisotropy that we discuss below. The residual isotropic component presents no difficulties in the case of rigid solutes where it has no effect at all on the predicted order parameters since these quantities depend strictly on the purely anisotropic component of the potential, $U_n^{aniso}(\omega)$. The situation for flexible molecules is quite different. Inspection of Eq. (3.54) clearly shows that in calculating the conformer probabilities, any isotropic component contained in a mean-field potential used to model the supposedly anisotropic $U_n^{aniso}(\omega)$ will be absorbed into the calculated U_n^{iso}, and will thus affect the resulting value of E_{tg}. Thus, an improperly calculated E_{tg}^{false} will be obtained, where

$$E_{tg}^{false} = E_{tg} + \langle U_{SS}^{trans} \rangle - \langle U_{SS}^{gauche} \rangle \tag{3.56}$$

This point was not considered in any of the previous studies of oriented flexible molecules that used a SS model, and calls into question the values for E_{tg} that were obtained. We return to this point later in the discussion section of this chapter. To calculate properly the conformer probabilities, it is necessary simply to subtract out the isotropic component of U_{SS}:

$$U_n^{aniso}(\omega) = U_{SS}^n(\omega) - \langle U_{SS}^n \rangle \tag{3.57}$$

Model A$_1$. This is the original SS model, in which the mean-field orientation-dependent

potential energy is given by [33]

$$U_{SS}^n(\omega) = \frac{1}{2}k(C_n(\omega))^2, \tag{3.58}$$

where $C_n(\omega)$ is the minimum circumference traced out by the projection of the solute onto a plane perpendicular to the nematic director, as shown in Figure 3.7.

Model A_2. This model is a slight variation of A_1 [33]:

$$U_{SS}^n(\omega) = \frac{1}{2}k(D_n(\omega))^2, \tag{3.59}$$

where $D_n(\omega)$ is the maximum circumference traced out by the projection of the solute onto the plane perpendicular to the nematic director, as shown in Figure 3.8

Model A_3. This two-parameter model was the first extension of A_1 [34] in which

$$U_{SS}^n(\omega) = \frac{1}{2}k(C_n(\omega))^2 - \frac{1}{2}\xi k C_n(\omega) Z_n(\omega) \tag{3.60}$$

where $Z_n(\omega)$ is the length of the projection of the solute along the nematic director (see Figure 3.8). In order to use this as a one-parameter model, we fix the second parameter to ξ=3.9, the value obtained from a fit to the order parameters for a collection of 46 solutes using this model in which both k and ξ were treated as free parameters [36]. This should be a valid assignment since the model parameters associated with a particular zero-EFG mixture are, in principle, solute-independent.

Model A_4. The model potential is given by [36]

$$U_{SS}^n(\omega) = -\frac{1}{2}k_s \int_{Z_{min,n}}^{Z_{max,n}} C_n(Z,\omega)dZ \tag{3.61}$$

where Z is the position along the nematic director bounded by the minimum, $Z_{min,n}$, and maximum, $Z_{max,n}$, points of the orientation-dependent projection of the solute along this axis. $C_n(Z,\omega)$ is the minimum circumference traced out by the solute at position Z along the director. Thus, $C_n(Z,\omega)dZ$ is the area of an infinitesimally thin ribbon that

Figure 3.7: Illustration of Orientation-Dependent Parameters Used in Size and Shape Models (I).
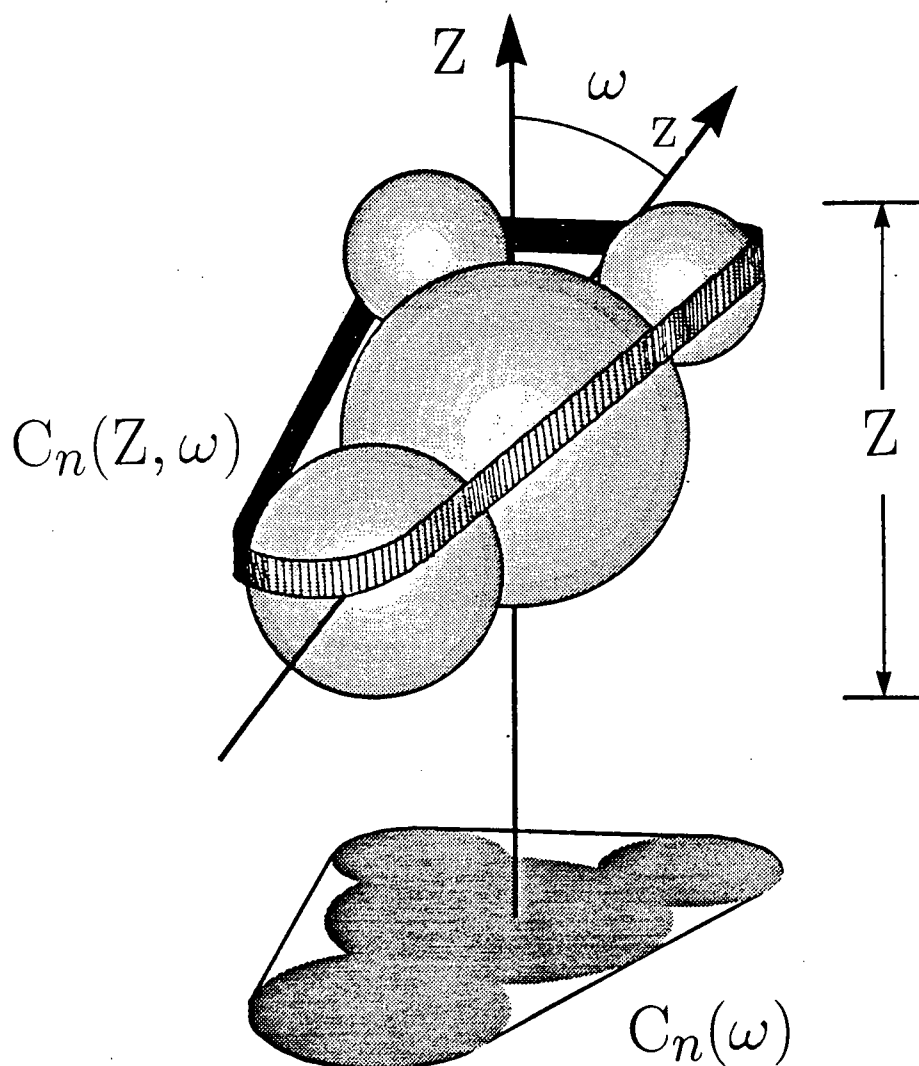
A hypothetical solute constructed from van der Waals spheres. The mean-field potentials of models A_1, A_3, A_4 and A_5 depend on parameters defined in this figure. See the text for a further description.

Figure 3.8: Illustration of Orientation-Dependent Parameters Used in Size and Shape Models (II).
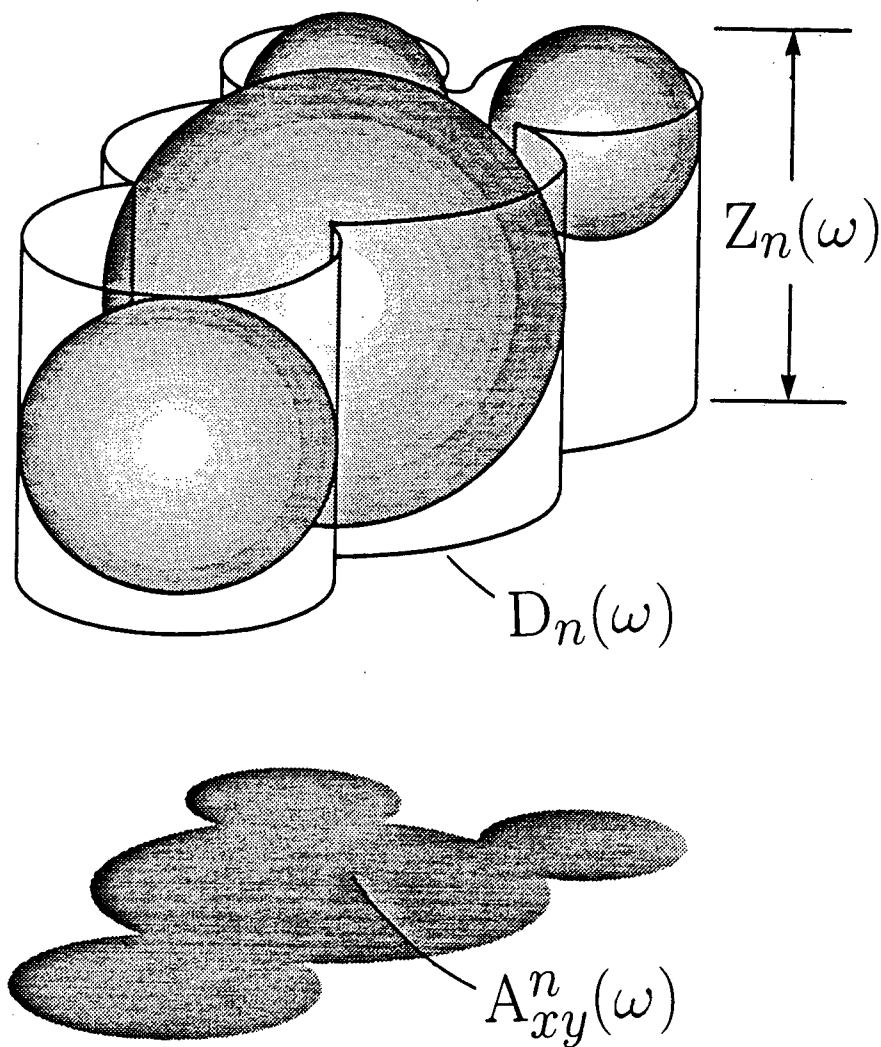
A hypothetical solute constructed from van der Waals spheres. The mean-field potentials of models A_2, and A_6 depend on parameters defined in this figure. See the text for a further description.

traces out this circumference, and the integral is the area of the full projection of the surface of the molecule onto a plane parallel to the nematic director (see Figure 3.7). Thus A_4 can be interpreted as an anisotropic surface potential. Note that the equation for A_4 is a generalization of the second term for the potential A_3 which can be obtained if one neglects the Z-dependence of $C_n(Z, \omega)$ and sets all values equal to $C_n(\omega)$. This model is similar to another by Ferrarini *et al.* [37] in which surface area elements of the van der Waals spheres contribute an energy proportional to $P_2(\cos \psi)ds$, where ψ is the angle between the surface normal and the nematic director, and ds the area of the surface element. In Model A_4, the interaction energy effectively is proportional to $| \sin \psi | ds$.

Model A_5. This model is a combination of models A_1 and A_4:

$$U_{SS}^n(\omega) = \frac{1}{2}k(C_n(\omega))^2 - \frac{1}{2}k_s \int_{Z_{min,n}}^{Z_{max,n}} C_n(Z, \omega)dZ \qquad (3.62)$$

Again, it is necessary to fix the ratio of parameters to the value obtained from the previous study by Zimmerman *et al.* [36], where $k_s/k = 23.529$. Note that this particular model was the most successful for predicting order parameters for molecules oriented in a zero-EFG liquid crystal mixture.

Model A_6. The potential is given by [36]

$$U_{SS}^n(\omega) = 2k_{xy}A_{xy}^n(\omega) - k_z D_n(\omega)Z_n(\omega) \qquad (3.63)$$

where, again, $D_n(\omega)$ is the maximum circumference traced out by the projection of the solute onto the plane perpendicular to the nematic director Z-axis, and Z_n is the length of the projection of the solute along the Z-axis. Also, A_{xy}^n is the area of the projection contained within the maximum circumference, $D_n(\omega)$, as shown in Figure 3.8. For this study, we fix $k_z/k_{xy} = 0.327$, the optimal value obtained in ref. [36]. Note that the quality of the fit to experimental order parameters for the solutes in that study using A_6 was comparable to the best fit obtained using A_5.

3.2.4.2 Model B: Moment of Inertia Model

Model B uses a mean-field potential based on the expansion of $U_n^{aniso}(\omega)$ in Equation (8) truncated to second rank:

$$U_n^{aniso}(\omega) = \sum_{m=-2}^{2} c_{2,m}^n Y_{2,m}(\theta, \phi) \qquad (3.64)$$

The expansion coefficients, $c_{2,m}^n$, are parameterized by using a model developed by Straley [120] in which the interacting molecules are represented by parallelepipeds. The symmetry of the parallelepipeds causes this expansion to be reduced to [44, 45]

$$U_n^{aniso}(\omega) = c_{2,0}^n Y_{2,0} + \sqrt{\frac{3}{2}} c_{2,2}^n \sin^2(\theta) \cos(2\phi) \qquad (3.65)$$

For a solute modeled as a parallelepiped of length, L, width, W, and breadth, B:

$$c_{2,0}^n = \frac{1}{3}\epsilon \left[6LBW + L(W^2 + B^2) - 2W(L^2 + B^2) - 2B(W^2 + L^2) \right] \qquad (3.66)$$

$$c_{2,2}^n = \frac{\epsilon}{\sqrt{6}} \left[(L^2 - BW)(B - W) \right] \qquad (3.67)$$

for $L \geq W \geq B$, where ϵ is a parameter that characterizes the solute-solvent interaction. The parallelepiped dimensions can be calculated in terms of the principal-axis components of the moment of inertia tensor, $I_{\alpha\beta}^n$, for each conformer, n [46]:

$$l_\alpha = 2\sqrt{\frac{5(I_{\beta\beta}^n + I_{\gamma\gamma}^n - I_{\alpha\alpha}^n)}{2m}} \qquad (3.68)$$

where L, B and W are written as the elements l_α.

3.2.4.3 Model C: The Chord Model

Photinos, Samulski and coworkers have developed a mean-field model for molecular orientation in a uniaxial phase that is specially tailored for molecules comprised of repeating identical units [47, 48]. Thus, it is not surprising that this model gives remarkably

good results in the analysis of ^{1}H dipolar coupling constants of oriented hydrocarbons [45, 49, 118]. Indeed Rosen *et al.* [45] concluded this to be the superior model in their study of oriented alkanes. This potential is derived from the leading terms in a rigorous expansion of the mean-field interaction. Photinos *et al.* [49] write

$$U_n^{aniso}(\omega) = -\sum_{i=1} \left[\tilde{w}_0 P_2(\mathbf{s}^i, \mathbf{s}^i) + \tilde{w}_1 P_2(\mathbf{s}^i, \mathbf{s}^{i+1}) \right] \tag{3.69}$$

where $\mathbf{s}^i$ is a unit vector describing the orientation of the ith C–C bond of the hydrocarbon chain, and where the sum is over all of the bonds in the chain. The factors $P_2(\mathbf{s}^i, \mathbf{s}^{i+m})$ are given by

$$P_2(\mathbf{s}^i, \mathbf{s}^{i+m}) = \frac{3}{2} \cos \theta_Z^i \cos \theta_Z^{i+m} - \frac{1}{2} \mathbf{s}^i \cdot \mathbf{s}^{i+m} \tag{3.70}$$

where θ_Z^i is the angle between the ith bond and the nematic director, which aligns with the static magnetic field direction along the Z-axis. The parameters, $\tilde{w}_m$, are proportional to the liquid crystal order parameter. The first term in Eq. (3.69) corresponds to the independent alignment of separate C–C bonds that may arise, for example, from the anisotropy of the polarizability of the bonds [121]. The second term incorporates correlations between adjacent-bond orientations, and therefore distinguishes between conformations that may have equal numbers of *trans* and *gauche* bonds but significantly different shapes; thus, it accounts for shape-dependent excluded-volume interactions. In the present study, we consider the specific case, $\tilde{w}_0 = \tilde{w}_1$. This is called the "chord model", since it can be shown to be equivalent to a model in which the chords connecting the midpoints of the C–C bonds are the elemental submolecular units interacting with the external field.

The mean-field potential defined in Eq. (3.69) can be written in a more convenient form. Following Rosen *et al.* [45], we define the components of a second rank tensor:

$$u_{\alpha\beta} = -2\tilde{w}_0 \sum_i \left[T_{\alpha\beta}(\mathbf{s}^i, \mathbf{s}^i) + \frac{1}{2}(T_{\alpha\beta}(\mathbf{s}^i, \mathbf{s}^{i+1}) + T_{\alpha\beta}(\mathbf{s}^{i+1}, \mathbf{s}^i)) \right] \tag{3.71}$$

where

$$T_{\alpha\beta}(\mathbf{s}^i, \mathbf{s}^{i+m}) = s_\alpha^i s_\beta^{i+m} - \frac{1}{3}\delta_{\alpha\beta}\mathbf{s}^i \cdot \mathbf{s}^{i+m} \tag{3.72}$$

where s_α^i is the α-component of the ith C–C bond vector. The principle-axis components of $u_{\alpha\beta}$, $u_{33} \geq u_{22} \geq u_{11}$, can be used to parameterize the leading terms in the expansion

$$U_n^{aniso}(\omega) = c_{2,0}^n Y_{2,0} + \sqrt{\frac{3}{2}} c_{2,2}^n \sin^2(\theta) \cos(2\phi) \tag{3.73}$$

according to

$$c_{2,0}^n = \frac{1}{\sqrt{6}}\left(2u_{33} - (u_{11} + u_{22})\right) \tag{3.74}$$

$$c_{2,2}^n = \frac{1}{2}(u_{22} - u_{11}) \tag{3.75}$$

3.2.5 Other Details of the Calculations

3.2.5.1 Torsional Fluctuations

While the RIS model provides a convenient method for the analysis of experimental data to obtain information about the conformational behaviour of hydrocarbons, the high quality of the experimental dipolar coupling constants that may be obtained for these systems means that the crudeness of this approximation may be the limiting factor for the accuracy with which information can be determined. The principle restriction of this model is the limitation of the dihedral angle, ϕ, to the three angles, $0°$, $\pm\phi_g$, associated with the *trans* and $\pm gauche$ states. Thus, it would be useful to examine the role of torsional fluctuations of ϕ about these minima of the rotational potential energy. A simple approach is provided in a study by Photinos *et al.* [118] in which the dihedral angle can assume values at $\pm\Delta\phi$ about the RIS state values, in addition to the RIS values themselves. For butane, this corresponds to nine conformers with dihedral angles of $\phi = 0°$, $\pm\Delta\phi$, $\pm\phi_g$, and $\pm(\phi_g \pm \Delta\phi)$. We use this extended-RIS model in addition

to the regular RIS model to determine the importance of torsional fluctuations on the determined E_{tg}, conformer probabilities and molecular order parameters. We fix the population ratios of each extended-RIS triplet to 1:2:1 and set $\Delta\phi=20°$ to approximate roughly the shape of each peak in the torsional probability distribution.

3.2.5.2 Dihedral Angle

Experimental estimates of the dihedral angle, ϕ_g, vary widely, ranging from 110° from an electron diffraction study [122] to a value of 118° obtained from an analysis of the Raman spectrum [94]. Because the dipolar couplings have a sensitive dependence on ϕ_g, we examine the variation in the results of our analysis to changes in ϕ_g.

3.2.5.3 Methyl Groups

Since four of the seven butane dipolar coupling constants involve protons in methyl groups, it is important to model the rotation of these groups in a reasonable way. We employ a methyl group rotation barrier of 12.5 kJ/mol and sample different molecular geometries in steps of 5°, with probabilities weighted by the Boltzman factor.

3.3 Experimental

A liquid-crystal mixture of 55 wt% Merck ZLI 1132 and 45 wt% EBBA was prepared. Approximately 500 mg of the mixture was placed into a 5 mm o.d. standard NMR tube and was thoroughly degased through several freeze-pump-thaw cycles. Enough gaseous butane was condensed into the tube at liquid nitrogen temperature to achieve a $\approx$5 mol% solute to liquid crystal ratio under the assumption that all of the gas dissolved in the liquid crystal. The tube was then flame-sealed under vacuum. Since a fraction of the gas in the tube filled the space above the sample, the true solute concentration was

<5 mol%. To provide a lock, the NMR tube was equipped with a capillary tube, filled with acetone-d_6, that was held coaxial to the NMR tube with teflon spacers.

The ^{1}H-NMR spectra were acquired on a Bruker AMX-500 spectrometer at 301.4 K at 500 MHz. The MQ spectra were acquired using the following pulse sequence:

$$\left(\frac{\pi}{2}\right)_\phi - \tau - \left(\frac{\pi}{2}\right)_\phi - t_1 - \left(\frac{\pi}{2}\right) - \tau' - t_2(acquire)$$

To detect selectively a $\pm n$-quantum spectrum, the phase ϕ of the first two pulses relative to the third pulse were cycled through $2n$ steps in increments of π/n with alternating addition and subtraction of the signal for each value of t_1 [52]. Thus, the acquisition of the seven-quantum spectrum required a phase cycle employing 14 steps of 25.7°, while that of the eight-quantum spectrum used 16 steps of 22.5° increments.

Both spectra were acquired using a preparation time, τ, of 12 ms, a recycle delay of 3.5 s, and a t_1 increment time of 41.7 μs, which corresponds to an f_1 sweep width of 24 kHz. There were 1250 increments of t_1 collected for the seven-quantum spectrum and 1200 increments for the eight-quantum spectrum. For both spectra, a delay of τ'=1 ms was used to minimize the contribution of the liquid-crystal signal that is generated after the third pulse. For every t_1 increment, there were 1024 data points collected in t_2. The total time for acquisition of each spectrum was approximately 20 hours.

Both data sets were zero-filled to 2048 in the t_1 dimension prior to the 2D magnitude fourier-transform. Each MQ spectrum was obtained by performing a summed projection of the 2D spectrum onto the f_1 axis. Peak positions of both the one-quantum and MQ spectra were calculated using the Bruker UXNMR peak-peaking routine. The one-quantum spectrum was analyzed using the computer program LEQUOR; the MQ spectra were analyzed using a suitably modified version of LEQUOR.

3.4 Results and Discussion

3.4.1 NMR Spectra

The experimental one-quantum spectrum of partially oriented butane is shown in Figure 3.9. The ^{1}H-NMR spectrum of butane consists of a thick mass of lines spanning a frequency range of 10 kHz with essentially no notable features and sits on the broad liquid-crystal ^{1}H spectrum. A horizontally expanded region of the spectrum is shown in the lower half of Figure 3.10. It is apparent that while the spectral-line density is high, overlap is not so severe as to make it impossible to determine the frequencies of most of the lines; thus, a fit of the experimental spectrum is certainly possible. However, the complexity of the spectrum makes it extremely difficult to do so without very accurate initial estimates of the coupling constants and chemical shifts. Small deviations from the true values of these parameters would alter the line frequencies and intensities enough to generate a spectrum with significantly different fine structure from that of the experimental spectrum.

These problems can be circumvented with the help of MQ spectra. The seven-quantum and eight-quantum spectra for oriented butane are shown in Figures 3.11 and 3.12. There are far fewer lines than appear in the one-quantum spectrum, though they are spread out over a comparable frequency range. The strategy used to fit these spectra employed the Model A_5 described earlier, with parameters optimized to the zero-EFG liquid-crystal mixture according the results of an earlier study [36] to predict molecular order parameters and thus dipolar coupling constants. A value for E_{tg} of 3.0 kJ/mol was used to generate initial conformer probabilities. Chemical shifts and J-coupling constants were initialized to their isotropic values [123]. The trial spectrum that was generated provided an adequate starting point to fit simultaneously the two MQ spectra. In total, 19 lines from the eight-quantum spectrum and 35 lines from the seven-quantum

Figure 3.9: Experimental (bottom) and Simulated (top) Spectra of Partially Oriented Butane.

Frequency /kHz
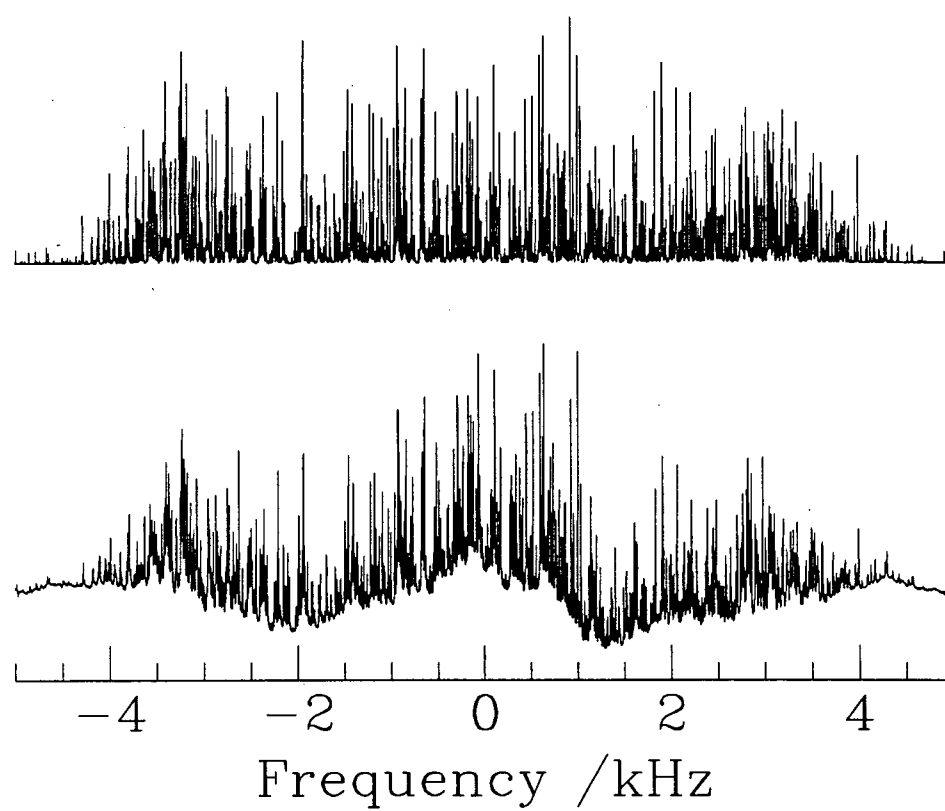
Figure 3.10: Expanded Region of Experimental and Simulated Spectra of Partially Oriented Butane.
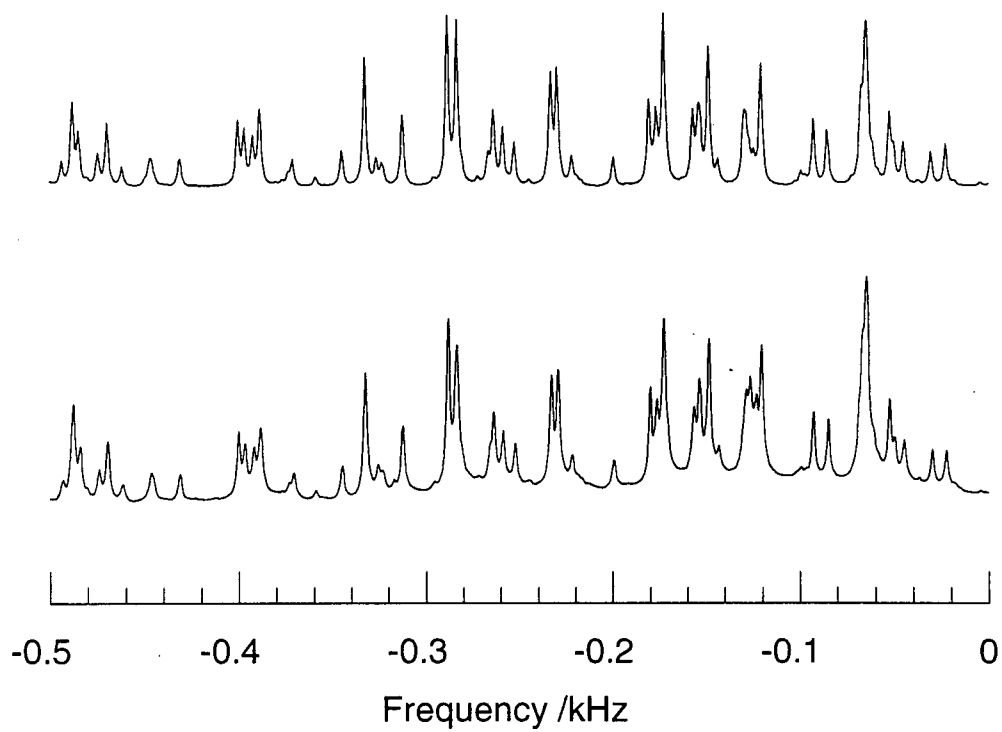
Figure 3.11: Experimental and Simulated Seven-Quantum Spectra of Partially Oriented Butane.
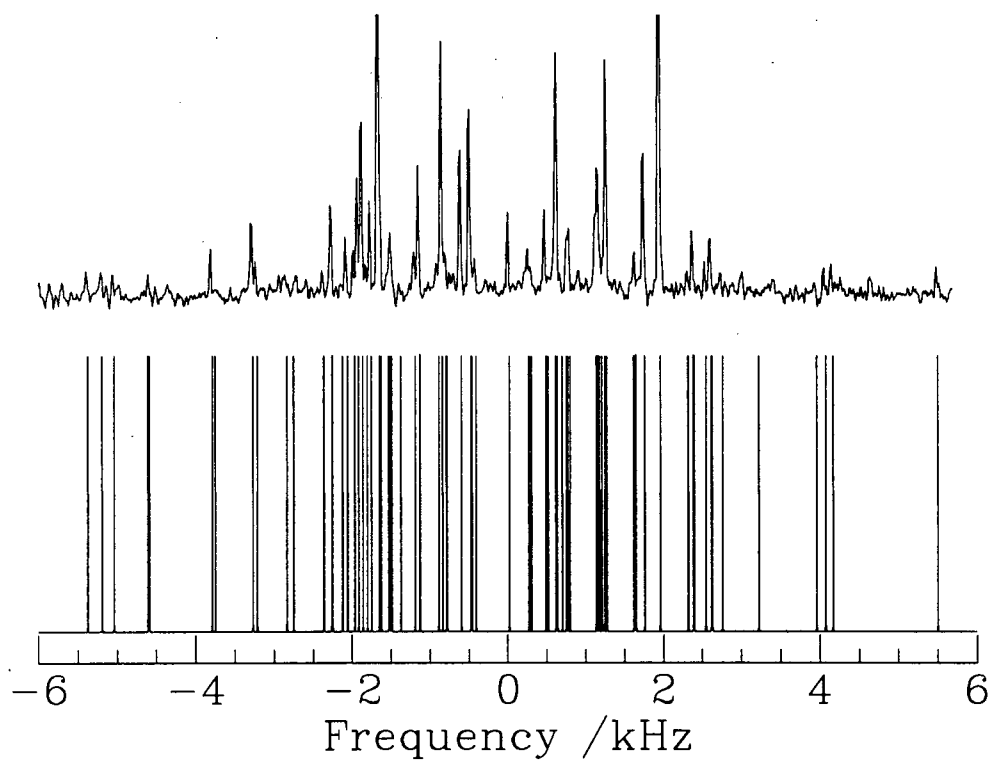
For the simulated spectrum, the line intensities have been arbitrarily set equal since the intensity of each MQ transition is a complicated function of the preparation time τ and the parameters in the spin Hamiltonian, and does not provide any information for the present study.

Figure 3.12: Experimental and Simulated Eight-Quantum Spectra of Partially Oriented Butane.
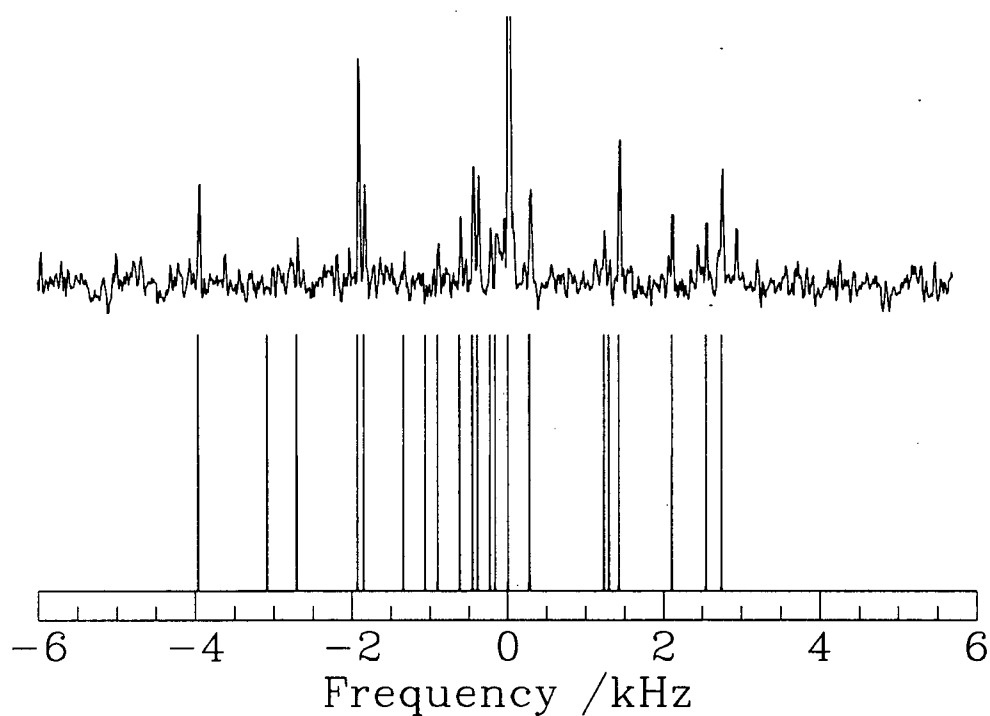
For the simulated spectrum, the line intensities have been arbitrarily set equal since the intensity of each MQ transition is a complicated function of the preparation time τ and the parameters in the spin Hamiltonian, and does not provide any information for the present study.

spectrum were fit successfully. Figures 3.11 and 3.12 show the frequencies of all of the lines calculated in the fit of the MQ spectra. A large number of these lines in the experimental seven-quantum spectrum have very weak intensity and are barely discernible, if at all, from the fluctuations in the noise. Note that the line intensities have a very complex and sensitive dependence on the preparation time, τ. Ideally one uses an optimum τ, if one exists, for which all of the associated MQ coherences are appreciably populated. A practical approach is to coadd a series of spectra acquired with different values of τ. In the present case, we found the spectra acquired with a single τ to be sufficient.

The trial one-quantum spectrum that was predicted from the fit of the MQ spectra proved to be an excellent starting point in the fit of the experimental one-quantum spectrum; assignment of spectral lines was tedious, but trivial. A simulated one-quantum spectrum using the fitted dipolar coupling constants, chemical shift difference and J-couplings is shown in Figure 3.9 with the experimental spectrum. The high quality of the fit is more evident in the expanded plot of a region of the spectrum shown in Figure 3.10. Table 3.5 lists the final values of the fitting parameters obtained in both the one-quantum and MQ spectral fits. The protons are labeled according to Figure 3.13. Note that the predicted coupling constants and chemical shift difference are almost exactly the same for both fits; the J-couplings are shifted only slightly from their literature values. Thus, an analysis of the MQ spectra for this particular ten-spin system is shown to provide information sufficiently accurate for the type of analysis that we describe below. This is a significant point when considering the accuracy of MQ spectral information of molecules of slightly greater complexity for which the one-quantum spectrum cannot be analyzed.

3.4.2 Conformational and Orientational Behaviour of Butane

Table 3.6 summarizes the results of the fit of the experimental dipolar coupling constants using the eight mean-field models described in Section 3.2.4, for three different ϕ_g

Table 3.5: Fitting Parameters (Hz) from the Multiple-Quantum and One-Quantum Spectral Fits.

Parameter	MQ	1Q
D_{12}	817.8(2)	817.63(3)
D_{14}	−199.6(2)	−199.57(5)
D_{16}	−389.2(2)	−388.84(2)
D_{18}	−196.4(2)	−196.14(2)
D_{45}	1601.3(3)	1601.09(4)
D_{46}	65.3(5)	65.61(8)
D_{47}	34.5(5)	33.98(8)
$\delta_1 - \delta_4$	309.5(2)	309.40(7)
J_{14}	7.4^a	7.37(5)
J_{16}	-0.2^a	−0.19(2)
J_{46}	5.7^a	6.04(2)
J_{47}	8.6^a	8.83(2)

^{a}Isotropic values from Ref. [123].

Figure 3.13: Labeling of Butane Protons
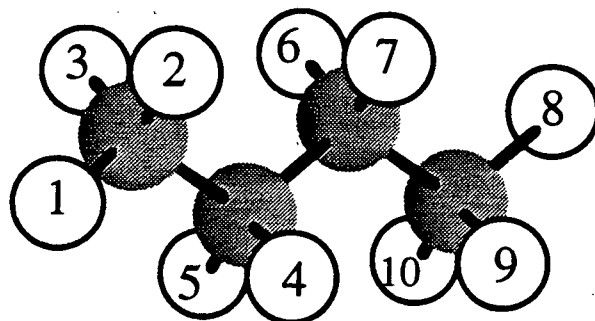
dihedral angles, with and without corrections for torsional fluctuations about the RIS states. Among the SS models, A_1, A_2 and A_3 yield fits of comparable quality, with root-mean-square (RMS) deviations of approximately 30 Hz, regardless of the variation in the geometrical parameters. Models A_4, A_5 and A_6 yield fits of substantially improved quality with RMS values roughly half those of the fits with the other three models. This trend is entirely consistent with the results of the study by Zimmerman *et al.* [36] in which these SS models were tested on a series of rigid solutes oriented in the same zero-EFG liquid-crystal mixture. This probably is due to the fact that models A_4, A_5 and A_6 incorporate much more detail into their descriptions of the molecular size and shape than do the others. Model B yielded by far the poorest fit of the experimental dipolar coupling constants. This is surprising in light of the results of Rosen *et al.* [45] in which this model yielded particularly good fits, especially so for the shorter alkanes. Model C gave the best fit, consistent with the results of Rosen *et al.* and as one may expect for a model specially tailored for molecules composed of identical repeating units. The quality of the fits for all mean-field models is generally insensitive to the value of ϕ_g, and is only marginally improved by incorporating torsional fluctuations into the fits. Table 3.7 lists the experimental and calculated dipolar coupling constants for all of the mean-field models for the case of ϕ_g=116° and $\Delta\phi$=20° and clearly highlights the relative success of each model in describing the orientational ordering of butane. Note that the simulated dipolar coupling constants for all models do not fall within the uncertainties of the highly accurate experimental coupling constants. This discrepancy is due to a variety of factors, including small uncertainties in the molecular geometry, molecular vibrations, as well as the limitations in the mean-field models themselves.

The principal goal of the present study is an accurate determination of E_{tg}, the effective energy difference between the *trans* and *gauche* states of butane in an anisotropic condensed phase. The results summarized in Table 3.6 clearly show that the value for

Table 3.6: Results of the Fits to the Experimental Dipolar Coupling Constants.

Model	Parameter	$\phi_g=112°$		$\phi_g=116°$		$\phi_g=120°$	
		$\Delta\phi=0°$	$20°$	$\Delta\phi=0°$	$20°$	$\Delta\phi=0°$	$20°$
A_1	E_{tg} /kJ·mol^{-1}	2.22	2.22	2.33	2.34	2.43	2.45
	k /10^3 N·m^{-1}	5.81	5.92	5.75	5.86	5.69	5.80
	RMS /Hz	32	32	29	29	26	26
A_2	E_{tg} /kJ·mol^{-1}	2.35	2.36	2.43	2.45	2.50	2.54
	k /10^3 N·m^{-1}	4.64	4.74	4.62	4.72	4.60	4.69
	RMS /Hz	34	33	30	30	27	27
A_3	E_{tg} /kJ·mol^{-1}	2.27	2.26	2.37	2.38	2.47	2.49
	k /10^3 N·m^{-1}	4.74	4.81	4.70	4.77	4.66	4.73
	RMS /Hz	32	32	29	29	26	27
A_4	E_{tg} /kJ·mol^{-1}	2.58	2.67	2.74	2.84	2.90	3.01
	k_s /10^3 N·m^{-1}	70.4	71.0	68.8	69.6	67.2	68.1
	RMS /Hz	17	15	19	19	22	20
A_5	E_{tg} /kJ·mol^{-1}	2.48	2.54	2.62	2.68	2.75	2.82
	k_s /10^3 N·m^{-1}	46.4	47.0	45.6	46.2	44.7	45.4
	RMS /Hz	17	15	16	14	17	15
A_6	E_{tg} /kJ·mol^{-1}	2.62	2.70	2.78	2.85	2.93	3.01
	k_{xy} /10^3 N·m^{-1}	18.5	18.7	18.1	18.3	17.7	18.0
	RMS /Hz	13	12	15	14	18	17
B	E_{tg} /kJ·mol^{-1}	2.94	3.07	3.18	3.32	3.46	3.59
	ϵ /10^4 kJ·m^{-3}	4.50	4.56	4.37	4.44	4.23	4.32
	RMS /Hz	44	41	48	44	52	48
C	E_{tg} /kJ·mol^{-1}	2.09	2.09	2.15	2.17	2.22	2.26
	$\tilde{w}_0$ /kJ·mol^{-1}	0.736	0.744	0.725	0.734	0.713	0.723
	RMS /Hz	12	11	9	7	9	7

Table 3.7: Experimental and Calculated Dipolar Coupling Constants (Hz) for $\phi_g=116°$ and $\Delta\phi=20°$.

D_{ij}	Exp.	A_1	A_2	A_3	A_4	A_5	A_6	B	C
D_{12}	817.3	842.9	822.5	843.0	821.7	829.8	822.5	776.6	821.8
D_{14}	-199.6	-195.3	-207.9	-194.7	-211.3	-206.2	-207.9	-206.5	-192.2
D_{16}	-388.8	-392.2	-360.5	-393.5	-352.6	-366.6	-360.5	-339.4	-390.0
D_{18}	-196.1	-229.2	-199.9	-229.2	-198.7	-208.7	-199.9	-160.6	-203.0
D_{45}	1601.1	1536.2	1609.1	1535.1	1615.3	1588.7	1609.1	1700.9	1591.0
D_{46}	65.6	70.1	63.5	70.8	66.1	67.9	63.5 ·	66.0	66.5
D_{47}	34.0	66.8	42.0	67.1	34.3	46.4	42.0	-13.4	52.7
RMS		29	30	29	19	14	14	44	7

this quantity obtained from an analysis of dipolar coupling constants is sensitive to the model used to describe the orientational ordering. Model C yields an E_{tg} of ≈ 2.1 kJ/mol, the lowest estimate of any of the models. Model B gives the highest value, with $E_{tg} \approx$ 2.9–3.6 kJ/mol, while the various SS models predict values that lie between these two extremes. Thus, the estimates for E_{tg} are spread over a fairly wide range. Note that while increasing the value of ϕ_g consistently leads to higher estimates of E_{tg}, the range of values obtained from each model is small compared to differences between the predictions of different models, with the exception of some of the SS models which predict very similar values of E_{tg}. Including torsional fluctuations in the calculations causes only a very slight shift towards a higher E_{tg}.

To assess the accuracy of each model prediction we must consider the quality of each fit to the experimental dipolar coupling constants. Since model B yielded such a poor fit, the high calculated E_{tg} values must be treated skeptically. The poorness of this fit relative to those for other models is emphasized in Table 3.7. The dipolar coupling constant D_{47}, for example, which is highly sensitive to E_{tg}, is actually predicted to have a

different sign from the experimental value. In light of this consideration, we exclude the range of values of E_{tg} predicted by model B. The low value of E_{tg} obtained using model C mirrors the results of Rosen *et al.*, in which a consistently low E_{tg} for alkanes of various lengths was determined. Thus, we take 2.1 kJ/mol as the lower limit in our estimate of E_{tg}. The values for E_{tg} predicted by the SS potentials span a fairly wide range, 2.2–3.0 kJ/mol. Of particular importance are models A_5 and A_6, which account for the oriented molecule's shape in the most detailed manner and thus yielded the best fits among the SS models. These models also gave the highest estimates of E_{tg}, with a range of 2.5–3.0 kJ/mol, and thus provide an upper limit to the estimate of E_{tg} for butane in this study. To summarize, our analysis of the ^{1}H dipolar coupling constants of partially oriented butane using a variety of mean-field models suggests that $E_{tg} \approx$ 2.1–3.0 kJ/mol.

While a model-independent estimate of E_{tg} would have been preferred, the results of our analysis are significant, nevertheless. The range 2.1–3.0 kJ/mol is below most experimental gas-phase values which lie in the range 3.3–3.7 kJ/mol [92, 93, 94, 95, 96], with the exception of the value of 2.9 kJ/mol reported in ref. [97]. Thus, our study provides evidence that *gauche*-conformer populations of butane in an anisotropic condensed phase are enhanced relative to the gas-phase values, in accord with much experimental evidence for butane in isotropic condensed phases [98, 99, 100].

Table 3.8 lists the *trans*-state probabilities calculated for the various models employed in our analysis. As expected the probabilities increase with increasing calculated E_{tg}, with model B predicting the highest probabilities and model C predicting the lowest. Considering only the successful models that were used to establish a range of values for E_{tg}, we estimate that the *trans* probabilities lie in the range 0.54–0.62. Also shown in Table 3.8 are the *trans* probabilities for an isotropic phase obtained by setting $U_n^{aniso}(\omega)$=0 in Eq. (3.54). The isotropic probabilities are consistently slightly lower than the nematic-phase probabilities, indicating that the anisotropy in the mean-field has the effect of

Table 3.8: Nematic (N) and Isotropic (I) Phase *trans* Probabilities.

Model	Phase	$\phi_g=112°$		$\phi_g=116°$		$\phi_g=120°$	
		$\Delta\phi=0°$	$20°$	$\Delta\phi=0°$	$20°$	$\Delta\phi=0°$	$20°$
A_1	N	0.547	0.549	0.559	0.561	0.570	0.573
	I	0.537	0.539	0.549	0.551	0.560	0.544
A_2	N	0.559	0.562	0.562	0.572	0.577	0.582
	I	0.550	0.552	0.559	0.562	0.567	0.572
A_3	N	0.551	0.553	0.563	0.565	0.573	0.576
	I	0.541	0.543	0.553	0.555	0.563	0.567
A_4	N	0.580	0.590	0.596	0.607	0.612	0.624
	I	0.573	0.584	0.589	0.600	0.606	0.618
A_5	N	0.571	0.606	0.585	0.592	0.599	0.607
	I	0.563	0.570	0.577	0.585	0.591	0.599
A_6	N	0.585	0.592	0.600	0.608	0.615	0.624
	I	0.577	0.586	0.592	0.602	0.609	0.618
B	N	0.615	0.629	0.638	0.652	0.664	0.677
	I	0.608	0.622	0.632	0.646	0.658	0.671
C	N	0.535	0.537	0.543	0.546	0.551	0.555
	I	0.523	0.526	0.531	0.534	0.538	0.544

Table 3.9: Calculated Principal Axis System (PAS) Order Parameters, and PAS Euler-Angle, for *trans* and *gauche* Conformers of Butane.

Model	Conformer	S_{zz}	$S_{yy}-S_{xx}$	β_{rot}
A_1	*trans*	0.177	0.007	43.6
	gauche	0.107	-0.037	25.6
A_2	*trans*	0.175	0.010	43.3
	gauche	0.108	-0.035	27.2
A_3	*trans*	0.177	0.006	43.5
	gauche	0.108	-0.037	25.7
A_4	*trans*	0.151	0.034	44.6
	gauche	0.101	-0.616	25.0
A_5	*trans*	0.160	0.025	44.1
	gauche	0.103	-0.053	23.2
A_6	*trans*	0.154	0.028	44.1
	gauche	0.100	-0.059	24.3
B	*trans*	0.140	0.061	42.0
	gauche	0.078	-0.064	23.8
C	*trans*	0.179	0.013	41.6
	gauche	0.089	-0.07	23.6

Calculated for ϕ_g=116° and $\Delta\phi$=20°. For both conformers, the PAS y-axis bisects the C–C–C–C dihedral angle, and the PAS z-axis makes an angle of β_{rot} with the central C–C bond towards the methyl groups.

favouring the elongated *trans* state relative to the *gauche* states. Since these shifts are very small, it appears that the conformational distribution is essentially determined by the isotropic "solvent pressure" of the liquid crystal, in agreement with the findings of Rosen *et al.* for longer alkanes.

Table 3.9 summarizes the model-dependence of the calculated Principal Axis System (PAS) order parameters for both the *trans* and *gauche* states of butane for the special case of ϕ_g=116° and $\Delta\phi$=20°. It is interesting to note that the calculated principal order matrix component, S_{zz}, for the *trans* state varies inversely with the calculated E_{tg} and *trans* state probabilities. Thus, the calculated S_{zz} is lowest for model B and highest for

model C. Also shown for both conformers is the Euler angle β_{rot}, defined as the angle between the central C–C bond and the Principal Axis System (PAS) z-axis. As the results clearly show, the PAS orientation is not particularly sensitive to the choice of models used to describe the orienting potential. Thus, an interesting result of these calculations is that the orientation of the PAS system predicted for each model is essentially identical to that for the PAS system of the moment of inertia tensor for both conformers, which is the axis system calculated using model B.

An important result of the present study is the fact that, with the exception of model B, all of the mean-field models for molecular orientation in a nematic phase employed here yielded physically reasonable results in the fits of the experimental dipolar coupling constants. This is in marked contrast to the results of Rosen *et al.* [45] who concluded that the SS models that were tested (models A_1 and A_3) were deficient and unable to adequately describe the orientation of flexible alkanes. One major complaint against model A_1, for example, was that the calculated E_{tg} was unusually high, and found to increase with increasing alkane chain length. However, it is important to note that these calculations failed to account for the fact that each SS potential is *not* purely anisotropic, but has a residual isotropic component (see Eq. (3.55)) that must be subtracted away from the potentials defined in Eqs. (3.57)–(3.63) in order to calculate correctly E_{tg}. In the case of butane, failure to incorporate this correction leads to an incorrect value, E_{tg}^{false}, defined by Eq. (3.56), that was found to be $\approx 10\%$ higher for model A_1 compared to the correct value, a result of the fact that $\langle U_{SS}^{trans} \rangle > \langle U_{SS}^{gauche} \rangle$. It is entirely conceivable that this effect may become more pronounced as the shape anisotropy increases with increasing hydrocarbon chain length and yield results similar to those of Rosen *et al.* Their results for model A_3 contain unrealistically low values for E_{tg}. For butane it was found that $\langle U_{SS}^{trans} \rangle < \langle U_{SS}^{gauche} \rangle$, the opposite of what was observed for model A_1 as a result of the large negative term in Eq. (3.60), which yielded $E_{tg}^{false} < E_{tg}$. Thus, the

apparent deficiencies in the SS models may arise from the failure to account for the isotropic component inherent to all of these potentials. In addition, the results of the present study strongly suggest that the more recent forms of the SS potentials are much more successful than are the earlier versions in fitting experimental dipolar coupling constants and therefore of describing the orientation of flexible molecules.

3.5 Conclusions

In this chapter, we have investigated the conformational and orientational behaviour of butane aligned in a nematic liquid crystal. Information obtained from the analysis of the seven-quantum and eight-quantum ^{1}H-NMR spectra provided an excellent starting point to analyze the highly complex one-quantum spectrum and thus to obtain extremely accurate estimates of the seven independent ^{1}H dipolar coupling constants. An analysis of the coupling constants was carried out with the aid of several different mean-field models for molecular orientation in a nematic environment. It was found that recent versions of the "Size and Shape" potential proposed by Burnell and coworkers, and, in particular, the Chord model proposed by Photinos *et al.*, were able to describe successfully the intermolecular interaction of butane in a liquid crystal, while a model based on the molecular moment of inertia tensor was found to be inadequate. An effective *trans-gauche* energy difference in the range of 2.1–3.0 kJ/mol was determined, suggesting that the *gauche*-state probabilities are enhanced in a condensed anisotropic environment relative to the gas-phase values. Varying the dihedral angle, ϕ_g, between *trans* and *gauche* states, and inclusion of torsional fluctuations about the internal rotational potential minima were found to have only small effects on the results. The anisotropic potential was found to cause a very minor shift towards higher probabilities of the elongated *trans* conformer relative to the isotropic values, in agreement with studies of longer alkanes, suggesting

that the conformational behaviour of butane is similar to that found in the neat liquid phase.

Chapter 4

Monte Carlo Simulations of Oriented Solutes (I): Shape Anisotropy and Mean-Field Models

The material presented in this chapter has been accepted for publication in *Molecular Physics*.

4.1 Introduction

The task of elucidating by experimental means the details of the intermolecular forces that induce orientational order in nematic liquid crystals is challenging. In the case of NMR studies, acquiring information from direct probing of the nematogens is complicated by their structural complexity and significant conformational freedom. An alternative approach that has been fruitful has been to study small, rigid molecules dissolved in nematic solvents. The basic assumption is that these molecules will probe the forces present in the ordered fluid, which may be observed indirectly through the orientational ordering of the probes. The choice of probe molecules permits some means of disentangling the many factors that influence the behaviour of liquid crystalline systems. An important example is the case of dideuterium, in which the interaction between the molecular electric quadrupole moment with the average electric field gradient sampled by the molecule was shown to be the principal interaction responsible for its orientational ordering [13, 119]. More recently, studies of halogenated alkanes with localized dipole moments have indicated that the dipole-dipole interaction is also an important orienting mechanism [47, 48]. In both cases, it is postulated that these interactions are significant for the orientational

ordering of the nematogens as well.

While long-range electrostatic forces contribute to the orientational ordering in nematics, it is the anisotropic short-range repulsive forces that are generally believed to be the dominant orienting mechanism. These short-range repulsive interactions have also been incorporated into the analysis of orientational order of probe molecules. The basic approach is to construct a mean-field orientation-dependent potential characterized by one or two parameters that is sensitive to the details of the size and shape of the molecule. This potential then is used to fit the experimentally measured molecular order parameters for a collection of solutes. The values of the model parameters give a measure of the strength of the short-range repulsive forces that give rise to the ordering. Several mean-field models proposed by Burnell and coworkers [33, 34, 35, 36] and a closely related model due to Ferrarini *et al.* [37] have been highly successful, yielding fits where the calculated principal molecular order parameters are within 10% of their experimental values. Generally, the models which are most sensitive to the details of the molecular shape provide the most accurate description of orientational order.

It is interesting to note that these models are formulated as anisotropic surface interactions or as an elastic distortion of the liquid crystal, but are assumed to arise physically from the short-range repulsive forces between molecules. Thus, some insight into the relationship between the mean-field models and these interactions may be gained by using computer simulations to study orientational ordering of solutes in model systems in which molecules interact solely by short-range forces. The ability to focus on the effects of specific forces without the complicating effects of the other interactions is an important advantage of the computer simulation approach, and provides an additional tool for the interpretation of experimental data.

Computer simulation techniques have been a very effective method to study liquid

crystal systems. In these studies, mesogens have been modeled to various degrees of complexity, ranging from simple hard convex bodies (HCB's) [6], to models of intermediate complexity such as the Gay-Berne mesogen [26, 124, 125, 126], which include long-range attractive forces, to models which attempt to incorporate full molecular detail [38, 39]. The case of HCB's such as hard ellipsoids has attracted much attention over the last decade [5, 60, 127, 128]. For this model, the basic requirement of non-overlap between the bodies approximates the effects of short-range repulsive forces sufficiently to induce the formation of orientationally ordered mesophases for systems of sufficient density.

The purpose of the present study is to investigate the general nature of the size and shape dependence of solute orientational ordering in a nematic solvent without attempting to simulate the behaviour of any particular real molecule. We model both solvent-solvent and solvent-solute interactions with hard-core repulsive forces in an attempt to elucidate the role of this important ordering mechanism. Specifically, solvent and solute molecules are modeled as hard ellipsoids. We follow the approach taken in experimental NMR studies and study the second-rank orientational order parameters of a large collection of solutes of a variety of sizes and shapes. In addition, we investigate the detailed orientational behaviour of two dissimilar ellipsoidal solutes, including an examination of the singlet orientational distribution function and the dependence of the degree of solute orientational order on the nematic order parameter, $\bar{P}_2^{(nem)}$. The MC results are analyzed in terms of four mean-field potentials that were designed to describe orientational order for arbitrary solutes in a uniaxial nematic phase. The simplicity of the approach used here contrasts with and complements that taken in two recent studies which investigated the orientational and dynamical behaviour of benzene [65] and the conformational behaviour of hexane [66] as solutes in a liquid crystalline solvent modeled using the more complex Gay-Berne potential.

4.2 Monte Carlo Simulations

4.2.1 Order Parameters for a Collection of Solutes

Constant-volume Monte Carlo (MC) simulations were conducted for a system composed of 95 liquid crystal molecules and one solute. The usual periodic boundary conditions were employed. Nematogens were modeled as hard prolate ellipsoids of revolution with an axis ratio of 5:1. Solutes of a variety of sizes and shapes also were modeled as hard prolate ellipsoids of revolution. Solute shape anisotropy was varied by adjusting the axis length ratio. Overlap between ellipsoids was tested for trial moves using the procedure described by Vieillard-Baron [129]. All calculations were performed using a reduced density of $\rho^* = Nv_0/V$=0.488, where N=96 is the number of particles confined to the cell, v_0 is the volume of a solvent ellipsoid, and V is the volume of the cell. Although the true density of the system varied between calculations by $\leq 1\%$ as a result of varying the solute volume, changes in the ordering of the solvent were negligible and too small to be detected to within statistical uncertainty.

Particles were randomly chosen for trial moves, which consisted of a simultaneous translation and rotation, the maximum magnitudes of which were chosen so that the translation and rotation would contribute about equally to the likelihood that the move would be rejected. The overall acceptance ratio was 30–40%. Solute trial moves were attempted as frequently as those for individual solvent ellipsoids; no configurational biasing technique was used to increase the sampling rate for the solute. For each translation, a random displacement vector was calculated with individual components in the range of $[-\delta, \delta]$. The orientational displacements were generated by adding a vector of fixed length r but with an orientation chosen at random from an isotropic distribution to the unit vector specifying the orientation of a given particle. The resulting vector was normalized to yield the new orientational unit vector. The values of δ and r were chosen to

give an average acceptance ratio of the combined translation-rotation move of 30-40%. Further, the ratio of δ and r was fixed by the requirement that a translation and rotation contributed about equally to the likelihood that a particle would be rejected. The values of δ and r for solute ellipsoids varied considerably and were generally larger than those for the larger solvent ellipsoids.

The orientational order parameter of the nematic solvent, $\bar{P}_2^{(nem)}$, was measured by finding the largest eigenvalue of the average second-rank tensor defined by

$$\langle \mathbf{Q} \rangle = \frac{1}{N} \sum_{i=1}^{N} \left\langle \frac{3}{2} \hat{u}_i \hat{u}_i - \frac{1}{2} \mathbf{I} \right\rangle \tag{4.76}$$

where $\hat{u}_i$ is a unit vector describing the orientation of the ith solvent ellipsoid. The nematic director is given by the axial-symmetry axis of the principal axis system of this tensor. Solute orientational order was monitored by measuring the second-rank order parameter $\bar{P}_2 = \langle P_2(\cos\theta) \rangle$, where θ is angle between the solute symmetry axis and the nematic director. An equilibration period of 1–2×10^5 sweeps was used, where one sweep represents an attempt to move on average each particle once, starting from an initial configuration where the particles were perfectly aligned and placed on an FCC lattice. Typically 80–90 block averages of 10^4 sweeps each were used to calculate the ensemble averages and provide an estimate of the uncertainties. A total of 31 calculations were performed, each with a solute of a different size and shape. Solute dimensions were chosen to span the range of dimensions less than those of the solvent ellipsoids and were not intended to represent those of real molecules.

The nematic order parameter $\bar{P}_2^{(nem)}$ was determined to be 0.883±0.004, and is consistent with the results of Samborski *et al.* [128]. In order to check that the small size of the system did not in any way influence the outcome of the simulations, several calculations were repeated using a larger system of N=240 particles and yielded identical

results. Attempts to conduct simulations for a system with a lower degree of orientational order that is more comparable to that measured in a typical nematic phase were found to be not practical for conducting a large number of simulations involving different solutes. While reducing the density lowers $\bar{P}_2^{(nem)}$, it also brings the system close to the nematic-isotropic phase transition at $\rho^*=0.37$ [128] where we found the effects of using a small system ($N=96$) to be severe, generally resulting in an overestimate of $\bar{P}_2^{(nem)}$. Since an appropriate increase in the system size required an unacceptable increase in computation time, the higher density was used.

4.2.2 Further Simulations for Two Solutes

Since an important objective of the study is to compare the results of the simulations with experimental results, it is necessary to have a means to scale the results to correspond to a system having a realistic value of $\bar{P}_2^{(nem)}$. To this end, additional simulations were performed for a dissimilar pair of ellipsoidal solutes in the model nematic liquid crystal at lower densities. The simulation method is almost identical to that described in the previous section. In this case, however, a larger system size of $N=240$ particles was used to minimize finite-size effects. Solute A had dimensions of $l=2.0$ and $w=1.0$, while solute B had dimensions of $l=3.33$ and $w=0.25$, where l and w are the dimensions of the ellipsoid parallel and perpendicular to the symmetry axis, respectively, and where the dimensions are measured in units of the solvent ellipsoid width d. Simulations were performed for both solutes at a density of $\rho^*=0.388$, where the nematic order parameter was found to be very close to $\bar{P}_2^{(nem)}=0.634$, the value reported for the order parameter of the analine ring of the nematogen EBBA in the experimental NMR studies of Burnell and coworkers [33, 36]. Simulations were also conducted for solute A and B at intermediate densities of $\rho^*=0.444$, 0.425 and 0.405, as well as those at $\rho^*=0.488$ and 0.388, in order to study the solute orientational ordering as a function of $\bar{P}_2^{(nem)}$.

In addition to calculating the second-rank order parameters $\bar{P}_2$, the full singlet orientation distribution functions were also calculated for these solutes. The probability distribution was calculated for $\cos \theta$ ranging from 0 to 1 in increments of 0.01. Solute orientations were measured with respect to the local director which was recalculated after every 1000 attempted moves per particle.

4.3   Mean-Field Models

The MC simulation data were analyzed using four mean-field model potentials that have been used previously for the analysis of molecular order parameters obtained from NMR data for solutes in nematic liquid crystals.

Model I. The first potential, introduced by van der Est *et al.* [33], is given by

$$U(\omega) = \frac{1}{2}k(C(\omega))^2 \qquad (4.77)$$

where $C(\omega)$ is the circumference traced out by the projection of the solute onto a plane perpendicular to the nematic director, and where $\omega = (\theta, \phi)$ are the angles describing the orientation of the nematic director in the molecular frame. For the axially symmetric solutes considered here, the ϕ-dependence vanishes. This model was also employed in Chapter 3 (Model A_1). See Figure 3.7 for an illustration of the orientation-dependent solute parameters.

Model II. The second potential is an anisotropic surface potential introduced by Zimmerman *et al.* [36], and is given by

$$U(\omega) = -\frac{1}{2}k_s \int_{Z_{min}}^{Z_{max}} C(Z, \omega)dZ \qquad (4.78)$$

where Z is the position along the nematic director bounded by the minimum, Z_{min}, and maximum, Z_{max}, points of the orientation-dependent projection of the solute along this axis. $C(Z, \omega)$ is the circumference traced out by solute at this position along the

director. Thus, $C(Z, \omega)dZ$ is the area of an infinitesimally thin ribbon that traces out this circumference, and the integral is the area of the full projection of the surface of the solute onto a plane parallel to the nematic director. For the case of the convex model solutes studied here, the potential of Eq. (4.78) may also be written as

$$U(\omega) = -\frac{1}{2}k_s \int dS_{\hat{n}} \mid \sin \theta_{\hat{n}} \mid \qquad (4.79)$$

where $\hat{n}$ is the unit vector normal to a solute surface-area element $dS_{\hat{n}}$, and $\theta_{\hat{n}}$ is the angle between $\hat{n}$ and the nematic director. This model was also used in Chapter 3 in the study of butane (model A_4). See Figure 3.7 for details.

Model III. Third, we consider another anisotropic surface potential due to Ferrarini *et al.* [37] given by

$$U(\omega) = \epsilon \int dS_{\hat{n}} P_2(\cos \theta_{\hat{n}}), \qquad (4.80)$$

which has a form similar to that of the previous potential. A noteworthy point regarding this potential is that it may be expanded in terms of second-rank spherical harmonics generally, and is proportional to $P_2(\cos \theta)$ for axially symmetric molecules, where θ is the angle between the symmetry axis and the nematic director.

Model IV. Finally, we consider the two-parameter potential formed by combining the potentials of Models I and II [36] (Model A_5 of Chapter 3):

$$U(\omega) = \frac{1}{2}k(C(\omega))^2 - \frac{1}{2}k_s \int_{Z_{min}}^{Z_{max}} C(Z, \omega)dZ \qquad (4.81)$$

The four mean-field potentials described above were designed to fit experimental solute orientational order parameters according the following relation:

$$S_{\alpha\beta} = \int \left(\frac{3}{2}\cos \theta_\alpha \cos \theta_\beta - \frac{1}{2}\delta_{\alpha\beta}\right) f(\omega)d\omega, \qquad (4.82)$$

where the solute orientational distribution function is related to the mean-field potentials according to

$$f(\omega) = \frac{\exp(-U(\omega)/k_B T)}{\int \exp(-U(\omega)/k_B T)d\omega}. \qquad (4.83)$$

The mean-field potentials are of the following form:

$$U(\omega) = ch(\omega), \qquad (4.84)$$

where c is any of the solute-independent solvent parameters (k, k_s and ϵ), and $h(\omega)$ gives the orientational dependence of the potential, specific for each solute. Model IV is simply a sum of two such terms. Defining a reduced potential $U^*(\omega) \equiv U(\omega)/k_B T$, we can rewrite Eq. (4.83):

$$f(\omega) = \frac{\exp(-U^*(\omega))}{\int \exp(-U^*(\omega))d\omega} = \frac{\exp(-c^* h(\omega))}{\int \exp(-c^* h(\omega))d\omega}, \qquad (4.85)$$

where $c^* \equiv c/k_B T$ (i.e. $k^* = k/k_B T$, $k_s^* = k_s/k_B T$ and $\epsilon^* = \epsilon/k_B T$). To apply these models to fit the order parameters generated in the MC simulations, we must first recognize that the hard-particle system is not characterized by a temperature, since it is fixed at one finite energy value, while also noting that the orientational distribution function in Eqs. (4.83) is defined in terms of temperature. To circumvent this problem, we simply reinterpret Eq. (4.85) as the definition of the mean-field potential $U^*(\omega)$, characterized by the parameters k^*, k_s^* and ϵ^* for the four models above, which, for a system that is characterized by temperature, may be used to define $U(\omega)$, k, k_s and ϵ. In a real system, the temperature-dependence of k^*, k_s^* and ϵ^* can be correlated to the variation of degree of nematic solvent orientational order with density which is an inverse monotonic function of the temperature. Thus, these fitted reduced interaction strength parameters for simulation and experiment may be compared directly in the case of equal nematic solvent order parameters.

4.4 Results and Discussion

4.4.1 Order Parameters for a Collection of Solutes

Solute order parameters vs. solute length for the 31 solutes in a nematic solvent with a density of $\rho^*=0.488$ are plotted in Figure 4.14. The solute length and width are measured in units of the solvent ellipsoid width, d. For solutes of the same width, there is a smoothly varying increase in $\bar{P}_2$ with increasing length. For the case of solutes with a width of $w=1.0$ (Figure 4.14(a)), $\bar{P}_2$ initially rises rapidly with increasing length, and levels off as it approaches the solvent order parameter for a length of $l=5$. For smaller widths, this change in the slope of the graph is less pronounced. Interestingly, there is only a slight decrease in $\bar{P}_2$ at the maximum length, that is when the solute length is equal to the solvent length, as the width is decreased to $w=0.25$.

The solute order parameters calculated from the four fits are plotted with the MC results in Figure 4.14. Each fit corresponds to using one model potential to fit simultaneously the order parameters of all 31 solutes. Thus, the fitting curves shown in Figure 4.14 correspond to a single value of the model parameters for each potential for all four solute widths employed. The root-mean-square (RMS) deviations and the values of the model parameters (Value(1)) for each of the fits are presented in the second and fourth columns, respectively, of Table 4.10.

The curves calculated using the potential of Model I demonstrate that this potential is unable to calculate accurate order parameters for both short and long solutes simultaneously for any solute width. For example, in Figure 4.14(a), the $\bar{P}_2$ for short solutes are underestimated while those for longer ones are fit fairly well. The calculated $\bar{P}_2$ for narrower molecules shown in Figures 4.14(c) and 4.14(d) are reasonably accurate for short molecules, but significantly overestimated for longer molecules. This model deficiency

Figure 4.14: Solute Order Parameters vs. Solute Length
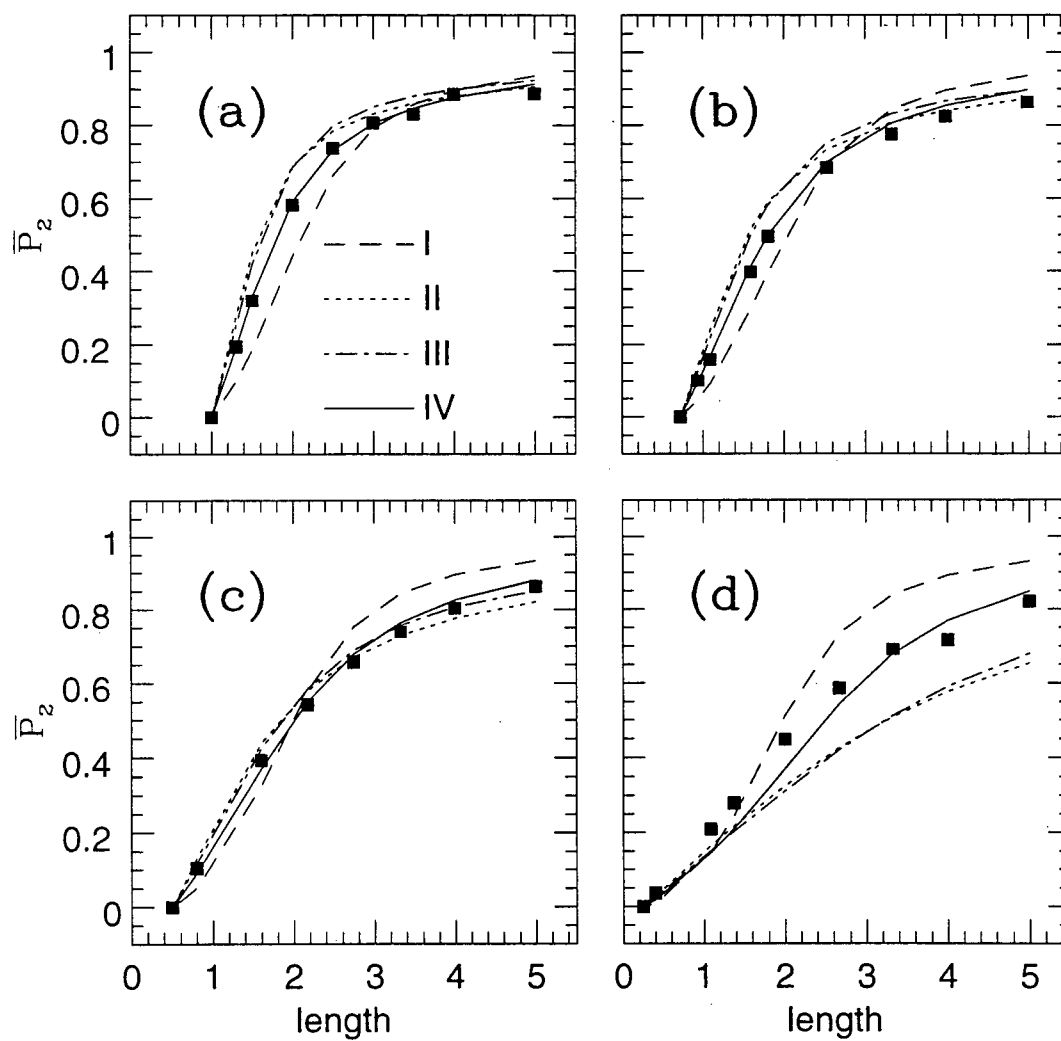
Fits were calculated using the four model potentials. (a) Solute width of $w=1.0$; (b) $w=0.7241$; (c) $w=0.5$; (d) $w=0.25$. In each simulation, a system of 95 solvent ellipsoids and one solute was used.

Table 4.10: Comparison of Results for Fits of MC and Experimental Solute Order Parameters.

Model	RMS	Parameter	Value(1)[a]	Value(2)[b,c]	Value(3)[b,d]	Value(4)[b,e]	Exp.[b,f]
I	0.087	k^*	0.45	0.028	0.0093	0.010	0.013[g]
II	0.083	k_s^*	10.7	0.67	0.20	0.21	0.18[g]
III	0.080	ϵ^*	2.4	0.15	0.049	0.053	0.05[h]
IV	0.031	k^*	0.16	0.0099	0.0031	0.0034	0.0049[g]
		k_s^*	6.1	0.38	0.12	0.13	0.115[g]

[a]Units of d^{-2}.

[b]Units of Å^{-2}.

[c]Value(2) obtained from Value(1) by fixing the length scale by setting the length of a solvent ellipsoid to be 20 Å . For a system with $\bar{P}_2^{(nem)} = 0.883$.

[d]Value(3) calculated by scaling Value(2) by the ratios for the model parameters for solute A listed in Table 4.13. For a system with $\bar{P}_2^{(nem)} = 0.634$.

[e]Value(4) calculated by scaling Value(2) by the ratios for the model parameters for solute B listed in Table 4.13. For a system with $\bar{P}_2^{(nem)} = 0.634$.

[f]Experimental values for a nematic mixture of 55 wt% 1132/EBBA. Order parameter of the analine ring on EBBA given by $\bar{P}_2^{(nem)} = 0.634$.

[g]From Ref. [36].

[h]From Ref. [37].

was also noted previously in analyses of experimentally measured molecular order parameters. In that case, $\bar{P}_2$ calculated for solutes like 1CB, whose length approaches that of the nematogens, were overestimated when using this potential to fit order parameters of a collection of otherwise predominantly small solutes [34].

The fits using models II and III show the opposite trends. In this case, the tendency is to either overestimate $\bar{P}_2$ for shorter solutes or underestimate $\bar{P}_2$ for longer solutes. Again, this trend has been noted previously. For example, model III was found to underestimate the orientational order of the nematogen 5CB using an interaction strength parameter suitable to a collection of shorter solutes [37]. Also noteworthy are the near identical predictions of these two potentials. This is perhaps not surprising, given their similar forms. Both are anisotropic surface potentials in which surface area elements have similar orientation dependencies with respect to the nematic director. RMS deviations for fits of the order parameters of the solutes using models II and III are similar to that of the fit using the model I.

The two-parameter potential of model IV yields by far the best fit to the MC data. The RMS deviation of this fit is less than half of those using the three other potentials. In this case, the deficiencies of models I and II cancel out, yielding accurate fits to solute order parameters for both long and short solutes for all solute widths studied. This is a significant factor underlying the high quality of this fit despite the fact that varying two parameters generally should give an improved fit relative to that of one-parameter models. Among the several models investigated in the study of Zimmerman *et al.* [36], this potential gave the most accurate fit to experimental data. In that case, the deficiences of the individual terms of the potential canceled out in an analogous manner to that observed here.

4.4.2 Analysis of Singlet Orientational Distribution Functions for Two Solutes

To gain further insight into the mean-field models, we focus on the detailed orientational behaviour of two very differently shaped solutes from the full collection analyzed above. Specifically, we investigate the singlet orientational distribution function, $f(\theta)$, and the angular-dependence of the corresponding reduced mean-field potential, $U^*(\theta)$.

Figures 4.15 and 4.16 show the singlet orientational distribution functions and the corresponding orientation-dependence of the mean-field potential for solutes A (l=2, w=1) and B (l=3.33, w=0.25). The potentials of Figures 4.15(b) and 4.15(b) are defined to be zero for θ=0. The orientational distribution functions and mean-field potentials calculated using the model parameter values obtained from the fits of the $\bar{P}_2$ of the full collection of 31 solutes are also shown in the figures.

For the case of solute A in Figure 4.15, the strength of the interaction described by model I clearly is underestimated, leading to an underestimate of the probability for orientations parallel to the director and an overestimate of the probability for orientations perpendicular to the director. In contrast, the strength of the interactions described by models II and III are overestimated, which results in the opposite behaviour for the orientational distribution function. Finally, the interaction strength for model potential IV is exactly right, yielding a very accurate description of orientational order for this solute. This behaviour is consistent with the predictions of $\bar{P}_2$ for this solute, as shown in Figure 4.14(a), which is underestimated by model I, overestimated by models II and III and accurately predicted by model IV.

For the case of solute B in Figure 4.16, model potential I significantly overestimates the degree of solute orientational order, while potentials II and III underestimate the order. Model IV by far gives the most accurate description of orientational order. As expected,

Figure 4.15: Singlet Orientational Distribution Functions and the Corresponding Mean-Field Potential for Solute A ($l=2$, $w=1$)
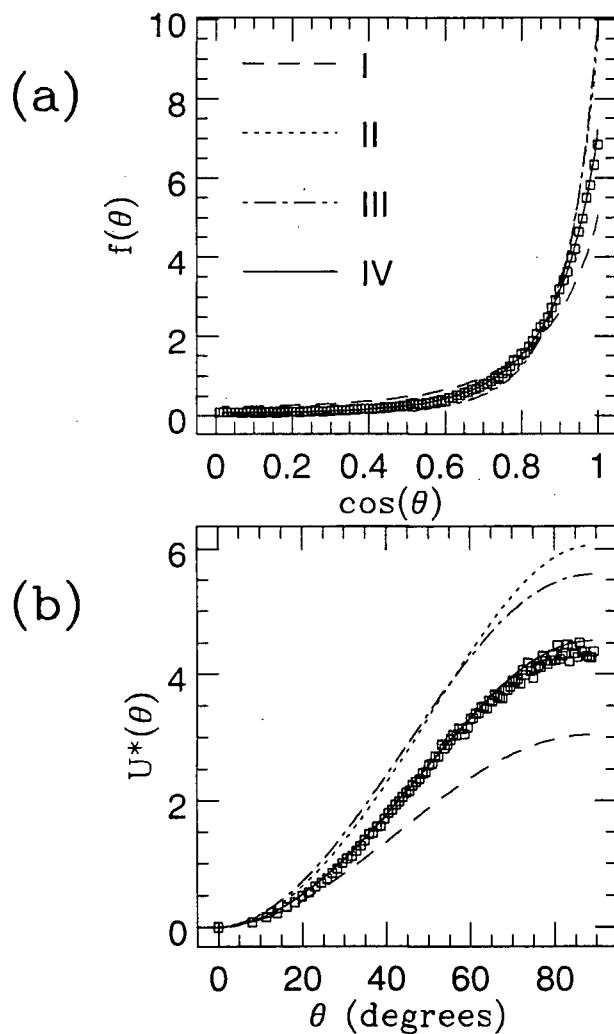
MC calculated distribution and potential (squares). Model predictions calculated using model parameter values obtained from the fit to the $\bar{P}_2$ of 31 solutes. For the simulation, a system of 95 solvent ellipsoids and one solute was used.

Figure 4.16: Singlet Orientational Distribution Functions and the Corresponding Mean-Field Potential for Solute B (l=3.33, w=0.25)
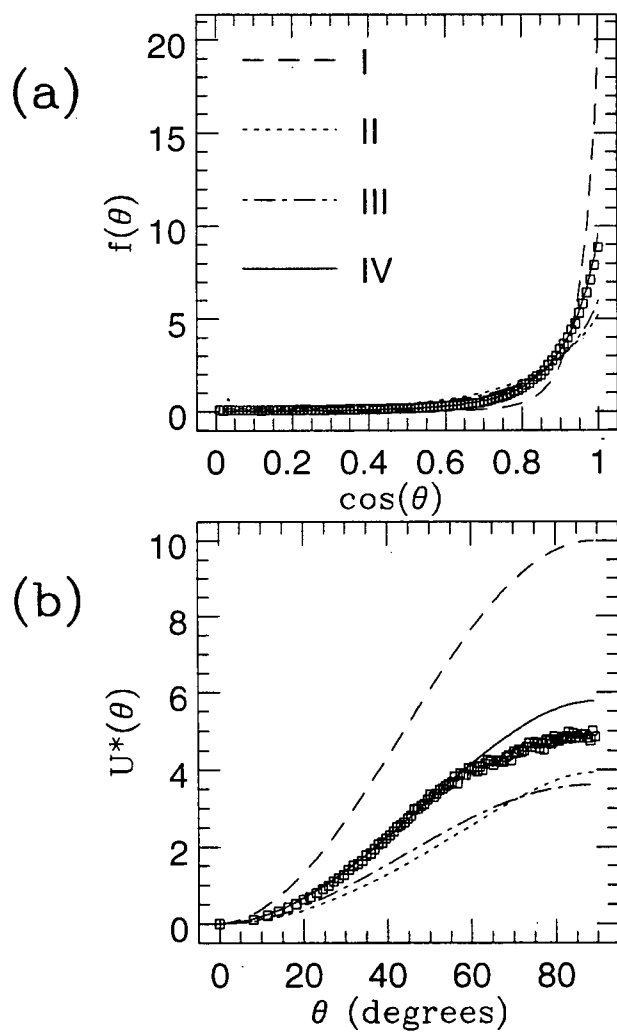
MC calculated distribution and potential (squares). Model predictions calculated using model parameter values obtained from the fit to the $\bar{P}_2$ of 31 solutes. For the simulation, a system of 95 solvent ellipsoids and one solute was used.

these results are consistent with the model predictions of $\bar{P}_2$ shown in Figure 4.14(d) for this solute.

In the analysis of the orientational distribution function and the corresponding mean-field potential for the two solutes above, the predictions from the model potentials used model parameter values based on the fits to the $\bar{P}_2$ for the full collection of solutes. An alternative approach is to fit the distribution functions with each model potential directly. Comparison of the fitted and calculated curves provides more detailed insight into the strengths or deficiencies of the models. Further, an analysis of the $\bar{P}_2^{(nem)}$-dependence of the fitted model parameters would provide a means of scaling the results of the fit above to a system with a more realistic $\bar{P}_2^{(nem)}$. In this way, the results of the MC simulations can be compared directly to those of experimental studies.

Singlet orientational distribution functions were calculated by MC simulations of solutes A and B in the model solvent with densities of ρ^*=0.488, 0.444, 0.425, 0.405 and 0.388. Each distribution function was fit using the four model potentials. For the fits using the two-parameter potential of model IV, the ratio of parameters were fixed to the value of k^*/k_s^*=0.0262 obtained from the fit of the $\bar{P}_2$ of the 31 solutes above. Rather than showing the fitted singlet orientational distribution functions, we present instead the corresponding calculated mean-field potentials together with the model predictions. These are shown in Figures 4.17 and 4.18. The presentation of the results in this form amplifies the deficiencies of the models more clearly. Again, we choose a potential energy of zero at θ=0.

For each solute, the anisotropy of the potentials calculated in the MC simulations decreases with decreasing density. This is qualitatively the same behaviour expected for solutes in real nematic systems as the temperature is increased. In either case this is related to a decrease in $\bar{P}^{(nem)}$. The potential energy profiles predicted from fits to all the model potentials are generally better for the wider solute (A) than for the narrow

Figure 4.17: Orientation-Dependence of the Mean-Field Potential for Solute A ($l=2$, $w=1$).
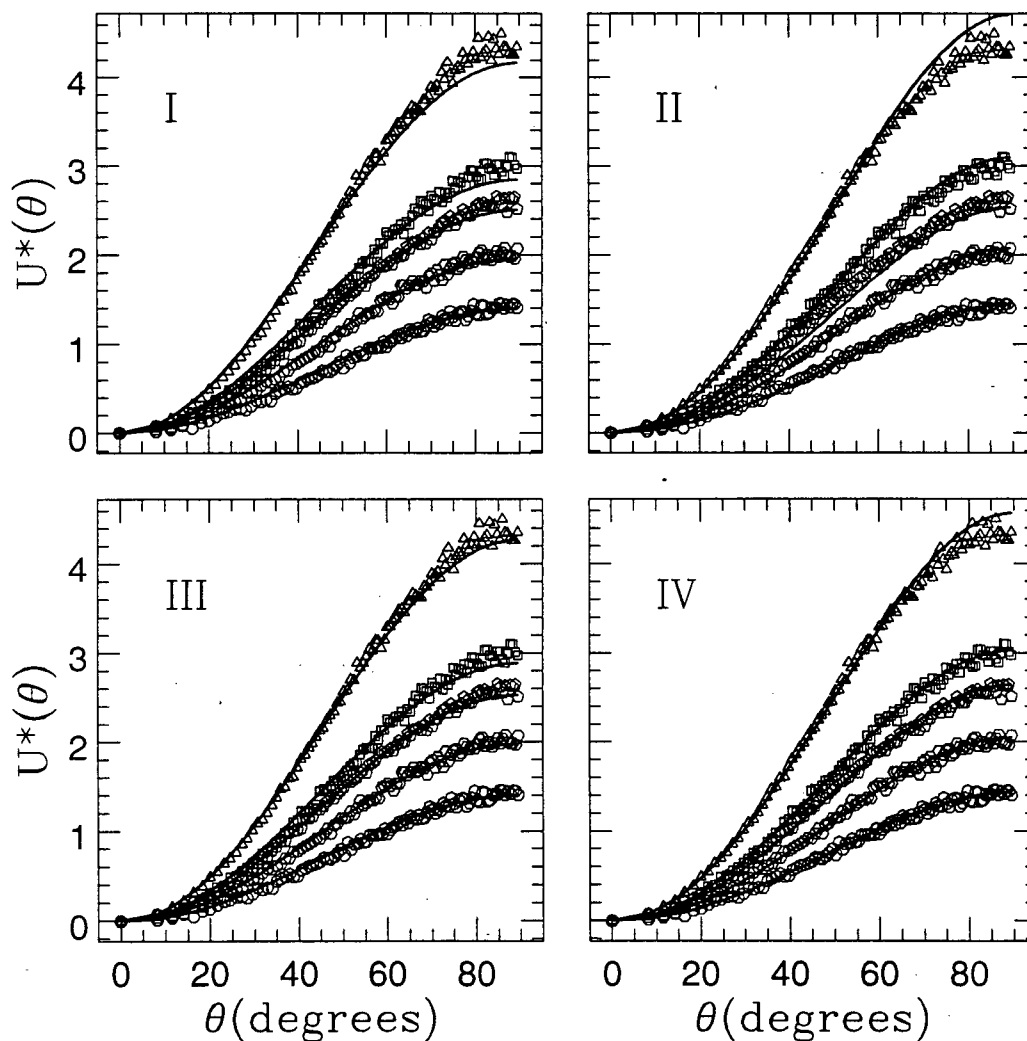
Calculated for $\rho^*=0.488$ (triangles), 0.444 (squares), 0.425 (pentagons), 0.405 (hexagons) and 0.388 (heptagons). The predictions of model potentials I, II, III and IV were obtained by optimizing the model parameters in fits to the corresponding singlet orientational distribution function. The potential energy is chosen to be zero for $\theta=0$. A system of 239 ($\rho^*=0.444$, 0.425, 0.405, 0.388) or 95 ($\rho^*=0.488$) solvent ellipsoids and one solute ellipsoid was used for each simulation.

Figure 4.18: Orientation-Dependence of the Mean-Field Potential for Solute B (l=3.33, w=0.25).

The predictions of model potentials I, II, III and IV were obtained by optimizing the model parameters in fits to the corresponding singlet orientational distribution function. The potential energy is chosen to be zero for θ=0. A system of 239 (ρ^*=0.444, 0.425, 0.405, 0.388) or 95 (ρ^*=0.488) solvent ellipsoids and one solute ellipsoid was used for each simulation.

solute (B). This is evident both from the plots in the figures and in the relative size of the RMS deviations of the fits listed in Tables 4.11 and 4.12. Also noteworthy is the significant difference in the shapes of the mean-potential profiles predicted by models II and III. This feature contrasts with the fact that orientational order predicted by these potentials for a collection of solutes tends to be very similar, as illustrated in the fits to the order parameters in Figure 4.14. Thus, while the similarity in the forms of these two anisotropic surface potentials leads to a similar parameterization among solute shapes, the difference in the details of the surface interaction is manifested in the angular-dependence of the potentials.

The results of the fits for solutes A and B are presented in Tables 4.11 and 4.12, respectively. There are two important results. (1) The solute order parameters have been calculated from the predictions of the model potentials using the model parameter values from these fits. For both solutes, these calculated values fall within $\sim$5% of the MC values. This suggests that fitting solute order parameters using model potentials gives essentially the same results as fitting the orientational distribution functions which provide complete information about one-particle orientational behaviour. This is a significant consideration for the analysis of NMR experiments which yields only the solute order parameters. (2) Although the model potentials provide comparable descriptions of the orientational distribution functions when separately fitting the data from individual solutes, this is not true if the results are analyzed simultaneously. This is evident from a comparison of the values of the same model parameters for solutes A and B. Since the purpose of a model potential is to provide an accurate description of orientational order for solutes of arbitrary size and shape, the parameter corresponding to the same model and nematic solvent should be independent of the characteristics of the solute. However, the parameter values for the potentials of I, II and III vary roughly by a factor of two between the different solutes for all values of $\bar{P}_2^{(nem)}$. By contrast, the parameter values for potential IV

Table 4.11: Results of Fits to Singlet Orientational Distribution Functions for Solute A with Dimensions of $l=2$ and $w=1$.

ρ^*	$\bar{P}_2^{(nem)a}$	$\bar{P}_2^a$	Model	Parameter	Value/d^{-2}	$\bar{P}_2$(calc)	RMS[b]
0.488	0.886(2)	0.58(1)	I	k^*	0.614	0.575	0.097
			II	k_s^*	8.36	0.604	0.049
			III	ϵ^*	1.81	0.583	0.062
			IV[c]	k_s^*	6.15	0.597	0.037
0.444	0.817(2)	0.44(1)	I	k^*	0.418	0.416	0.082
			II	k_s^*	5.48	0.441	0.056
			III	ϵ^*	1.22	0.422	0.066
			IV[c]	k_s^*	4.08	0.435	0.051
0.425	0.780(2)	0.38(1)	I	k^*	0.368	0.367	0.047
			II	k_s^*	4.48	0.367	0.051
			III	ϵ^*	1.07	0.372	0.035
			IV[c]	k_s^*	3.56	0.383	0.038
0.405	0.729(3)	0.30(1)	I	k^*	0.304	0.287	0.049
			II	k_s^*	3.89	0.303	0.040
			III	ϵ^*	0.884	0.295	0.040
			IV[c]	k_s^*	2.91	0.299	0.035
0.388	0.636(6)	0.21(2)	I	k^*	0.171	0.199	0.037
			II	k_s^*	2.11	0.208	0.034
			III	ϵ^*	0.494	0.201	0.033
			IV[c]	k_s^*	1.60	0.206	0.031

[a]Uncertainties in the last digit are given in parentheses.
[b]Root-mean-square deviation from fits to singlet orientational distribution functions.
[c]Fixing $k^*/k_s^*=0.0262$ as obtained from the two-parameter fit of $\bar{P}_2$ for the full set of solutes at $\rho^*=0.488$.

Table 4.12: Results of Fits to Singlet Orientational Distribution Functions for Solute B with Dimensions of l=3.33 and w=0.25.

ρ^*	$\bar{P}_2^{(nem)a}$	$\bar{P}_2^a$	Model	Parameter	Value/d^{-2}	$\bar{P}_2$(calc)	RMS[b]
0.488	0.883(2)	0.69(1)	I	k^*	0.235	0.663	0.067
			II	k_s^*	18.5	0.695	0.123
			III	ϵ^*	3.48	0.667	0.053
			IV[c]	k_s^*	6.03	0.676	0.047
0.444	0.821(2)	0.53(2)	I	k^*	0.164	0.518	0.10
			II	k_s^*	12.2	0.557	0.106
			III	ϵ^*	2.42	0.522	0.087
			IV[c]	k_s^*	4.14	0.533	0.078
0.425	0.782(2)	0.47(2)	I	k^*	0.145	0.466	0.080
			II	k_s^*	10.5	0.502	0.187
			III	ϵ^*	2.13	0.468	0.093
			IV[c]	k_s^*	3.62	0.480	0.11
0.405	0.712(5)	0.39(3)	I	k^*	0.115	0.369	0.063
			II	k_s^*	8.13	0.408	0.13
			III	ϵ^*	1.69	0.379	0.066
			IV[c]	k_s^*	2.85	0.389	0.078
0.388	0.616(9)	0.26(3)	I	k^*	0.078	0.252	0.070
			II	k_s^*	5.28	0.273	0.051
			III	ϵ^*	1.14	0.253	0.069
			IV[c]	k_s^*	1.90	0.260	0.054

[a]Uncertainties in the last digit are shown in parentheses.
[b]Root-mean-square deviation from fits to singlet orientational distribution functions.
[c]Fixing k^*/k_s^*=0.0262 as obtained from the two-parameter fit of $\bar{P}_2$ for the full set of solutes at ρ^*=0.488.

are very close for the two solutes. This is consistent with the results shown in Figure 4.14 which illustrates the superiority of this model in its ability to predict order parameters for an arbitrary collection of solutes simultaneously.

The dependence of the model parameter values on nematic order parameter $\bar{P}_2^{(nem)}$ is shown for the two solutes in Figure 4.19. The parameter values have been scaled to be unity for the highest density of ρ^*=0.488. For each solute, the values scale very similarly for all four models. Further, the $\bar{P}_2^{(nem)}$-dependence for both solutes is very similar despite the substantially different shapes of the two solutes. For each case, there is a significant increase in the slope of the curves with increasing $\bar{P}_2^{(nem)}$.

4.4.3 Comparison with Experiment

We now compare the results of the MC simulations with those of previous experimental NMR studies of solute orientational order in nematics. Specifically, we compare the interaction strength parameters obtained from the previous fit to the MC solute order parameters for each of the model parameters with those obtained from a fit to the experimental values. In order to make this comparison it is necessary to scale the parameter values in two ways.

First, it is necessary fix the length scale of the MC system. In the experimental NMR studies of Burnell and coworkers [33, 36], a 55 wt% ZLI 1132/EBBA mixture was used as the nematic solvent. Thus, we fix the solvent ellipsoid length to 20 Å , the approximate length of an EBBA nematogen and roughly the average length of the various components of the ZLI 1132 mixture. For a length to width ratio of 5:1 for the solvent ellipsoids used in the MC simulations, this corresponds to a nematogen width of 4 Å . This is narrower than a phenyl-ring width of $\sim$5 Å, but wider than the thickness of the biaxial nematogen. Thus, this is a quite reasonable approximation to the nematogen size and shape given that we are employing an axially symmetric ellipsoid.

Figure 4.19: Model Parameter Values vs. $\bar{P}_2^{(nem)}$ for (a) Solute A (l=2, w=1) and (b) Solute B (l=3.33, w=0.25).
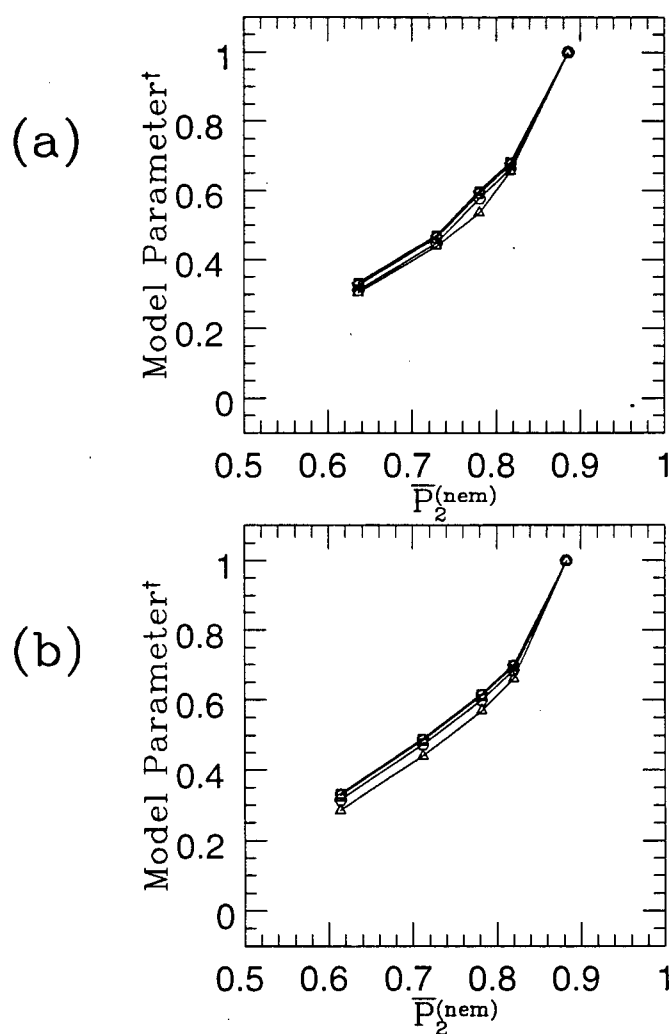
Calculated using the potentials I (triangles), II (squares), III (pentagons), and IV (hexagons). [†]Parameter values are scaled to unity for ρ^*=0.488.

Table 4.13: Scaling Ratios from Results of Fits to Singlet Orientational Distribution Functions for Solutes A and B at $\bar{P}_2^{(nem)}$=0.884 and $\bar{P}_2^{(nem)}$=0.634.

Model	Param.	Solute A[a]			Solute B[b]		
		Value(1)[c,d]	Value(2)[d,e]	Ratio[f]	Value(1)[c,d]	Value(2)[d,e,g]	Ratio[f]
I	k^*	0.614	0.205	0.333	0.235	0.0843	0.358
II	k_s^*	8.36	2.55	0.305	18.5	5.77	0.312
III	ϵ^*	1.81	0.592	0.327	3.48	1.24	0.355
IV[h]	k_s^*	6.15	1.92	0.313	6.03	2.07	0.343

[a]Solute A has dimensions of l=2 and w=1.
[b]Solute B has dimensions of l=3.33 and w=0.25.
[c]Value(1) calculated for $\bar{P}_2^{(nem)}$=0.884.
[d]Dimensions of d^{-2}.
[e]Value(2) calculated for $\bar{P}_2^{(nem)}$=0.634.
[f]Ratio = Value(2)/Value(1).
[g]Interpolated value using the results of Table 4.12.
[h]Fixing k^*/k_s^*=0.0262 as obtained from the two-parameter fit of $\bar{P}_2$ for the full set of solutes at ρ^*=0.488.

Second, it is necessary to scale the results of the fit of the MC solute order parameters to correspond to the lower experimental value of $\bar{P}_2^{(nem)}$=0.634. We therefore scale the values of the model parameters by the ratios of the values obtained by fitting the orientational distribution functions for $\bar{P}_2^{(nem)}$=0.634 and 0.884. The scaling ratios have been calculated separately for all model potentials for solutes A and B. For solute B, the nematic order parameter was slightly smaller than that for the experimental value; hence, it was necessary to interpolate the model parameter values to correspond to $\bar{P}_2^{(nem)}$=0.634, although the correction was very small. For solute A, a similar correction was negligible. The scaling ratios are listed in Table 4.13. It is encouraging that the differences in the ratios between the two solutes are small despite the significantly different shapes of the solutes.

The scaled model parameter values corresponding to the fit of the MC simulation order parameters is compared to those obtained from a fit to experimental order parameters in Table 4.10 The parameter values are remarkably close, independent of whether the scaling ratio for solutes A or B was used. The agreement is particularly noteworthy for the two-parameter potential of model IV, for which the potential strength is partitioned between its two components very similarly for fits to experimental and MC data. The fact that MC order parameters, calculated using very crude models for nematogens and solutes, reproduce the basic results observed for experimental data when analyzed using the model potentials is highly significant. It firmly establishes the physical origin of these potentials as arising from the short-range repulsive interactions in the nematic solvent. As well, it highlights the ability to gain significant insight into the nature of liquid crystal systems without the need to resort to complex intermolecular interactions.

4.5 Conclusions

Monte Carlo simulations were used to study the orientational behaviour of solutes in a uniaxial nematic liquid crystal and its dependence on the solute size and shape. Solvent and solute molecules were both modeled as hard ellipsoids. The results were analyzed in terms of four model mean-field potentials. There was remarkable agreement between the results of these simulations and those of previous experimental studies in the analysis of solute orientational order parameters: the values of the model parameters and the trends of the model predictions were very close between simulation and experiment. The results confirm that the model potentials closely approximate short-range repulsive forces in nematic liquid crystals. Further, the detailed orientational behaviour of two differently shaped solutes was investigated. The models were able to describe the angular dependence of the mean-field potential reasonably well generally, though more poorly for

the narrower solute. Finally, the degree of orientational ordering scales with the nematic order parameter $\bar{P}_2^{(nem)}$ in a solute-independent manner.

Chapter 5

Monte Carlo Simulations of Oriented Solutes (II): Shape Anisotropy and Quadrupole-Quadrupole Interactions

5.1 Introduction

There is significant experimental evidence that anisotropic short-range repulsive interactions provide an important orienting mechanism for molecules in liquid crystal phases. The orientational order parameters for a wide variety of solutes used to probe the environment of a nematic solvent can be predicted accurately by using various empirical mean-field potentials which are sensitive to the details of the size and shape of the molecules. The importance of molecular shape in describing orientational order has been seen as evidence that short-range forces are the dominant ordering mechanism. In Chapter 4, we presented results of a computer simulation study which firmly established the connection between the model potentials and the underlying repulsive forces. In this case, there were no anisotropic long-range interactions incorporated into the model system; thus, there was no ambiguity in the interpretation of the results.

While molecular shape anisotropy is a key factor in the ordering behaviour of solutes in a nematic phase, there are other important contributions to orientational ordering as well. These include long-range electrostatic and dispersion interactions. The former arise from the presence of permanent electrostatic multipole moments, while the latter arise from correlated fluctuations of the charge distributions of polarizable molecules. Interactions between permanent and induced moments are also present in such systems.

An experimental study of deuterated molecular hydrogen as a solute in a nematic liquid crystal provided direct evidence that a specific electrostatic interaction provides a mechanism for orientational ordering [13, 14]. In particular, it was found that the interaction of the molecular quadrupole moment of both D_2 and HD with a measured average electric-field gradient (EFG) provided an accurate description of orientational ordering for these particular solutes. The important results of this study were summarized in Section 1.3.2.1 of this thesis. A reasonable conclusion from this study is that all probe solutes experience a similar interaction between their quadrupole moments and an average EFG. However, to apply this result to the analysis of order parameters of other solutes, it is necessary to assume that the EFG is a property of the nematic solvent alone, and not influenced significantly by solute properties. This approximation is necessary because the EFG can only be measured directly for the deuterated hydrogens, where the internal EFG contribution to the NMR quadrupolar coupling constant can be calculated accurately.

Emsley, Luckhurst and coworkers have discussed the significance of the EFG and its effects on orientational ordering in the context of a theory for orientational ordering which is closely related to the Maier-Saupe theory of nematics [22, 24, 25]. The important results of their studies were summarized in Section 1.3.2.2. It was shown that the nematogen quadrupole moment was the lowest order multipole that provided a non-vanishing contribution to the EFG. Further, it is possible to derive an expression for both the EFG and the contribution to a potential of mean-torque arising from the presence of the EFG. However, the expressions for these quantities are complicated by their dependence on the orientational distribution of solute-solvent intermolecular vectors, a property which is not readily determinable by experimental methods. Thus, the theory and its assumptions cannot be tested easily by an analysis of available experimental data.

The description of the contribution to orientational ordering from electrostatic interactions by means of a solute-independent average EFG has been criticized by Photinos

et al. [27, 28, 29]. They provided experimental evidence that the interaction between local dipole moments on solute and solvent molecules, in conjunction with short-range repulsive forces, provide an additional ordering mechanism [27, 28]. In the context of the electrostatic mean-field approach introduced by Burnell and coworkers and developed theoretically by Emsley and Luckhurst, solute dipole moments interact with an average electric field, which is necessarily zero for an apolar nematic phase; thus, the contribution to the mean-field potential should vanish. Further, Terzis *et al.* have constructed a theory to account for the contributions from both short-range repulsive forces and arbitrary electrostatic interactions [29]. A surprising result of this study was that electrostatic interactions were predicted to provide a contribution to orientational ordering which was roughly equal to that from the anisotropic repulsive forces. In addition, it was shown that the mean-field electrostatic model of a solute molecular quadrupole moment interacting with a solute-independent mean EFG was inconsistent with their theoretical calculations. The results from these studies were summarized in Section 1.3.2.3.

The studies of Emsley, Luckhurst *et al.* and Photinos *et al.* represent the only attempts to date to provide a theoretical understanding of the orientational behaviour of molecules in nematic liquid crystals. The goal of these theories is to derive a mean-field orientational potential which incorporates the molecular properties, such as shape anisotropy and electric multipole moments, that give rise to the intermolecular interactions responsible for the alignment of molecules. There have been many other mean-field models developed to describe orientational ordering, such as those examined in Chapter 4, but these are empirical in nature and cannot be related directly to molecular properties. In the derivation of true theoretical models, there are two types of approximations employed whose validity determines the accuracy of the theory: (1) the modeling of the molecules and the pair potential, and (2) the statistical approximations required when integrating over the pair potential to obtain the mean-field potential. Unfortunately, it is

difficult to test the theory and the validity of the approximations using the experimental data alone. This problem is due to the fact that there are multiple contributions to orientational ordering. Experiment provides only a few orientational order parameters per solute, and no estimate of the relative magnitude and effect from each contribution.

Computer simulations of solutes in nematic solvents can provide an effective bridge between experiment and theory. The molecular models employed in the various theories can easily be incorporated into the simulations. A comparison of the simulation results with theory and experiment can then provide valuable insight into the validity of the models for the pair potential and the statistical approximations used in the theory. In addition, it provides a simple method for examining the importance of each component of the intermolecular pair potential as an orienting mechanism and how the complex interplay between the different contributions varies with the properties of the solute.

In this chapter, we employ the Monte Carlo computer simulation method to study the combined effects of shape anisotropy and electrostatic interactions on orientational ordering of solutes in a nematic phase. We employ a minimal model in order not to obscure the interpretation of the results. Specifically, we model both the solvent and solute molecules as cylindrically symmetric hard ellipsoids with point quadrupoles placed at their centres. The modeling of the molecular shape is precisely that used in Chapter 4, and approximates the effects of shape anisotropy on the short-range repulsive forces while keeping the model computationally convenient. In the study presented in the previous chapter, this model yielded results that were quantitatively similar to those observed in earlier experimental studies.

The use of point quadrupoles to describe the electrostatic properties of the solvent and solute molecules is likely a far more drastic approximation. At short intermolecular distances, the quadrupole-quadrupole interaction may yield an unrealistic estimate of the electrostatic interactions between molecular charge distributions. This limitation

may be particularly problematic at the high densities typical of a condensed phase. Nevertheless, there are important reasons why this model deserves to be investigated. It is important to determine the simplest model which can reproduce the main qualitative behaviour observed experimentally in real nematic systems. Further, the molecular models used in the theories of orientationally ordering described above also employ point electrostatic multipole moments. Thus, the simulations can provide a test of the statistical approximations employed in the derivation of the theoretical mean-field potentials. We focus on the effects of quadrupole moments alone, since a principal goal of this study is to investigate the interaction of the solute quadrupole moment with the EFG generated by the solvent, and because the quadrupole moment is the lowest order multipole that the Emsley-Luckhurst theory predicts to contribute to a non-vanishing EFG. There are also important practical considerations for choosing this model. More realistic descriptions of the molecular charge distributions, such as the distribution of several point multipole moments within the volume of the molecule, would involve considerably more computational effort to calculate the pair potential in the MC simulations. As well, quadrupole-quadrupole interactions decay as r^{-5}, which may be sufficiently rapid to neglect very long-range contributions to the total energy. This also has a major influence on determining the speed with which the calculations can be performed. Dipole-dipole interactions, by comparison, decay as r^{-3} and require the inclusion of much longer range contributions to the total energy, as well as the use of Ewald sums to induce the convergence of the total energy with increasing system size [130]. The result is a much more time-consuming calculation.

To summarize, the description of a solvent or solute molecule as a hard ellipsoid with a point quadrupole represents a simple model with the following attributes: (1) it is computationally convenient; (2) it can be used to test the statistical approximations in current theories of solute ordering; (3) it is a starting point to determine the basic

molecular properties required to explain orientational behaviour of solutes in nematics; (4) it can be used to investigate the individual effects of the contributions to orientational ordering from shape anisotropy and electrostatic interactions, information which is not readily obtained by experiment.

In the following section, we outline the basic ideas of the theoretical models developed by Terzis and Photinos (TP) [29] and Emsley and Luckhurst *et al.* (EL) [19, 22, 24]. Section 5.3 describes the technical details of the Monte Carlo simulations. In Section 5.4 we present the results of the simulations and discuss their significance in terms of both theoretical predictions and experimental observation. Section 5.5 summarizes the key results of this study.

5.2 Theory

5.2.1 TP Theory

Terzis *et al.* have developed a theory for the description of orientational order of solutes in a nematic solvent which can incorporate dispersion, induction, short-range repulsive, and electrostatic interactions between the solute and solvent molecules [29]. We present a brief outline of the derivation of the mean-field orientational potential, considering only the effects of the latter two interactions.

The theoretical approach involves the reduction of the singlet distribution function of the solute, which is given by the following exact expression:

$$P(X) = Z^{-1} \int dX_1 dX_2 ... dX_N \tilde{P}_N(X_1, X_2, ..., X_N) \exp\left[-\sum_{i=1}^{N} u(X, X_i)/k_B T \right], \quad (5.86)$$

where $X \equiv (\vec{r}, \omega)$, $\tilde{P}_N(X_1, X_2, ..., X_N)$ is the N-particle solvent distribution function in the absence of the solute, $u(X, X_i)$ is the pair potential between the solute and the ith solvent molecule, and Z is a normalizing factor. The principal approximation of the

theory is to neglect the correlations between solvent molecules,

$$\tilde{P}_N(X_1, X_2, ..., X_N) \approx \tilde{P}(X_1)\tilde{P}(X_2)...\tilde{P}(X_N), \tag{5.87}$$

which simplifies the expression of the solute distribution function to the following:

$$P(X) \sim \left[\int dX' \tilde{P}(X') \exp\left(-u(X, X')/k_B T\right) \right]^N \tag{5.88}$$

Short-range repulsive forces are approximated by a hard-core (HC) interaction between molecules, which can take the values of zero or infinity depending on whether the molecules overlap. Anisotropic long-range interactions are restricted in this treatment to electrostatic forces. Thus, the pair potential can be written as

$$u(X, X_i) = u_{HC}(X, X_i) + u_{ES}(X, X_i) \tag{5.89}$$

Further, for spatially homogeneous systems, $P(X) = f(\omega)/V$ and $\tilde{P}(X) = \tilde{f}(\omega)/V$. Thus, the solute orientational distribution function can be written as the following:

$$f(\omega) \sim \left[V^{-1} \int d\omega' d\vec{r} \tilde{f}(\omega') \left\{ 1 - K(\vec{r}, \omega, \omega') \right\} \right]^N \equiv \left[1 - \langle K \rangle \right]^N \tag{5.90}$$

where

$$K(\vec{r}, \omega, \omega') = 1 - g_{HC} \exp(-u_{ES}/k_B T), \tag{5.91}$$

and where

$$g_{HC} = \exp\left(-u_{HC}/k_B T\right) \tag{5.92}$$

Note that $K = 1$ for overlapping particles and decays to zero with increasing r, though it has appreciable values for a small localized volume v_a, where $v_a^{1/3}$ is of the order of a few molecular diameters. The solute distribution function may be written

$$f(\omega) \sim \exp\left(N \ln(1 - \langle K \rangle)\right). \tag{5.93}$$

Expanding the logarithm and neglecting terms of order $(v_a/V)^2$ and higher, it is trivial to show that

$$f(\omega) \sim \exp\left[-N\langle K(\omega)\rangle\right]. \tag{5.94}$$

This corresponds to the following terms for the mean-field potential:

$$U(\omega) = U_{HC}(\omega) + U_{ES}(\omega), \tag{5.95}$$

where

$$U_{HC}(\omega)/k_BT = \rho \int d\vec{r}d\omega' \tilde{f}(\omega') \left[1 - g_{HC}(\vec{r}, \omega, \omega')\right] \tag{5.96}$$

and

$$U_{ES}(\omega)/k_BT = \rho \int d\vec{r}d\omega' \tilde{f}(\omega') \left[1 - \exp\left(-u_{ES}(\vec{r}, \omega, \omega')/k_BT\right)\right] g_{HC}(\vec{r}, \omega, \omega') \tag{5.97}$$

As a final remark on the mean-field potential, we note that the contribution from the hard-core component of the pair potential can be written as

$$U_{HC}(\omega)/k_BT = \rho \int d\omega' V_{ex}(\omega, \omega')\tilde{f}(\omega'), \tag{5.98}$$

where $V_{ex}(\omega, \omega')$ is the orientation-dependent solute-solvent excluded volume. As discussed in Section 1.3.2.3, this is the same form of the potential that appears in the self-consistent expression in Onsager's theory for the distribution function for a system of long hard rods [7], as described in Section 1.2.2.1. This is not surprising, since both theories consider the effects of interactions of pairs of molecules while neglecting correlations due to three and more particles. Onsager's theory is valid in the limit of very long rods where the effects of these higher order correlations are negligible. While the typical nematogen and solute molecules do not satisfy this condition, Terzis *et al.* have argued that neglecting solvent-solvent interactions should have minor effects if the system is sufficiently far removed from the phase transition. This assumption can be tested by comparing the results of computer simulations and the theoretical predictions for solutes in nematic systems.

5.2.2 EL Theory

A theoretical model for describing the orientational ordering of solutes in a uniaxial nematic solvent which was developed by Emsley, Luckhurst *et al.* [19] was introduced in Section 1.3.2.2. The approach of this theory is closely related to that used in the Maier-Saupe theory of nematic liquid crystals. A mean-field orientational potential is derived using some simplified model for the pair potential between solvent and solute molecules and averaging over the magnitude and direction of the intermolecular displacement, and over the orientation of the solvent molecules. The relationship between the mean-field and pair potentials is given by:

$$U(\omega_1) = \rho \int d\vec{r} d\omega_2 u(\vec{r}, \omega_1, \omega_2) \tilde{f}(\omega_2) g(\vec{r}) \tag{5.99}$$

where $\omega_1 \equiv (\theta_1, \phi_1)$ and $\omega_2 \equiv (\theta_2, \phi_2)$ are the polar angles describing the orientation of the nematic director in the solute and solvent molecular frames, respectively. Also, $\vec{r}$ is the intermolecular displacement, ρ is the number density of the solvent, $u(\vec{r}, \omega_1, \omega_2)$ is the solvent-solute pair potential, $\tilde{f}(\omega_2)$ is the solvent orientational distribution function (ODF), and $g(\vec{r})$ is the pair correlation function. The crucial approximation of this theory involves neglecting the orientational correlations between molecules, i.e. $g(\vec{r}, \omega_1, \omega_2) \approx g(\vec{r})$.

Most applications of the Emsley-Luckhurst theory to the analysis of experimental data have employed long-range anisotropic dispersion forces, though the incorporation of an electrostatic interaction between quadrupoles to the pair potential has been discussed [22, 24]. Below, we derive the mean-field potential between quadrupoles for the case of axially symmetric molecules.

The energy of two interacting axially symmetric quadrupole moments may be written

as

$$u_{QQ}(\vec{r}, \omega_1, \omega_2) = (4\pi)^{\frac{3}{2}} \sqrt{\frac{14}{45}} \left(\frac{Q_{2,0}^{(u)} Q_{2,0}^{(v)}}{4\pi\epsilon_0 r^5} \right) \sum_{m_1, m_2, m} C(224; m_1, m_2, m) Y_{2,m_1}(\omega_1)$$
$$\times Y_{2,m_2}(\omega_2) Y_{2,m}^*(\omega), \qquad (5.100)$$

where $C(224; m_1, m_2, m)$ are Clebsch-Gordon coefficients, $\omega \equiv (\theta, \phi)$ describe the orientation of the intermolecular vector in the frame of the nematic director, and $Q_{2,0}^{(\alpha)} = \sqrt{\frac{5}{4\pi}} Q_{zz}^{(\alpha)}$, where $Q_{zz}^{(\alpha)}$ is the principal cartesian component of the quadrupole moment tensor for the solute ($\alpha = u$) and solvent ($\alpha = v$). Substitution of Eq. (5.100) into Eq. (5.99) yields

$$U(\theta) = \frac{\sqrt{280\pi}}{3} \rho \left(\frac{Q_{zz}^{(u)} Q_{zz}^{(v)}}{4\pi\epsilon_0} \right) \sum_{m_1, m_2, m} C(224; m_1, m_2, m) Y_{2,m_1}(\omega_1) \langle Y_{2,m_2} \rangle \left\langle \frac{Y_{4,m}^*}{r^5} \right\rangle, \qquad (5.101)$$

where

$$\langle Y_{2,m_2} \rangle = \int d\omega_2 \tilde{f}(\omega_2) Y_{2,m_2}(\omega_2), \qquad (5.102)$$

and where

$$\left\langle \frac{Y_{4,m}^*}{r^5} \right\rangle = \int \frac{Y_{4,m}^*(\omega)}{r^5} g(\vec{r}) r^2 dr d\omega. \qquad (5.103)$$

In the case of axial symmetry considered here, Eq. (5.102) reduces to

$$\langle Y_{2,m_2} \rangle = \sqrt{\frac{5}{4\pi}} \bar{P}_2^{(nem)} \delta_{m_2, 0}, \qquad (5.104)$$

where $\bar{P}_2^{(nem)}$ is the second-rank nematic order parameter, while Eq. (5.103) reduces to

$$\left\langle \frac{Y_{4,m}^*}{r^5} \right\rangle = 6\sqrt{\pi} \delta_{m,0} \int \frac{\bar{P}_4^+(r) g(r)}{r^3} dr, \qquad (5.105)$$

where

$$\bar{P}_4^+(r) = \int d\theta \sin\theta P_4(\cos\theta) P(\theta; r), \qquad (5.106)$$

and where $P(\theta; r)$ is the probability of finding a solvent molecule at angle θ relative to the nematic director for a particular intermolecular distance r given that the solute is at

the origin. Finally, substitution of Eqs. (5.104) and (5.105) into Eq. (5.101) yields

$$U(\theta) = 60\pi\rho \left(\frac{Q_{zz}^{(u)}Q_{zz}^{(v)}}{4\pi\epsilon_0} \right) \bar{P}_2^{(nem)} \left[\int \frac{\bar{P}_4^+(r)g(r)}{r^3} dr \right] P_2(\cos\theta) \qquad (5.107)$$

Noting that the form of the interaction between a quadrupole moment and an EFG is given by

$$U(\theta) = -\frac{1}{2}F_{ZZ}Q_{zz}P_2(\cos\theta), \qquad (5.108)$$

Eq. (5.107) can be used to define an average EFG:

$$\bar{F}_{ZZ} = -120\pi\rho Q_{zz}^{(v)} \bar{P}_2^{(nem)} \int \frac{\bar{P}_4^+(r)g(r)}{r^3} dr \qquad (5.109)$$

It is convenient to rewrite the expressions for the mean-field potential and the average EFG in terms of dimensionless quantities. We define a reduced mean-field potential $U^*(\theta) \equiv U(\theta)/k_BT$:

$$U^*(\theta) = 60\pi Q_u^* Q_v^* \rho^* \left(\frac{d^3}{v_0} \right) \left[\int \frac{\bar{P}_4^+(r^*)g(r^*)}{(r^*)^3} dr^* \right] P_2(\cos\theta), \qquad (5.110)$$

where $Q_\alpha^* = Q_{zz}^{(\alpha)}/\sqrt{4\pi\epsilon_0 k_B T d^5}$, $\rho^* = \rho v_0$, $r^* = r/d$, v_0 is the solvent ellipsoid volume, and where d, the diameter of the solvent ellipsoid, is used to fix the length scale in the system. Further, we define a dimensionless EFG:

$$\bar{F}_{ZZ}^* \equiv \frac{F_{ZZ}d^5}{\mid Q_{zz}^{(v)} \mid} = -120\pi\rho^* \left(\frac{d^3}{v_0} \right) \left(\frac{Q_{zz}^{(v)}}{\mid Q_{zz}^{(v)} \mid} \right) \bar{P}_2^{(nem)} \int \frac{\bar{P}_4^+(r^*)g(r^*)}{(r^*)^3} dr^*. \qquad (5.111)$$

Finally, comparing Eqs. (5.110) and (5.111), we can write

$$U^*(\theta) = -\frac{1}{2}\bar{F}_{ZZ}^* \mid Q_v^* \mid Q_u^* P_2(\cos\theta). \qquad (5.112)$$

In the context of the theory presented above, an essential requirement for the observation of a non-vanishing average EFG is a non-spherical distribution of solute-solvent inter-molecular vectors. If this distribution had spherical symmetry, then the factor defined in Eq. (5.103) would vanish for all values of m, along with the magnitude of the EFG. This

point was first noted by Emsley *et al.* who incorporated this factor into the derivation of the contribution to the mean-field orientational potential from quadrupole-quadrupole interactions [22]. However, this derivation had implicitly assumed the separability of averaging the pair potential over the magnitude and direction of the intermolecular vector $\vec{r}$:

$$\left\langle \frac{Y_{4,m}^*}{r^5} \right\rangle \approx \langle Y_{4,m}^* \rangle \langle r^{-5} \rangle \sim \bar{P}_4^+ \delta_{m,0} \langle r^{-5} \rangle \tag{5.113}$$

However, the computer simulations of Emerson *et al.* [26] indicate that the fourth-rank order parameter $\bar{P}_4^+$, which describes the non-sphericity of the intermolecular-vector distribution, is strongly dependent on the molecular separation r, and that therefore the separability of the averaging in Eq. (5.113) is invalid. The mean-field potential derived above for the quadrupole-quadrupole pair potential differs from that derived originally by Emsley *et al.* by using Eq. (5.105) rather than Eq. (5.113) for averaging over the intermolecular coordinates.

5.3 MC Simulations

The methods employed in the simulation of solutes in a nematic solvent are similar to those used in Chapter 4. The calculations were performed at constant volume for a fixed number of particles confined to a rectangular box subject to the usual periodic boundary conditions. The calculations used a system of 239 solvent particles plus one solute particle. Nematogens were modeled as cylindrically symmetric hard ellipsoids with an axis ratio of 5:1. Solutes were also modeled as cylindrically symmetric hard ellipsoids, though with a variety of sizes and axis ratios. An equilibration period of 1-2×10^5 trial moves per particle was used, starting from an initial configuration where all of the molecules were orientationally aligned and positioned on a FCC lattice.

The sequence of system configurations was generated using the Metropolis algorithm,

which was described in Section 1.5. In some of the simulations, only a hard-core pair interaction between molecules was considered. In this case, trial orientational and translational moves for each randomly chosen particle were rejected if it resulted in overlap with any of the other particles, and accepted if there was no overlap—precisely the same procedure as described Chapter 4. However, in the present study, most of the calculations involved systems of particles with an additional interaction between point quadrupoles positioned at the centres of the ellipsoids. For such systems, the Metropolis algorithm is applied as follows. Trial configurations are first tested for overlap. If particles overlap, then the configuration is rejected. If the particles do not overlap, the quadrupole-quadrupole energy of the total system is calculated and compared to that of the previous configuration. If $\Delta E < 0$, then the move is accepted; if $\Delta E > 0$, then the configuration is accepted with a probability given by $e^{-\Delta E/k_B T}$. The maximum displacements and rotations were chosen to contribute approximately equally to the likelihood that a particle move would be rejected, and to yield an overall acceptance ratio of in the range of 40–60% in order to achieve equilibrium as rapidly as possible.

The solvent-solvent quadrupolar pair potential was calculated using the following relation for the interaction between axially-symmetric quadrupoles:

$$
u_{QQ} = \frac{3}{4}\left(\frac{Q_{zz}^{(1)}Q_{zz}^{(2)}}{4\pi\epsilon_0 r^5}\right)[1 - 5\cos^2\theta_1 - 5\cos^2\theta_2 + 2\cos^2\theta_{12}
$$
$$
+35\cos^2\theta_1\cos^2\theta_2 - 20\cos\theta_1\cos\theta_2\cos\theta_{12}], \tag{5.114}
$$

where θ_1 and θ_2 are the angles between the quadrupole symmetry axis and the displacement vector between the point quadrupoles, and θ_{12} is the angle between the two quadrupole symmetry axes. The EFG at the site of the solvent was calculated using the following expression for the EFG due to a point quadrupole moment:

$$
F_{\mu\nu} \equiv \nabla_\mu E_\nu = -\nabla_\mu \nabla_\nu \phi
$$

$$= \frac{1}{r^5}[-2Q_{\mu\nu} + 10Q_{\alpha\nu}\hat{r}_\alpha\hat{r}_\mu + 10Q_{\mu\alpha}\hat{r}_\alpha\hat{r}_\nu + 5Q_{\alpha\beta}\hat{r}_\alpha\hat{r}_\beta\delta_{\mu\nu}$$

$$-35Q_{\alpha\beta}\hat{r}_\alpha\hat{r}_\beta\hat{r}_\mu\hat{r}_\nu], \tag{5.115}$$

where $\hat{r}$ is a unit vector describing the orientation of the displacement between the quadrupole pair, and where we have used the Einstein summation convention for repeated indices. The solute-solvent pair potential is a function of the EFG due to the solvent:

$$\begin{aligned} u_{QQ} &= -\frac{1}{6}Q_{\mu\nu}F_{\mu\nu} \\ &= -\frac{1}{6}Q_{\alpha\beta}^{(P)}\cos\theta_{\alpha\mu}\cos\theta_{\alpha\nu}F_{\mu\nu}, \end{aligned} \tag{5.116}$$

where $Q_{\mu\nu}$ and $Q_{\mu\nu}^{(P)}$ are the quadrupole moments in the laboratory and principal axis system (PAS) frames, respectively, and $\cos\theta_{\alpha\mu}$ is the angle between the PAS α-axis and the laboratory μ-axis.

The total energy is obtained by summing the pair potentials over all of the particles in the system and averaging over the sequence of configurations which are generated by the Metropolis algorithm. In certain cases for long-range interactions, it is necessary to include contributions to the total energy from particles that are very widely spaced in order to minimize truncation effects. For a finite-sized simulation system, this often requires a summation over molecules in repeated images of the system. However, this greatly increases the time required to perform a simulation. In the present case, the quadrupole-quadrupole pair potential decays as r^{-5}, which was found to be sufficiently rapid to eliminate the need to perform such a lattice summation. The energy of a single molecule was calculated by summing over the pair potentials between it and all other molecules within a radius given by half the smallest dimension of the sample cell. For a density of $\rho^*=0.42$, this corresponds to a distance of $r=4.96d$, where d is the width of a solvent ellipsoid. When this maximum distance was doubled, the calculated energy of the system and of each of the molecules, and the EFG sampled by the solute, was found

to change by <1% for each of several different system configurations. Further, ensemble averages of various quantities of interest were not affected by increasing the sampling range.

Most of the simulations for the quadrupolar systems were performed at $Q_v^* = -\sqrt{2.5}$ and ρ^*=0.42. The choice of Q_v^* falls at the lower end of a range of values ($\mid Q_v^* \mid \approx 0.75$–4.0) suitable for T=300 K and $d \approx 5$ Å using the results of a study which employed a simple atom-dipole method for approximating the quadrupole moment for rigid conformers of various real nematogens. The use of higher values of Q_v^* was found to promote the formation of a smectic phase in the model system and was therefore avoided. Note that we neglect the axial asymmetry of the $Q_{\alpha\beta}^{(v)}$ tensor present in real molecules.

The nematic order parameter $\bar{P}_2^{nem}$ was determined by calculating the largest eigenvalue of the following matrix:

$$\langle \mathbf{Q} \rangle = \frac{1}{N} \sum_{i=1}^{N} \left\langle \frac{3}{2} \hat{u}_i \hat{u}_i - \frac{1}{2} \mathbf{I} \right\rangle, \tag{5.117}$$

where N is the number of solvent molecules, and $\hat{u}_i$ is a unit vector describing the orientation of the ith solvent molecule. The brackets $\langle \ \rangle$ denote an ensemble averaging over the sequence of configurations generated by the MC Markov process. The nematic director is given by the eigenvector corresponding to this eigenvalue. In addition to the nematic order parameter, the following functions were also calculated:

- the solvent orientational distribution function $\tilde{f}(\theta)$

- the solvent-solvent pair correlation function $g_{vv}(r^*)$

- the second-rank solvent-solvent orientational correlation function $\bar{P}_2^{(vv)}(r^*)$ defined as follows:

$$\bar{P}_2^{(vv)}(r^*) = \frac{1}{N(N-1)} \sum_{i \neq j}^{N} \langle P_2(\cos \theta_{ij}) \rangle, \tag{5.118}$$

where θ_{ij} is the angle between solvent ellipsoids i and j

- the solute orientational order parameter $\bar{P}_2$

- the solute orientational distribution function $f(\theta)$

- the average EFG tensor at the center of the solute $\bar{F}_{\alpha\beta}$ in the frame of the nematic director

- the solute-solvent radial distribution function $g_{uv}(r^*)$

- the solute-solvent orientational correlation function $\bar{P}_2^{(uv)}(r^*)$, defined in an analogous manner as $\bar{P}_2^{(vv)}(r^*)$ above

- the fourth-rank orientational order parameter for the distribution of solute-solvent intermolecular displacements $\bar{P}_4^+(r^*)$ defined in Eq. (5.106)

All of the measured quantities described above were calculated by averaging over typically $8-9\times10^5$ configurations. In order to calculate properly all quantities that are measured with respect to the nematic director, which undergoes orientational fluctuations over the course of a simulation, the director was recalculated after every 10^1-10^2 attempted moves per particle. All calculated quantities which are functions of orientation with respect to the director were calculated for $\cos\theta$ in the range of 0 to 1 in increments of 0.01. Further, the quantities which depend on the intermolecular separation r were calculated to a distance of half the minimum dimension of the sample cell (e.g. 4.96d for $\rho^*=0.42$) in increments of 0.05d. Solute and solvent orientational order parameters and EFG tensor components were calculated in 80-90 block averages of 10^4 sweeps through the system. The fluctuations of these averages were used to provide an estimate of the uncertainties of these quantities.

Table 5.14: MC and Theoretical Solute Order Parameters for a Hard-Core System

ρ^*	l^a	w^a	$\bar{P}_2$ (MC)	$\bar{P}_2$ (Th)[b]	$\bar{P}_2^{nem}$
0.388	0.65	1.0	-0.05(1)	-0.030	0.627(4)
	2.0	1.0	0.24(1)	0.077	0.626(4)
	2.0	0.5	0.23(1)	0.083	0.629(4)
	5.0	1.0	0.63(1)	0.308	0.626(4)
0.44	0.65	1.0	-0.13(1)	-0.043	0.814(4)
	2.0	1.0	0.50(1)	0.077	0.811(4)
	2.0	0.5	0.34(1)	0.124	0.810(4)
	5.0	1.0	0.81(1)	0.458	0.811(4)

[a] Units of solvent ellipsoid width d.
[b] Calculated using Eq. (5.96).

5.4 Results and Discussion

5.4.1 Hard-Core System

Orientational distribution functions for four different solutes were calculated for two different densities for a system employing only hard-core interactions. The MC distributions are shown in Figures 5.20 and 5.21. The corresponding second-rank solute orientational order parameters are listed in Table 5.14. The variation of the distributions with solute shape and solvent density is similar to that observed for the calculations described in Chapter 4. Increasing the length of the solute results in an increase in the degree of orientational ordering. This is evident in Figure 5.20 which shows distributions for solutes with dimensions of l=5.0 and w=1.0, and l=2.0 and w=1.0. Further, increasing the solvent density, and therefore the degree of solvent orientational order, leads to a corresponding increase in solute orientational order. Note that the oblate solute with dimensions of l=0.65 and w=1.0 prefers to orient with its symmetry axis perpendicular

Figure 5.20: Calculated and Theoretical Solute Orientational Distribution Functions for a Hard-Core System (I)

$\rho^* = 0.388$ $\rho^* = 0.44$
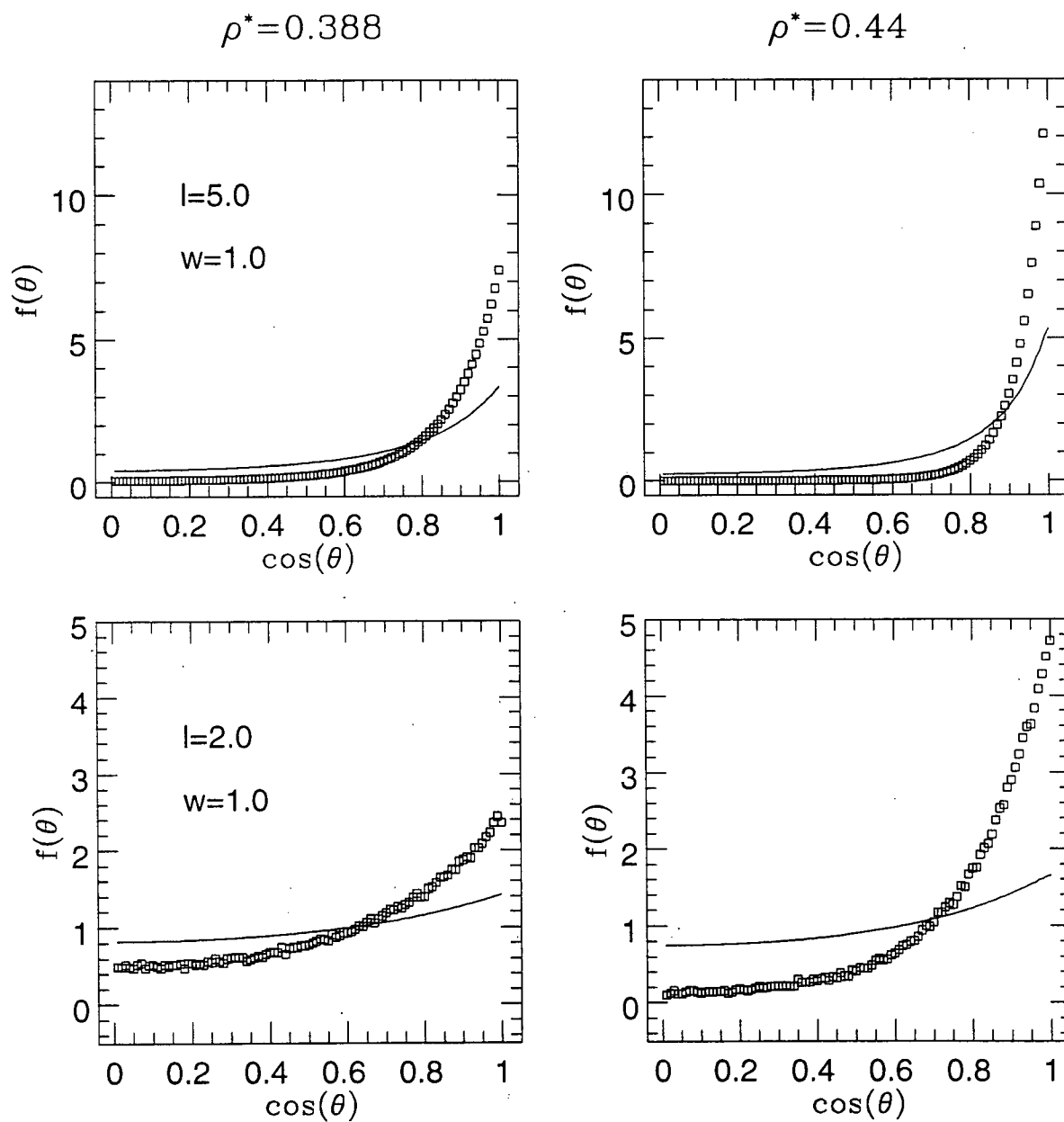
MC data (squares) and predictions from TP Theory using Eq. (5.96) (solid line).

Figure 5.21: Calculated and Theoretical Solute Orientational Distribution Functions for a Hard-Core System (II)
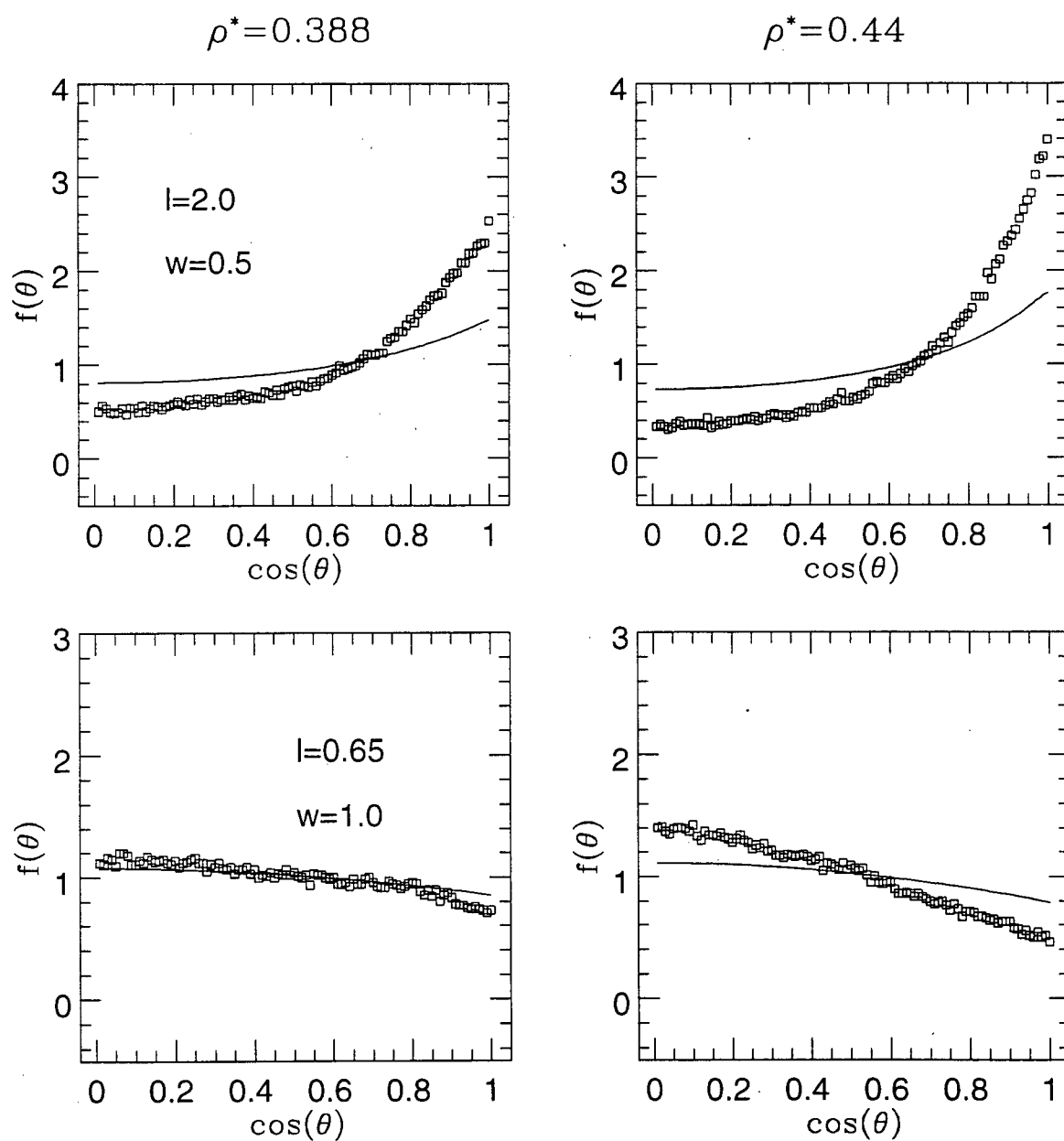
MC data (squares) and predictions from TP Theory using Eq. (5.96) (solid line).

to the nematic director resulting in a distribution maximum at $\theta=90°$ and a negative order parameter.

We use the results of these simulations to test the predictions of the TP theory using the mean-field potential due to hard body interactions given by Eq. (5.96) or equivalently by Eq. (5.98). The orientation-dependent excluded volume $V_{ex}(\omega, \omega')$, which for axially symmetric ellipsoids is a function of only the angle between the symmetry axes, was calculated through a numerical integration over the magnitude and direction of the solute-solvent intermolecular vector. The results for the case of identical 5:1 ellipsoids were consistent with those reported by Tjipto-Margo *et al.* [12] Note that the potential of Eqs. (5.96) and (5.98) is expressed in terms of the solvent orientational distribution function $\tilde{f}(\omega)$. Thus, in order to calculate the solute distribution, we use the solvent distribution calculated in the MC simulation. Note that in the study of Terzis *et al.*, the mean-field potentials were rewritten in terms of the solvent order parameters $\bar{P}_2^{(nem)}$ and $\bar{P}_4^{(nem)}$, with higher order contributions neglected. The values of these quantities are not reported and thus were estimated; values were chosen in order to yield calculated order parameters to be consistent with experimentally measured order parameters for several molecules. Clearly, the MC technique provides a superior method to test the approximations of the theory.

The calculated theoretical distribution functions are overlaid on the plots of the MC distributions in Figures 5.20 and 5.21 for the four different solutes for the densities of $\rho^*=0.388$ and 0.44. In all cases the TP theory drastically underestimates the degree of orientational order observed in these hard-core systems. This contrast is further illustrated by comparing the theoretical and calculated second rank order parameters $\bar{P}_2$ in Table 5.14. A notable case is that of the solute which is identical to the solvent particles ($l=5$, $w=1$). In this case, the MC orientational distribution function of the solute is identical to the solvent distribution which was used in the calculation of the theoretical solute

ODF; thus, the very poor agreement between theory and simulation highlights the lack of internal self-consistency of the theory. Clearly, the hard-core component of the TP mean-field potential given by Eq. (5.96) gives an inadequate description of orientational ordering for hard-core systems.

The flaw in the TP theory must be due to the approximation of neglecting solvent-solvent correlations, which is expressed in Eq. (5.87). This is not a surprising finding given the high density of the nematic phase, coupled with the short-range nature of the interaction. It is analogous to the poor quantitative predictions of Onsager theory, which accounts for only two-particle correlations, when applied to hard particles of realistic length/width ratios. In the study by Tjipto-Margo *et al.* [12], an additional term involving the third virial coefficient (which accounts for three-body correlations) in the expression for the free energy for a system of hard ellipsoids with a dimension ratio of 5:1 was included; this approach yielded an adequate quantitative description of nematogen ordering. Similarly, the TP theory requires a more careful treatment of many-particle correlations, beyond the consideration of solute-solvent effects alone, in order to provide a reasonable description of solute orientational behaviour. Such a modification, however, may be difficult to incorporate into the framework of the theory.

5.4.2 Quadrupolar Systems

Table 5.15 lists the $\bar{P}_2$ and $\bar{F}_{ZZ}^*$ calculated for simulations employing a wide variety of solute shapes and quadrupole moments. The nematic solvent was characterized by a reduced density of $\rho^* = 0.42$, and by quadrupole moments with values of $Q_v^* = -\sqrt{2.5}$. The nematic order parameter was found to be $\bar{P}_2^{(nem)} = 0.76 \pm 0.01$, with some minor variations between systems with different solutes; specific values are listed in Table 5.15. Further, the table shows the theoretical $\bar{F}_{ZZ}^*$ calculated using Eq. (5.111) and theoretical predictions of $\bar{P}_2$ for spherical solutes using the reduced mean-field potential of Eq. (5.112)

Table 5.15: EFG and Order Parameters for Several Solutes at ρ^*=0.42 and $(Q_v^*)^2$=2.5

Shape	Dimensions	$Q_u^* Q_v^{*a}$	$\bar{F}_{ZZ}^*(MC)^a$	$\bar{F}_{ZZ}^*(Th)^b$	$\bar{P}_2$ (MC)	$\bar{P}_2$ (Th)^c	$\bar{P}_2^{(nem)}$
Spherical	l=1.0	-2.5	1.8 (2)	1.5	0.26(2)	0.50	0.749(3)
	w=1.0	-2.0	1.0 (1)	0.9	0.15(2)	0.19	0.750(3)
		-1.5	0.5(1)	0.5	0.07(1)	0.08	0.761(2)
		0.0	0.05(3)	0.15	0.01(1)	0.0	0.751(3)
		1.5	0.5(1)	0.4	-0.03(2)	-0.05	0.756(2)
		2.0	1.4(1)	1.4	-0.10(2)	-0.22	0.756(2)
		2.5	2.2 (2)	2.4	-0.16(2)	-0.32	0.758(2)
Spherical	l=0.75	-1.5	3.8(2)	3.9	0.29(2)	0.59	0.757(2)
	w=0.75	-1.0	1.1(1)	1.1	0.09(1)	0.12	0.754(2)
		0.0	0.04(3)	0.07	0.01(1)	0.0	0.761(2)
		1.0	1.8(1)	1.7	-0.06(1)	-0.14	0.757(2)
		1.5	5.4(3)	4.9	-0.19(2)	-0.36	0.757(2)
Oblate	l=0.65	-1.5	-0.8 (1)	-0.9	-0.11(1)	–	0.759(2)
	w=1.0	-0.75	-0.32(4)	-0.39	-0.12(1)	–	0.751(2)
		0.0	-0.01(3)	-0.05	-0.09(1)	–	0.756(2)
		0.75	2.1(1)	2.0	-0.14(1)	–	0.761(2)
		1.5	11.8(4)	15.5	-0.37(2)	–	0.752(2)
Prolate	l=2.0	-2.5	2.7 (1)	3.0	0.56(2)	–	0.762(2)
	w=1.0	-1.5	1.0 (1)	1.0	0.39(3)	–	0.758(2)
		0.0	-0.01(3)	-0.02	0.30(2)	–	0.753(2)
		1.5	-0.39(3)	-0.39	0.37(2)	–	0.768(2)
		2.5	-0.66(4)	-0.70	0.40(2)	–	0.761(2)
Prolate	l=5.0	-2.5	3.5 (1)	4.6	0.81(1)	–	0.768(2)
	w=1.0	0.0	-0.04(3)	-0.14	0.80(1)	–	0.772(2)
		2.5	-1.16(5)	-1.50	0.78(2)	–	0.763(2)

^{a}Calculated using $Q_{zz}^{(v)} = -\sqrt{2.5} < 0$; using $Q_{zz}^{(v)} = +\sqrt{2.5} > 0$ simply reverses the sign of $\bar{F}_{ZZ}^*$.
^{b}Calculated using Eq. (5.111).
^{c}Calculate using Eq. (5.112).

of the EL theory. Note that $\bar{F}_{ZZ}^*$ calculated in both the MC simulations and by EL theory is proportional to $Q_{zz}^{(v)}$ (see Eqs. (5.115) and (5.111)). Thus, the sign of $\bar{F}_{ZZ}^*$ is determined by the sign of $Q_{zz}^{(v)}$, which in the present calculations was taken to be $Q_{zz}^{(v)} < 0$. Using a positive value of $Q_{zz}^{(v)}$ simply reverses the sign of $\bar{F}_{ZZ}^*$ but otherwise has no effect on the calculated quantities.

The most striking result is the strong dependence of $\bar{F}_{ZZ}^*$ on the shape and quadrupole moment of the solute. This is in contrast to the solute-independent model put forward by Burnell and coworkers. For the case of spherical solutes, $\bar{F}_{ZZ}^*$ increases in magnitude for increasing $|Q_u^*|$, though it is approximately symmetric with respect to changing the sign of Q_u^*, since the sign of $\bar{F}_{ZZ}^*$ is consistently positive. This is clearly not the case for the non-spherical solutes where the shape anisotropy breaks the symmetry and $\bar{F}_{ZZ}^*$ undergoes concomitant change in sign with Q_u^*. Thus, for the oblate solute, $\bar{F}_{ZZ}^* < 0$ for $Q_u^* Q_v^* < 0$, and $\bar{F}_{ZZ}^* > 0$ for $Q_u^* Q_v^* < 0$. The trend is the reverse for the small prolate solute ($l=2$, $w=1$).

The dependence of $\bar{F}_{ZZ}^*$ on Q_u^* is qualitatively consistent with the behaviour of the measured orientational order parameters $\bar{P}_2$ in the context of a mean-field EFG-quadrupole moment interaction given by Eqs. (5.108) or (5.112). In the case of the spherical solutes, the consistently positive $\bar{F}_{ZZ}^*$ is predicted successfully by Eq. (5.112) to give $\bar{P}_2 > 0$ for $Q_u^* > 0$ and $\bar{P}_2 < 0$ for $Q_u^* < 0$ (for the present case where $Q_v^* < 0$). This is also consistent with the expected behaviour of $\bar{P}_2$ based on a consideration of the quadrupole-quadrupole pair potential alone. For axially symmetric quadrupole moments of the same sign, the minimum energy orientational configuration is a perpendicular arrangement of the symmetry axes; thus, a negative order parameter is expected. For quadrupole moments of opposite signs, a parallel configuration corresponds to the lowest energy, and thus, a positive $\bar{P}_2$ is predicted.

The asymmetry of $\bar{F}_{ZZ}^*$ for the non-spherical solutes is also consistent with the behaviour of the calculated orientational order parameters $\bar{P}_2$, referenced with respect to the systems with $Q_u^*=0$. For the case of the oblate solute, the negative $\bar{P}_2$ is enhanced by the positive $\bar{F}_{ZZ}^*$, which is present for $Q_u^*Q_v^* > 0$. Again, this is consistent with the expectation based on the orientation-dependence of the quadrupole-quadrupole pair potential. However, a somewhat surprising result is the (minor) enhancement of the negative $\bar{P}_2$ for the case of opposite signs of solvent and solute quadrupole moments, where the lowest pair potential energy configuration corresponds to a parallel arrangement of the quadrupole symmetry axes. While the corresponding case for spherical solutes gave rise to an alignment of the solute symmetry axis along the nematic director, the nature of the shape anisotropy for the oblate solute appears to frustrate that outcome.

The analogous situation is present for prolate solute with dimensions of $l=2$ and $w=1$. In this case, the expected enhancement of the positive value of $\bar{P}_2$, relative to the case of $Q_u^*=0$, for $Q_u^*Q_v^* < 0$ is observed, as well as an unexpected enhancement of $\bar{P}_2$ for $Q_u^*Q_v^* > 0$. Again, the increase in solute orientational ordering with $\mid Q_u^*Q_v^* \mid$ regardless of the sign of $Q_u^*Q_v^*$ is consistent with the change in sign of $\bar{F}_{ZZ}^*$.

In the case of the large prolate solute, with dimensions equal to those of the solvent ellipsoids ($l=5.0$, $w=1.0$), $\bar{F}_{ZZ}^*$ has a similar dependence on $Q_u^*Q_v^*$ relative to the case of the smaller prolate ellipsoid. Note however that the orientational ordering is not significantly affected by the details of the electrostatic interactions. Thus, orientational ordering of highly elongated particles in a dense nematic phase appears to be dominated by entropic considerations, in keeping with the belief that molecular shape anisotropy, in conjunction with short-range repulsive forces, is the dominant ordering mechanism for nematogens.

The full orientational distribution functions for three solutes are plotted for $Q_u^*Q_v^* = 0, \pm 2.5$ in Figure 5.22. The trends present in the behaviour of the $\bar{P}_2$ for each of the solutes

Figure 5.22: Solute Orientational Distribution Functions at $(Q_v^*)^2 = 2.5$ and $\rho^* = 0.42$
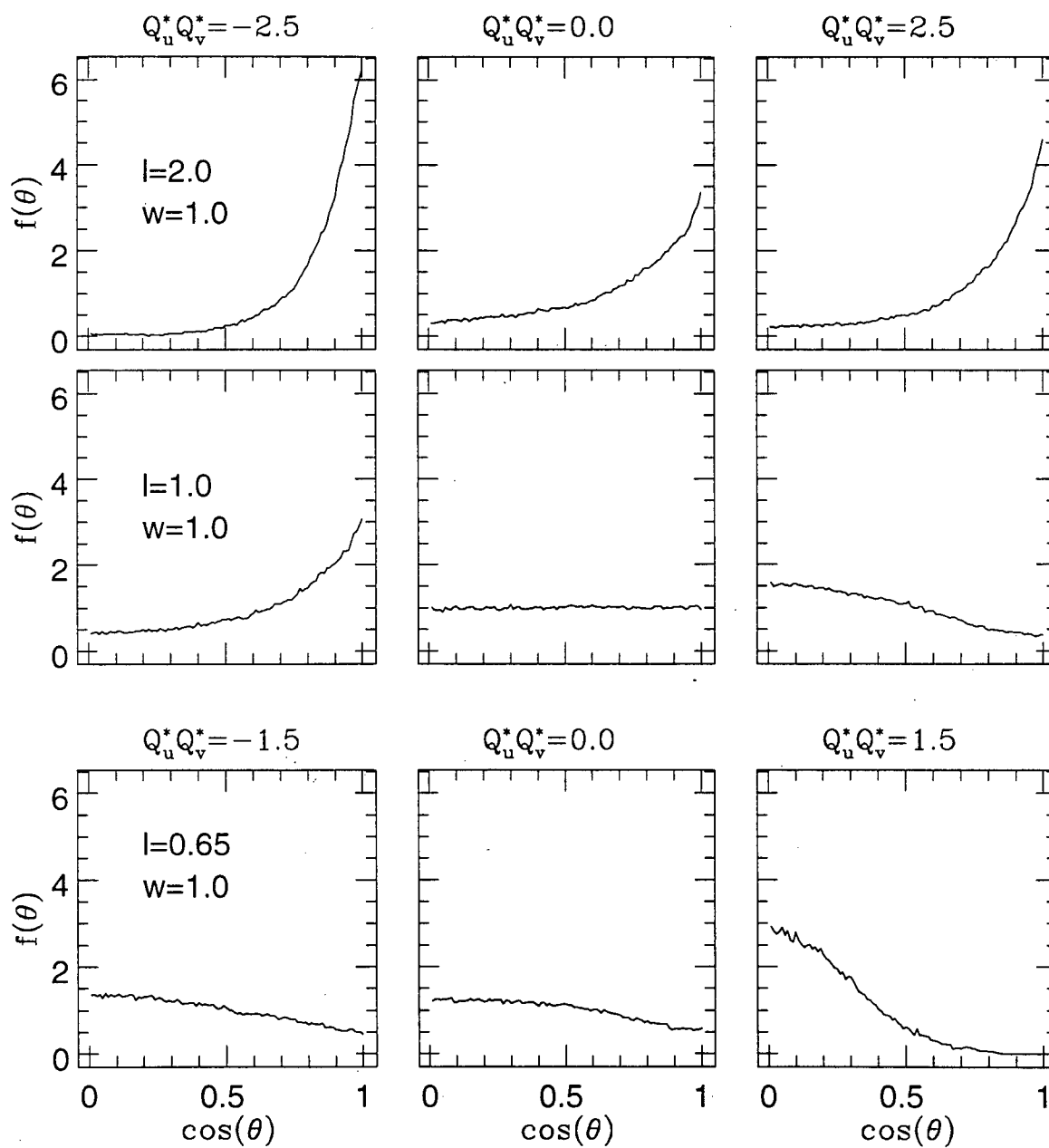
is mirrored by the behaviour of the distributions. Only in the case of the spherical solute is the orientational ordering consistent with an interaction between the solute quadrupole moment and a $\bar{F}^*_{ZZ}$ of a constant sign. The behaviour of the solute-solvent orientational correlation functions $\bar{P}_2^{(uv)}(r^*)$ for the same solutes, shown in Figure 5.23, provides some additional insight into the perturbing influence of the quadrupole-quadrupole pair interactions on the ordering of the solutes. Note that in the limit of wide separation r^*, $\bar{P}_2^{(uv)}(r^*) = \bar{P}_2 \cdot \bar{P}_2^{(nem)}$. Thus, the long-range limit of these functions provides a measure of the degree of solute orientational order. For all cases, except that of the spherical solute with $Q^*_u = 0$, there are both short-range and long-range orientational correlations. In the case of the spherical solute, both long-range and short-range correlations have the same pattern: enhancement of parallel configurations for solute and solvent quadrupole moments of the opposite sign, and enhancement of perpendicular configurations for quadrupole moments of the same sign. Note that the short-range correlations are indeed very short-range as they vanish within approximately one solvent ellipsoid width d from the nearest approach distance.

The case of the prolate solute is more interesting. While oppositely signed solute and solvent quadrupole moments corresponds to an enhancement of both short-range and long-range parallel configurations, quadrupole moments of the same sign lead to a slight enhancement of long-range parallel configurations, but a significant reduction of short-range parallel configurations. The latter feature is more in keeping with the expectations based on the orientation-dependence of the quadrupole-quadrupole pair potential. In the case of the oblate solute, there is no noticeable effect of the quadrupole-quadrupole pair potential on the short-range orientational correlations.

At this point, it is instructive to compare qualitatively the results of the simulations with certain previous experimental results. Table 5.16 lists the values of S_{zz} for D_2 benzene, hexafluorobenzene and acetylene measured in three different liquid crystals. The

Figure 5.23: Solute-Solvent Orientational Correlation Functions for $(Q_v^*)^2$=2.5 and ρ^*=0.42
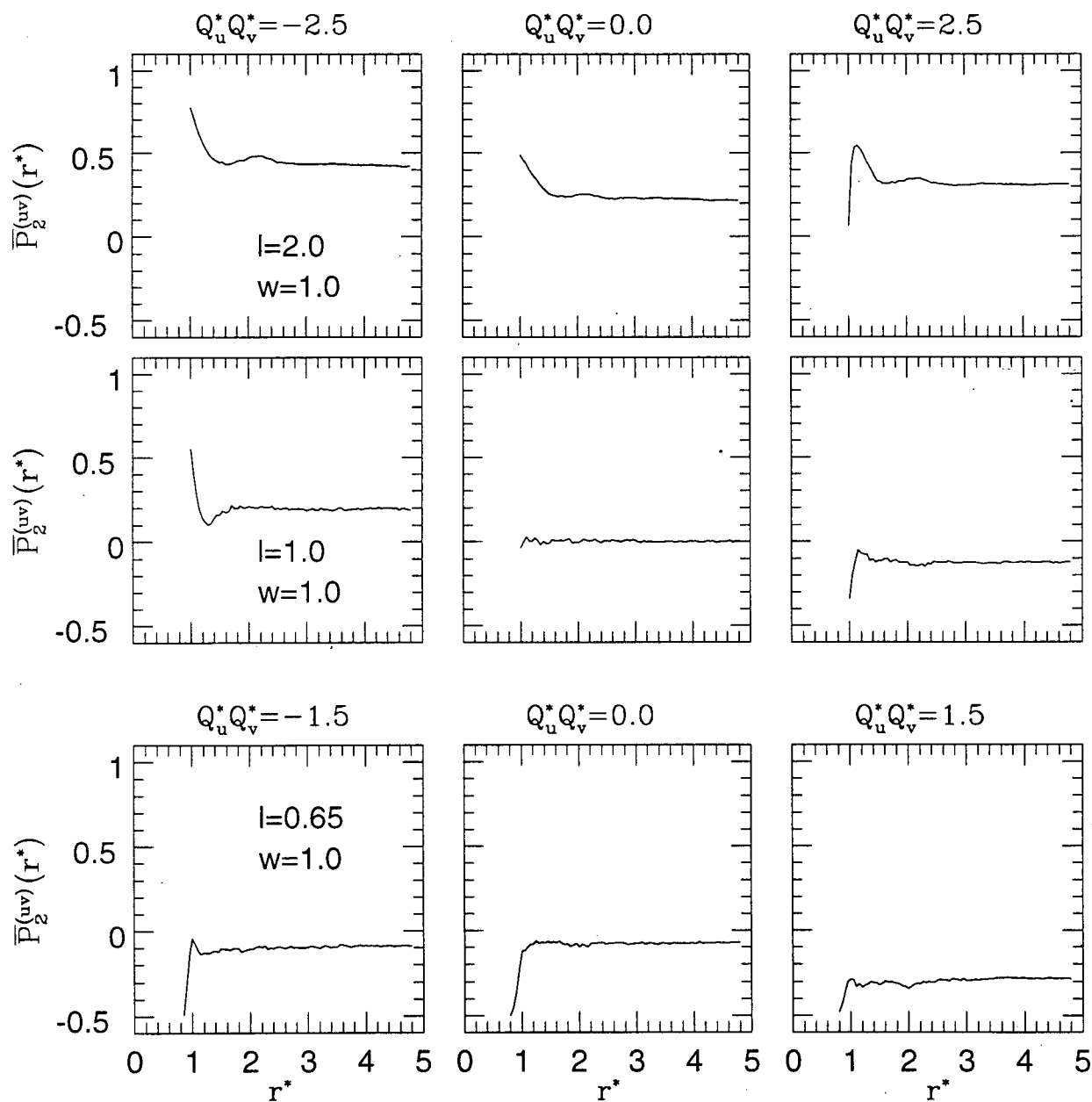
Table 5.16: Experimental Order Parameters for Three Solutes

Solute	$Q_{zz}{}^a$	$S_{zz}{}^b$		
		EBBA^c	55%^{d}	1132^e
dideuterium	0.649	-0.00965	-0.00082	0.00731
benzene	$-7.8(2.2)^f$	-0.1157	-0.1756	-0.2519
hexafluorobenzene	9.5^g	-0.3144	-0.2280	-0.2144
acetylene	$5.5(2.5)^h$	-0.0585	0.1123	0.1912

^{a}Units of 10^{-26} esu·cm^2.
^{b}From ref. [16].
$^c\bar{F}_{ZZ}$=-6.42×10^{11} esu for D_2.
$^d\bar{F}_{ZZ}$=0.0 esu for D_2.
$^e\bar{F}_{ZZ}$=6.07×10^{11} esu for D_2.
^{f}Average value of those reported in refs. [131] and [132].
^{g}From ref. [133].
^{h}Average value of those reported in refs. [134] and [135].

EFG has been measured for D_2 and HD in these nematics and was found to be positive for ZLI 1132, zero for the 55 wt% 1132/EBBA mixture and negative for EBBA [13, 31]. Further, benzene is known to have a large negative quadrupole moment, while hexafluorobenzene has a large positive value; approximate values are listed in the table. The magnitude of the negative value of $\bar{P}_2$ was found to increase with increasing $\bar{F}_{ZZ}$, while the opposite trend was observed for hexafluorobenzene. This behaviour can be explained by the interaction of the molecular quadrupole moments interacting with an external $\bar{F}_{ZZ}$ which has a sign that is *consistent* with that measured by molecular hydrogen for the three nematics. The values of orientational order parameters of acetylene are likewise consistent with this solute-independent mean-field prediction. In particular, note the negative value of $\bar{P}_2$ for acetylene in EBBA, a feature which is not easily rationalized except by an interaction between its positive Q_{zz} with a negative $\bar{F}_{ZZ}$. Further, note that

benzene and hexafluorobenzene have approximately the same shape, despite the large difference in quadrupole moments. Thus, the differences in $\bar{P}_2$ for the two molecules in the same liquid crystal likely arise principally from the difference in quadrupole moments. Again, the trend is consistent with a mean-field interaction between a quadrupole moment and a $\bar{F}_{ZZ}$ with a sign which is independent of the solute Q_{zz}: the magnitude of the negative $\bar{P}_2$ is enhanced for $Q_{zz}\bar{F}_{ZZ} < 0$, and reduced for $Q_{zz}\bar{F}_{ZZ} > 0$, where, again, we use values of $\bar{F}_{ZZ}$ measured using D_2. The slightly larger magnitude of $\bar{P}_2$ of hexafluorobenzene in the 55% mixture (where $\bar{F}_{ZZ} = 0$), compared to that of benzene, is probably due to the fact that hexafluorobenzene is slightly more oblate than benzene. To summarize, certain key experimental results strongly suggest that molecules of very different shapes and quadrupole moments interact with an average $\bar{F}_{ZZ}$ which, at the very least, has the same sign.

Clearly, the experimental results conflict with the results of the MC simulations which employ a simplified quadrupole-quadrupole potential to approximate the electrostatic interaction between molecules. As stated earlier, for example, the oblate solute in the simulations samples an average $\bar{F}_{ZZ}$ whose sign was directly proportional to the sign of the solute Q_u^* which was further manifested in an enhancement of $|\bar{P}_2|$ for increasing $|Q_u^*Q_v^*|$ relative to the case of $Q_u^*=0$ independent of the sign of $Q_u^*Q_v^*$. At this point, we cannot pinpoint precisely the origin of this sharply contradictory behaviour, but it is very likely a result of using such a highly simplified form for the electrostatic pair potential. At short range, the convergence of the multipole expansion is very slow. Thus, in dense systems, an interaction between point quadrupoles may be a very poor approximation and produce the kind of artifacts observed here. A significantly improved model of electrostatic interactions may be required to reproduce the qualitative trends observed in experimental studies. This consideration is important with regard to any theory of solute orientational order which uses such a highly simplified pair potential.

The EL theory has been applied to analyze the present results. Eqs. (5.111) and (5.112) were used to calculate values of $\bar{F}_{ZZ}^*$ and $\bar{P}_2$. However, note that the calculation of these averages requires $\bar{P}_2^{(nem)}$, $g_{uv}(r^*)$ and $\bar{P}_4^+(r^*)$, quantities which also must be calculated in the MC simulations. Thus, the "theory" simply provides a prediction of the relationship between various quantities that may be measured for the system, rather than a theory which requires exclusively external system parameters. Thus, it is not of a form which may be used to study real nematic systems using NMR spectroscopy, for example, since $g_{uv}(r^*)$ and $\bar{P}_4^+(r^*)$ are not measurable with this technique.

The results of the predictions of $\bar{F}_{ZZ}^*$ and $\bar{P}_2$ are summarized in Table 5.15 along with the values measured in the MC simulations. Note that $\bar{P}_2$ can only be calculated for spherical solutes, since the non-spherical solutes experience an additional orienting mechanism due to the shape anisotropy coupled with the short-range repulsive forces. The theoretical predictions of $\bar{F}_{ZZ}^*$ are consistently good for all solute shapes and quadrupole moments. This is true for both the signs and magnitudes of $\bar{F}_{ZZ}^*$. Considering this point, we may gain some insight into the dependence of $\bar{F}_{ZZ}^*$ on solute properties by investigating more closely the results in the context of the theory.

In Figures 5.24 and 5.25 we show the three solvent-solute pair distribution functions $g_{uv}(r^*)$, $\bar{P}_4^+(r^*)$ and $\bar{P}_4^+(r^*)g(r^*)(r^*)^{-3}$. Note that both the mean-field potential $U^*(\theta)$ (Eq. (5.110)) and $\bar{F}_{ZZ}^*$ (Eq. (5.111)) are directly proportional to the latter function. Figure 5.24 shows the distribution functions for a prolate solute ($l=2$, $w=1$) for $Q_u^* Q_v^* = 0, \pm 2.5$. For zero quadrupole moment, there is only a vague shell structure visible in $g_{uv}(r^*)$, while there is a very strong enhancement in minimum-distance positional correlation for $Q_u^* Q_v^* = -2.5$ and a smaller enhancement at $Q_u^* Q_v^* = 2.5$. The strong peak for $Q_u^* Q_v^* = -2.5$ is consistent with the a strong minimum in the quadrupole-quadrupole pair potential for parallel configurations between axially symmetric quadrupoles of opposite signs. The $\bar{P}_4^+(r^*)$ distribution also undergoes noticeable changes with varying

Figure 5.24: Solute-Solvent Distribution Functions for Solute with Dimensions of l=2.0 and w=1.0 at ρ^*=0.42 and $(Q_v^*)^2 = 2.5$.
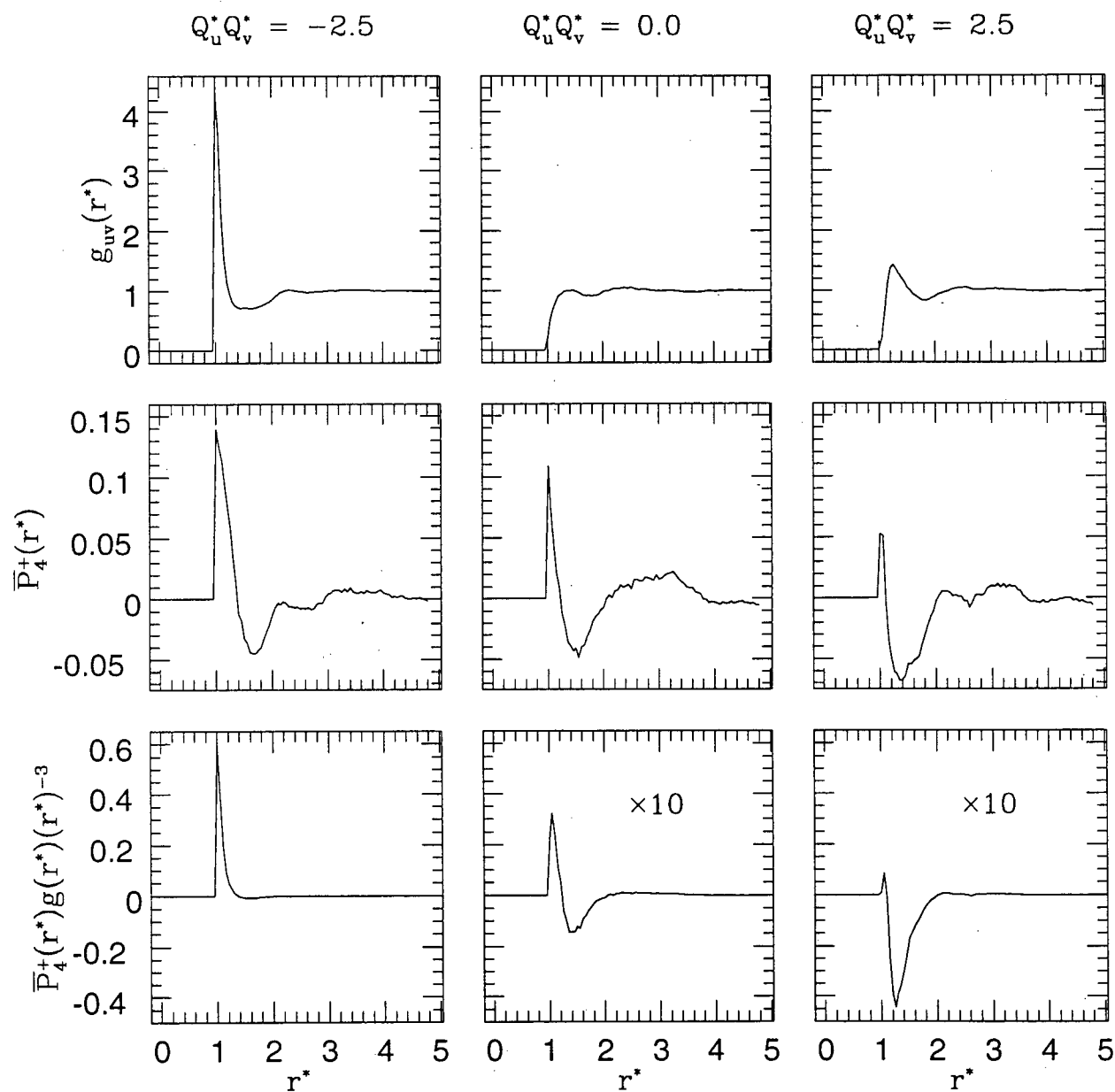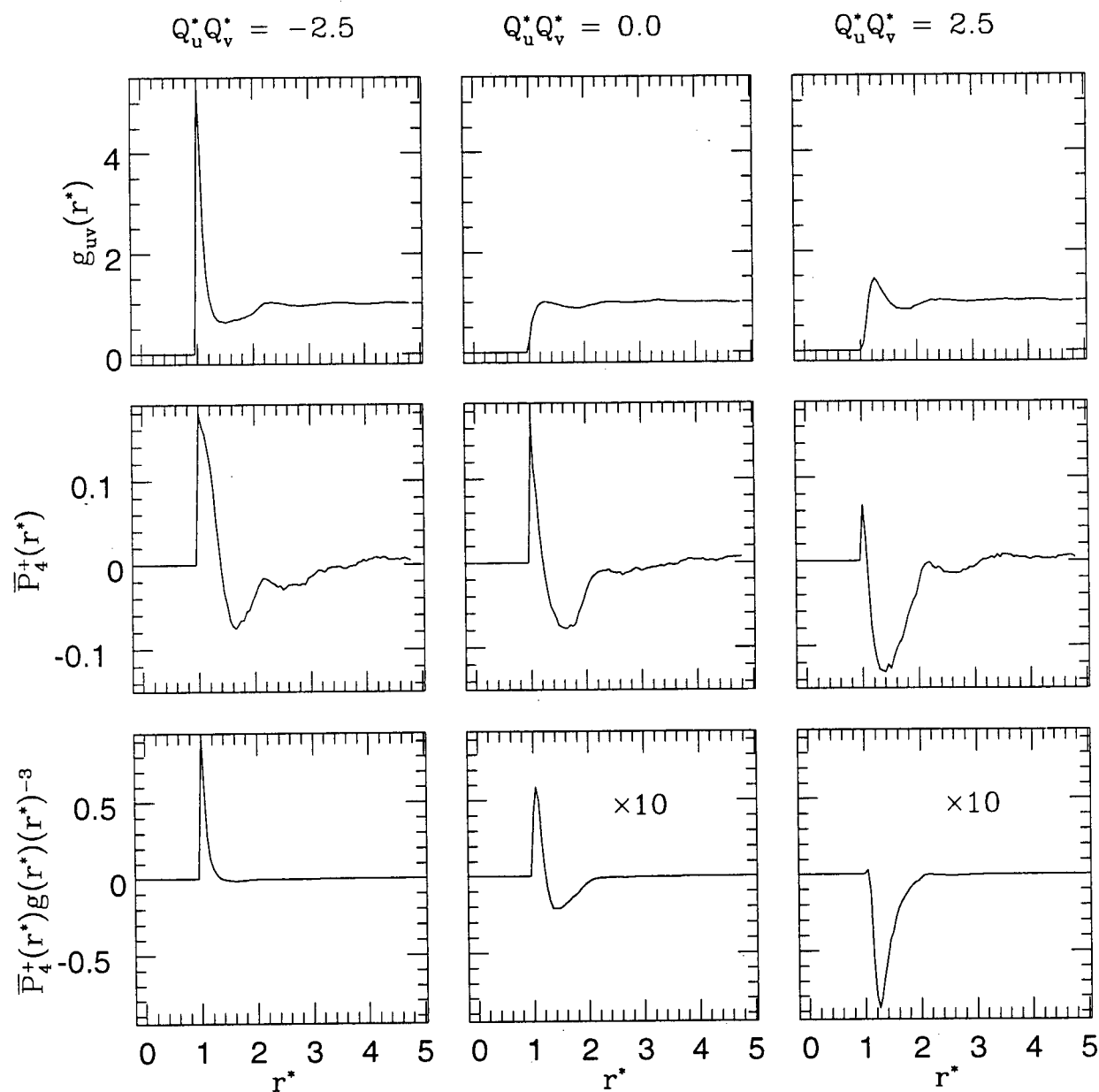
Figure 5.25: Solute-Solvent Distribution Functions for Solute with Dimensions of l=5.0 and w=1.0 at ρ^*=0.42 and $(Q_v^*)^2 = 2.5$.

$Q_u^* Q_v^*$: increasing $Q_u^* Q_v^*$ results in a decrease in the minimum-distance positive peak and a deepening of the negative "well" to the right of this peak. These effects result in significantly different $\bar{P}_4^+(r^*) g_{uv}(r^*)(r^*)^{-3}$ functions. Clearly, integration of the functions result in a $\bar{F}_{ZZ}^* > 0$ for $Q_u^* Q_v^* = -2.5$, $\bar{F}_{ZZ}^* < 0$ for $Q_u^* Q_v^* = 2.5$, and a near-vanishing $\bar{F}_{ZZ}^*$ for $Q_u^* Q_v^* = 0.0$. The results for the longer prolate ellipsoid (l=5, w=1) are virtually identical. Thus, changes in the $\bar{F}_{ZZ}^*$ arise from changes in the structure of the solvent in the vicinity of the solute as a result of changes in the solute properties.

The theoretical predictions of $\bar{P}_2$ for the spherical solutes listed in Table 5.15 are generally poor and deviate from the measured values typically by a factor of two. This result is somewhat surprising given the accuracy of the calculated $\bar{F}_{ZZ}^*$, whose theoretical expression (Eq. 5.111) is defined by the mean-field potential (Eq. 5.112) which is used to calculate $\bar{P}_2$. At the very least, however, the signs of the order parameters are accurately predicted. A comparison of the calculated and theoretical solute orientational distribution function for one spherical solute ($l = w = 1$) is shown in Figure 5.26. Note that the accuracy of the predicted curves appears to be poorer as the magnitude of the solute quadrupole moment increases. This discrepancy between the degree of orientational ordering calculated in theory and simulation suggests that the statistical approximations used in the EL methodology may be too severe to yield a useful and accurate theory for solute orientational order. Given that the theoretical predictions are slightly better for weaker solute-solvent couplings for the systems studied here, it may be generally a more accurate theory in the limit of small solute quadrupole moments. It is interesting to note that in the case of D_2 and HD, the only solutes for which the average EFG and order parameter can be simultaneously measured, the mean-field model gives excellent predictions of the measured $\bar{P}_2$. Perhaps it is significant that the solute quadrupole moments for these molecules are very small, in keeping with this argument. Unfortunately, it is very difficult to test this hypothesis using MC simulations for solutes with very weak

Figure 5.26: MC and Theoretical Orientational Distribution Functions for Spherical Solutes with $(Q_v^*)^2 = 2.5$ and $\rho^* = 0.42$
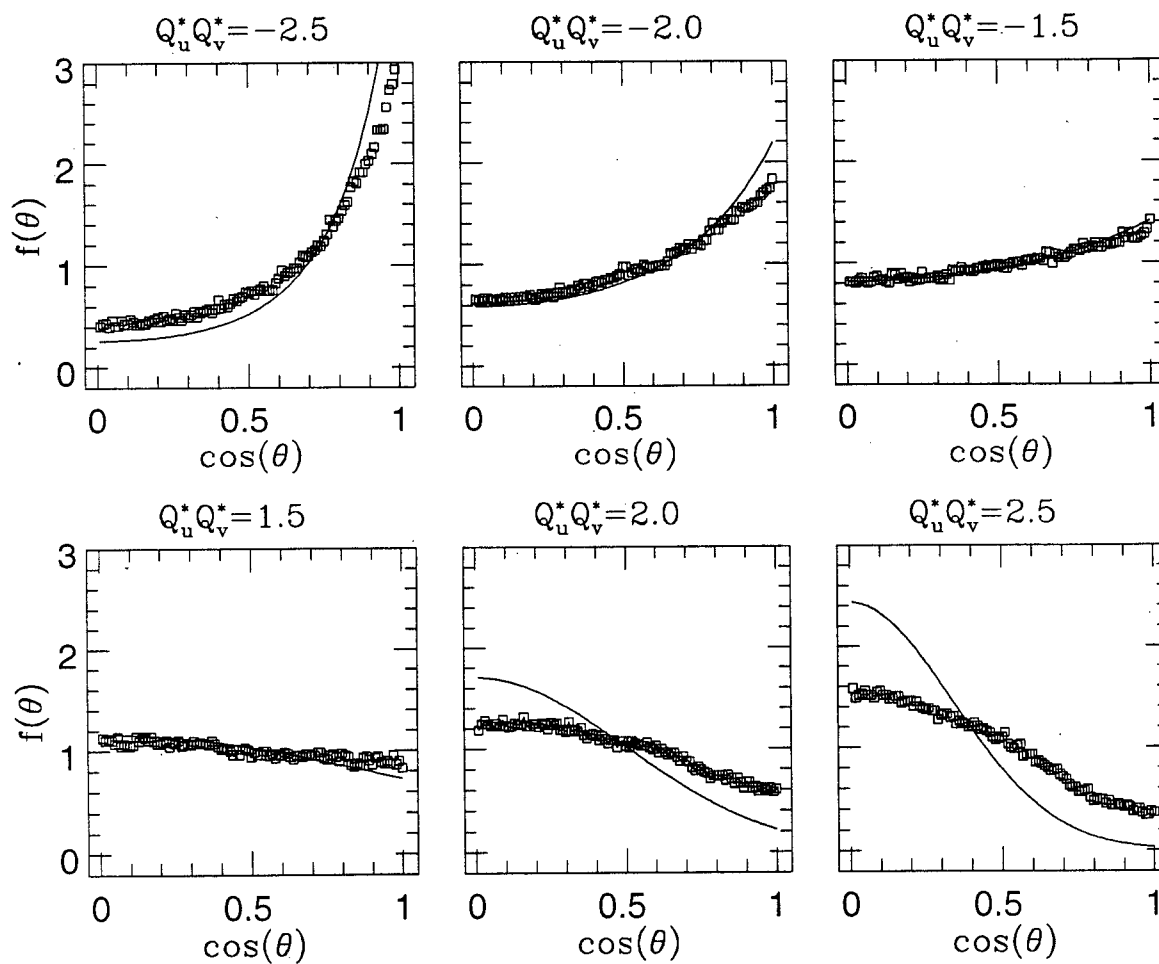
Table 5.17: EFG and Order Parameters for Several Solutes at ρ^*=0.39 and $(Q_v^*)^2$=2.5

Shape	Dimensions	$Q_u^* Q_v^{*a}$	$\bar{F}_{ZZ}^*$(MC)^a	$\bar{F}_{ZZ}^*$(Th)^b	$\bar{P}_2$ (MC)	$\bar{P}_2$ (Th)^c	$\bar{P}_2^{(nem)}$
Spherical	l=1.0	-2.5	1.8 (1)	1.2	0.26(2)	0.34	0.637(4)
	w=1.0	-1.5	0.29(5)	0.29	0.04(2)	0.04	0.645(4)
		0.0	0.04(3)	0.05	0.01(1)	0.0	0.641(6)
		1.5	0.43(6)	0.35	-0.01(1)	-0.05	0.622(7)
		2.5	1.5 (2)	1.5	-0.09(2)	-0.18	0.636(4)
Prolate	l=2.0	-2.5	2.0(1)	1.1	0.44(2)	–	0.638(4)
	w=1.0	-1.5	0.63(5)	0.45	0.30(2)	–	0.636(4)
		0.0	0.01(2)	0.06	0.23(2)	–	0.639(4)
		1.5	-0.33(3)	-0.21	0.25(2)	–	0.657(5)
		2.5	-0.48(4)	-0.30	0.29(2)	–	0.635(2)

^{a}Calculated using $Q_{zz}^{(v)} = -\sqrt{2.5} < 0$; using $Q_{zz}^{(v)} = +\sqrt{2.5} > 0$ simply reverses the sign of $\bar{F}_{ZZ}^*$.
^{b}Calculated using Eq. (5.111).
^{c}Calculate using Eq. (5.112).

quadrupoles: the statistical fluctuations of the measured $\bar{F}_{ZZ}^*$ and $\bar{P}_2$ rapidly become very large relative to their average values, a feature that greatly increases the statistical uncertainties of these averaged quantities.

To investigate further the details of solute orientational behaviour in a nematic solvent, we have conducted simulations for solutes in a nematic solvent at a lower density, and therefore, with a lower degree of orientational order. Table 5.17 presents results for the EFG and order parameters of spherical and prolate solutes with a variety of quadrupole moments oriented in a solvent at a reduced density ρ^*=0.39 and with an order parameter of $\bar{P}_2^{(nem)}$=0.64±0.01. As expected there is a significant reduction in

both $\bar{F}_{ZZ}^*$ and $\bar{P}_2$ as a result of the decrease of the degree of nematic ordering; otherwise, there is no qualitative difference with the results for the systems at $\rho^* = 0.42$.

Finally, we consider the effects of solvent-solvent correlations on the behaviour of solute average properties. In Section 5.4.1, it was shown that the TP theory drastically underestimates the degree of solute orientational order in hard-core systems. The cause of this problem was the severity of the approximation neglecting solvent-solvent correlations induced by the solvent-solvent hard-body interaction. A consideration which is related to that result concerns the importance of the solvent-solvent correlations due to the solvent-solvent electrostatic interactions on the solute properties. We have investigated this point by performing simulations in which solvent and solute interact both via hard-core and quadrupole-quadrupole interactions, but where solvent particles interact only with a hard-core pair potential. A comparison of the results of average solute properties with the corresponding results where all interactions have been properly included may provide some insight into this matter.

In Table 5.18, we present the calculated values for $\bar{F}_{ZZ}^*$ and $\bar{P}_2$ for three solutes with and without the solvent quadrupole-quadrupole interaction turned on. In the case of the spherical solute, there is a small difference in $\bar{F}_{ZZ}^*$ and no change in $\bar{P}_2$. However, for the prolate solute with $Q_u^* \neq 0$, there is a significant variation in both $\bar{F}_{ZZ}^*$ and $\bar{P}_2$. The difference is reduced by setting $Q_u^* = 0$ for a solute with the same shape. Thus, it appears that solvent-solvent correlations induced by solvent-solvent electrostatic interactions can indirectly affect solute properties, though in a way that clearly depends on the properties of the solute. Note that these differences do not arise from a change in the nematic order parameter: as shown in Table 5.18, $\bar{P}_2^{(nem)}$ is not significantly affected by the presence of solvent quadrupole-quadrupole interactions of the magnitude considered here. Nevertheless, there is a significant difference in the structure of the solvent between the hard-core and the hard-core plus quadrupole systems. This difference

Table 5.18: Comparison of MC Results With and Without Quadrupole-Quadrupole Interactions Between Solvent Ellipsoids

Dimensions	$Q_u^* Q_v^{*c}$	Q_v^*–Q_v^* off[a]			Q_v^*–Q_v^* on[b]		
		$\bar{F}_{ZZ}^*$	$\bar{P}_2$	$\bar{P}_2^{(nem)}$	$\bar{F}_{ZZ}^*$	$\bar{P}_2$	$\bar{P}_2^{(nem)}$
$l{=}1,\ w{=}1$	2.5	2.6(2)	-0.16(2)	0.764(2)	2.2(2)	-0.16(2)	0.758(2)
$l{=}2,\ w{=}1$	2.5	-1.03(5)	0.49(2)	0.766(2)	-0.66(4)	0.40(2)	0.761(2)
$l{=}2,\ w{=}1$	0.0	0.07(3)	0.32(2)	0.765(2)	-0.01(3)	0.29(2)	0.763(2)

[a]Solvent-solvent quadrupole interactions turned off.
[b]Solvent-solvent quadrupole interactions turned on; $Q_v^* = -\sqrt{2.5}$.
[c]$Q_u^* Q_v^*$ gives the solute-solvent interaction strength.

is manifest in the solvent-solvent pair distribution and orientational correlation functions shown in Figure 5.27.

5.5 Conclusions

In this chapter, we have presented a MC simulation study of the combined effects of shape anisotropy and one specific electrostatic interaction on the orientational order of solutes in a nematic solvent. Solute and solvent molecules were constructed using a minimal model to describe pair interactions. Anisotropic short-range repulsive forces were approximated by using a hard-core potential, and axially symmetric ellipsoids of rotation were used to describe the molecular shapes. Electrostatic effects were studied by incorporating an interaction between point quadrupoles embedded in the centers of the hard ellipsoids. We have analyzed the results of the simulations using two current theories of orientational ordering of solutes in nematic liquid crystals.

Figure 5.27: Comparison of Solvent-Solvent Pair Distribution and Orientational Correlation Functions for $(Q_v^*)^2 = 0$ and 2.5 at ρ^*=0.42.
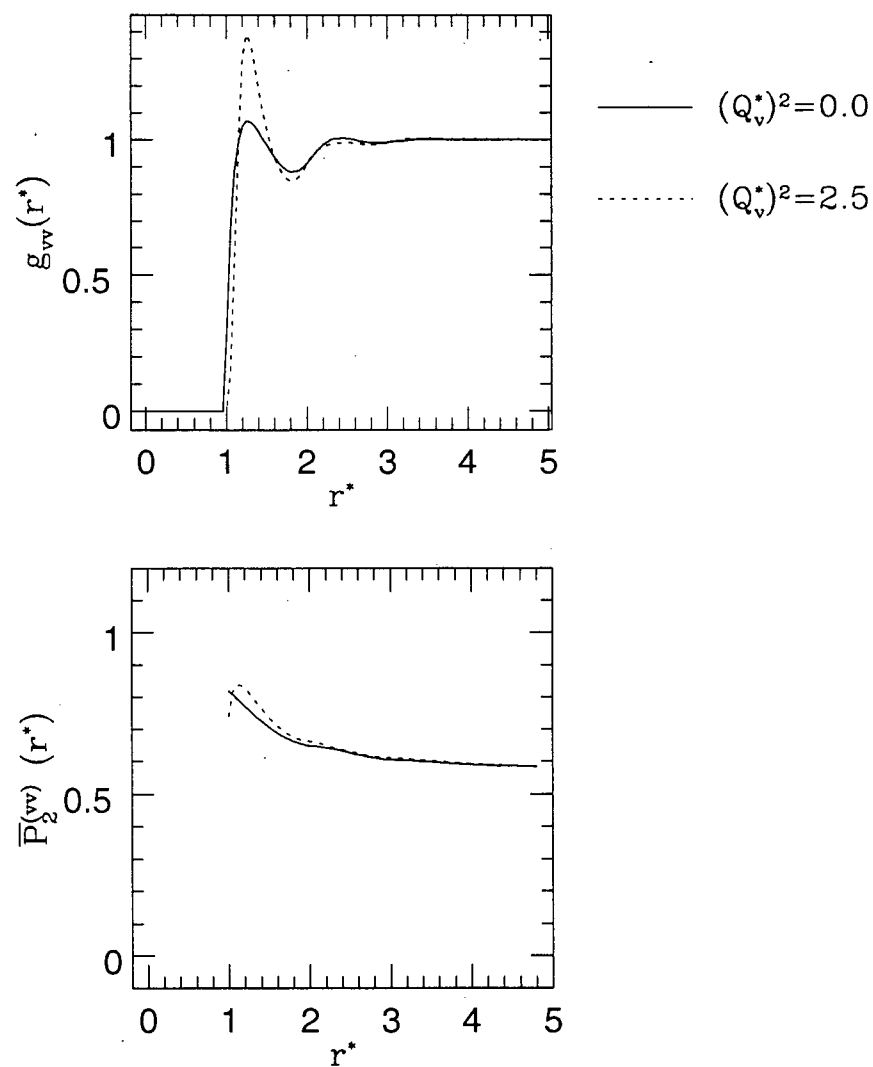
In a purely hard-core system, solute orientational order varies in a predictable manner: increases in solute shape anisotropy and solvent density enhance the degree of ordering. The orientational distribution functions were analyzed using a theory due to Terzis *et al.* which was found to drastically underestimate the solute ordering. This discrepancy is due to the complete neglect of solvent-solvent correlations in the derivation of the solute mean-field orientational potential. The severity of this approximation calls into question the results of the study which employed the theory to analyze orientational order parameters of solutes measured in previous NMR experiments.

In the quadrupolar systems, the relationship between the hard-core and electrostatic contributions to solute orientational ordering was investigated in detail. The behaviour of the properties for a large collection of solutes of varying shapes and quadrupole moments was examined. As well, we were particularly interested in testing the accuracy of a mean-field model proposed by Burnell and coworkers in which the interaction between the molecular quadrupole moment and a solute-independent average EFG sampled by the solute constitutes an important orientational ordering mechanism. To this end, the relationship between the measured average EFG and orientational order parameters was examined in detail. Further, a theoretical mean-field potential and average EFG can be derived using a method due to Emsley, Luckhurst and coworkers. The theory provides a simple relationship between the solute order and solvent-structure functions in the vicinity of the solute. This approach was found to give some insight into the solute orientational behaviour.

A significant result of the simulations employing the point quadrupole electrostatic model was that the measured EFG sampled by the solute was found to be highly sensitive to the details of the properties of the solute, in contrast to the model put forward by Burnell and coworkers. In the case of non-spherical solutes, the EFG was found to experience a concomitant change in sign with the solute quadrupole moment. This result is

in sharp contradiction with certain key experimental NMR results for which it was found that the order parameters of several molecules conform to the mean-field model where the solutes interact with an EFG which, at the very least has the same sign. The origin of this discrepancy is very likely the inadequacy of using point quadrupoles for dense systems for which the convergence of the multipole expansion at short distances becomes an important consideration. Thus, an improved description of molecular electrostatic interactions will likely be essential in order to generate solute orientational behaviour consistent with that observed experimentally.

Despite the problems with the molecular model outlined above, the observed orientational ordering was qualitatively consistent with the predictions of the mean-field model, using the measured values of the EFG for each solute individually. In addition, the EL theoretical prediction of the solute EFG, which is related to the local solvent structure, was quite accurate. The EL prediction of the orientational order of spherical solutes, for which there is only the electrostatic contribution to ordering, was qualitatively correct, though quantitatively rather poor. Thus, the statistical approximations of the EL theory appear to be too severe. Note that the theory requires a simple form for the pair potential in order to yield a simple, tractable expression for the mean-field potential. Yet, as we described above, the interaction between point moments to represent electrostatic interactions was found to be inadequate for dense systems. Thus, given the combined inadequacy of both the basic electrostatic pair potential and the statistical approximations of the theory, an accurate theoretical description of the electrostatic contributions to the orientational ordering of solutes in a nematic liquid crystal is not yet available.

Chapter 6

Conclusions

In this thesis, we have presented several studies concerned with solutes partially oriented in nematic liquid crystal solvents. There are two main components to this work: the first part involves the application of Multiple-Quantum NMR spectroscopy as a tool to investigate the orientational, structural and conformational properties of specific molecules; the second part employs the Monte Carlo simulation technique to complement previous experimental studies and investigate the influence of various molecular properties on orientational ordering. In this chapter, we review the important results and present our final comments on the material.

A key component of the experimental work presented in Chapters 2 and 3 involved the application of MQ spectroscopy as an aid for the spectral analysis for oriented solutes with spectra which are highly complex, but which nevertheless are composed of resolvable lines. High-order MQ spectra have considerably fewer lines and are much more straightforward to solve. Estimates of the dipolar coupling constants obtained from such fits can provide excellent predictions of the conventional NMR spectrum, rendering its analysis trivial. Possible limitations of this approach as a standard method for the studies of oriented solutes include the difficulty of obtaining high-order spectra of sufficient signal/noise, and the inaccuracy of the estimates of the dipolar couplings as a result of the broader lines typical of 2-D NMR spectroscopy. It is important to note that the experimental methods employed in the present work were developed more than a decade ago. While standard MQ NMR is ideal for many studies of oriented solutes, this technique has been virtually

ignored in recent years. Thus, the subject of the present work is not a development of novel variations on the experiment, but is simply an illustration of the usefulness of the basic method.

In Chapter 2, we presented a study of biphenylene which was used as a simple illustrative example to demonstrate the effectiveness of MQ spectroscopy as an aid in spectral analysis. Solutions of the six-quantum and seven-quantum spectra were used to solve the one-quantum spectrum; the resulting dipolar coupling constants were used to determine a vibrationally averaged structure for this simple molecule. Clearly, this system is of very limited interest in its own right. However, the study did show a possible limitation of the MQ method: the fact that there were a large number of fitting parameters (ten dipolar couplings and two chemical shifts) resulted in an initially poor estimate of the one-quantum spectrum. Only by a reduction in the number of parameters, obtained by fitting the spectrum directly to the proton geometry and molecular order parameters, was a sufficiently good estimate of the spectrum obtained.

In Chapter 3, the MQ experimental method was applied to the study of oriented butane, a far more interesting system. The NMR spectrum of this ten-spin molecule is highly complex and essentially featureless, and presents a significant challenge to the most courageous spectral-analysis enthusiast. However, the relatively straightforward fitting of sufficiently good quality seven-quantum and eight-quantum spectra provided highly accurate estimates of the coupling constants and chemical shifts and rendered trivial the analysis of the one-quantum spectrum. Clearly, MQ spectroscopy is a very effective experimental technique that deserves far more serious consideration as a standard approach among NMR spectroscopists.

The principal focus of Chapter 3 was the elucidation of the conformational and orientational behaviour of butane in an anisotropic condensed phase, from an analysis of the dipolar coupling constants. The considerable attention given to butane over the last

two decades stems from the fact that it is the simplest multi-conformational alkane. One important question concerns the effect of the condensed-phase environment on the conformational equilibrium relative to that of the gas phase. We performed an extensive analysis of the coupling constants. This involved the use of mean-field models to describe the orientational ordering of the solute for each of its distinct conformations. We employed several very different models in order to avoid the pitfall of obtaining model-specific results. In addition, torsional fluctuations and the uncertainty of the *gauche*-state angle were considered. From the analysis of the couplings, the *trans-gauche* energy difference was established to be in the range of $E_{tg} \approx 2.1$–3.0 kJ/mol. This range of values is considerably lower than the values typically reported for gas-phase butane. Thus, it is clear that there is an enhancement of the *gauche* conformation of butane in a condensed-phase environment. Finally, the analysis suggests that the conformational biasing is primarily a result of the isotropic solvent "pressure"; the anisotropy of the external field has only minor effects. This latter observation is consistent with the conclusions of other studies of the conformational behaviour of longer alkanes oriented in a nematic solvent.

As described above, in the analysis of the dipolar coupling constants of butane, it was necessary to employ mean-field models which are designed to describe orientational ordering of solutes in uniaxial anisotropic solvents. Such models are necessary generally for flexible molecules for which the dipolar coupling constants involve a summation of products of conformational probabilities and orientational order parameters. Since several different models were used, the analysis could also be used to test the ability of each of the models to accurately predict the orientational ordering of the solute. In accord with previous studies of alkanes, the "Chord Model" of Photinos *et al.* [47] was found to give the highest quality fit of the coupling constants, and thus, the best description of orientational ordering. However, recent versions of the "Size and Shape" model of Zimmerman *et al.* [36] which employ potentials that are more sensitive to the details

of the molecular shape, also gave excellent results. Further, it was explained that all previous studies that used the size and shape models for flexible molecules are in error: an accurate estimate of the *trans-gauche* energy difference E_{tg} of alkanes can only be obtained if the non-vanishing isotropic component implicit to all of these potentials is removed to yield a truly anisotropic external mean-field potential. Failure to account for this factor yields erroneous results. For example, the improper application of early versions of this model to a series of oriented alkanes produced values of E_{tg} that varied considerably with the length of the chain, and which were well outside the "acceptable" range of values. In light of our results for butane, we propose the following project: the considerable collection of coupling constants for alkanes ranging from hexane to decane should be analyzed using the mean-field models of Zimmerman *et al.*, in which the isotropic components are properly removed. We expect significantly better results than those obtained by Rosen *et al.* [45] Further, we propose that a corresponding analysis of existing dipolar and quadrupolar coupling constants of nematogens be performed. Unfortunately, time limitations precluded such an analysis for this thesis.

A principal goal of studying the orientational ordering of collections of solutes in liquid crystals is to examine the nature of the anisotropic intermolecular forces which underlie the ordering of the liquid crystal molecules themselves. NMR spectroscopy is an excellent experimental technique for measuring the degree of solute order via second-rank orientational order parameters. An analysis of the order parameters themselves can be used to elucidate the role of various ordering mechanisms. In this way, previous experimental studies were able to show, for example, the importance of short-range repulsive and electrostatic interactions. Nevertheless, there can be some ambiguity associated with the interpretation of experimental results. For this reason, the use of computer simulations of suitable model systems can complement and test the interpretation of experimental results. Further, this method can be used to investigate the accuracy of current empirical

and theoretical models which have been recently developed and applied extensively to the interpretation of NMR data. In Chapters 4 and 5, we employed the Monte Carlo simulation technique to study solute ordering in nematic solvents. In contrast to many recent MC studies of ordering in nematics, we employ minimal models to describe the molecular properties and intermolecular interactions. Further, the work focused specifically on the role of short-range repulsive forces and long-range electrostatic interactions, the subject of many previous studies by Burnell and coworkers.

In Chapter 4, we investigated the role of short-range repulsive forces, modeled as hard-core interactions, between molecules. The shapes of the constituent molecules were treated in a highly simplified manner: solvent molecules were modeled as hard prolate ellipsoids of revolution with an axis ratio of 5:1; solute molecules were also treated as hard ellipsoids, though with a variety of shapes and sizes. Orientational order parameters and distribution functions were measured under a variety of conditions. The results were analyzed in terms of several empirical mean-field models in order to provide a bridge between simulation and experiment. It was very interesting to note that the application of the model potentials not only provided good fits to orientational order parameters and distribution functions, but also yielded the same patterns of accuracy and inaccuracy as observed in fits of experimental data. Further, the values of the interaction strength parameters, obtained from a simultaneous fit for each model to all measured order parameters and scaled in an appropriate manner, were found to be remarkably close to those obtained from a fit to experimental order parameters obtained from NMR measurements. These results clearly demonstrate the importance of anisotropic short-range forces on orientational ordering in nematic liquid crystals, and firmly establish the connection between the various shape models with these interactions.

In light of the conclusions described above, we recommend that the importance of molecular shape be investigated further. We propose the following: (1) The solvent

molecular shape should be more accurately modeled, but without incorporating unnecessary detail. For example, the hard ellipsoids of revolution could be replaced by general ellipsoids that approximate the shape biaxiality present in all nematogens. Previous studies have demonstrated the importance of nematogen "flatness" on stablizing the nematic phase [136], and on predicting magnitudes of phase-transition discontinuities more consistent with those observed experimentally [137]. In the present case, such a refinement of the solvent shape would very likely alter the structure of the solvent, and therefore influence the orientational behaviour of solutes. (2) Solute molecules should be realistically modeled in order to facilitate a more direct comparison with experimental results. A very useful approach could be to construct model solutes using hard van der Waals spheres for each of the atoms. This essentially is the approach taken in each of the "Size and Shape" models. With such a model, the complete Saupe order matrix could be calculated. Deviations between simulated and experimental order parameters could be used to assess the importance of additional interactions on the orientational ordering of specific solutes.

In Chapter 5, we presented results of a further study which employed MC simulations to study orientational ordering of solutes in nematic liquid crystals. As in Chapter 4, the solvent and solute molecular shapes were approximated by hard axially symmetric ellipsoids. However, in most of the simulations, an additional interaction between point quadrupole moments, fixed at the centers of the ellipsoids, was included. This simple model was employed to investigate the relative importance of different ordering mechanisms. In addition, two current theoretical model potentials, applied previously to analyze experimental data, were investigated. The advantage of using computer simulations is that it can separately test two different types of approximations: (1) a comparison of the MC results with experiment provides a test of the molecular model; (2) a comparison of the MC results with the theoretical predictions provides a test of the statistical

approximations employed in the theory.

Simulations of solute orientational ordering in hard-core systems were used to investigate a theory due to Terzis *et al.* [29] The theory was found to underestimate drastically the degree of orientational order for a variety of solutes and at different solvent densities. This deficiency is a result of the approximation of completely neglecting the solvent-solvent correlations in the reduction of the full distribution function of the complete system. Clearly, a more careful treatment of these correlations is essential in order for this theory to provide an accurate prediction of the contribution to orientational order due to short-range repulsive forces.

The principal focus of Chapter 5 was the investigation of the effect of electrostatic interactions, in addition to that of shape anisotropy, on orientational ordering of solutes in a nematic solvent. Particular interest was given to a mean-field model in which the solute molecular quadrupole moment interacts with a solute-independent average EFG which arises from the presence of solvent quadrupoles. A quantitative expression for the average EFG and contribution to the mean-field potential, derived using a method described by Emsley, Luckhurst and coworkers, was used to aid in the interpretation of the MC data.

There are several important results of this study. First, the average EFG sampled by the solute in the simulations was found to be highly sensitive to the properties of the solute, in contrast with the Burnell model. For example, the EFG was found to undergo a concomitant change in sign with the solute quadrupole moment for many solutes. This feature contradicts certain experimental results, in which solutes of a variety of sizes and quadrupole moments appear to interact with an average EFG which has a sign consistent with that which was measured directly using D_2 and HD. We believe that this contradiction is a result of the very simplistic form of the pair potential: at short distances the point quadrupole approximation may be inappropriate to describe a generally very

complex interaction between molecular charge distributions. This defect is not surprising, considering the high density of the systems investigated here. Thus, in order to produce results from MC simulations which are more consistent with experimental data, a better model of the electrostatic interactions must be developed. The new model must provide a more realistic description of the pair potential at short distances. One possible approach may involve a distribution of point electrostatic moments throughout the volume of the hard ellipsoids in a manner which preserves the net quadrupole moment and long-range pair potential behaviour.

Although the model employed in the MC simulations yielded results in which the EFG was highly solute-dependent, the orientational behaviour was nevertheless qualitatively consistent with the picture of the solute quadrupole interacting with this average field. However, quantitative theoretical predictions of order parameters and orientational distribution functions were found to deviate significantly from those measured in the simulations. Thus, it appears that the statistical approximations of the theory are not sufficiently valid. Given the poor model for the intermolecular pair potential employed, the present theory is currently inadequate to describe the effects of electrostatic interactions on orientational ordering of solutes in liquid crystals. We believe that further simulations employing improved molecular modeling will be required to guide the development of the theory to a sufficiently reliable form.

Bibliography

[1] Reinitzer, F., 1888, *Monatsch. Chem.*, **9**, 421.

[2] Lehmann, O., 1889, *Z. Phys. Chem.*, **4**, 462.

[3] P. G. de Gennes, *The Physics of Liquid Crystals*, (Clarendon Press, Oxford, 1974).

[4] G. Vertogen and W. H. de Jeu, *Thermotropic Liquid Crystals, Fundamentals*, (Springer, Heidelberg, 1989).

[5] Frenkel, D., Mulder, B. M., and McTague, J. P., 1984, *Phys. Rev. Lett.*, **52**, 287.

[6] Allen, M. P., Evans, G. T., Frenkel, D., and Mulder, B. M., 1993, *Adv. Chem. Phys.*, **136**, 1.

[7] Onsager, L., 1949, *Ann. N.Y. Acad. Sci.*, **51**, 627.

[8] Maier, W. and Saupe, A., 1958, *Z. Naturforsch*, **13a**, 564.

[9] Maier, W. and Saupe, A., 1959, *Z. Naturforsch*, **14a**, 882.

[10] Maier, W. and Saupe, A., 1960, *Z. Naturforsch*, **15a**, 287.

[11] P. G. de Gennes, *Liquid Crystals 3*, eds. G.H. Brown and M.M. Labes, (Gordon and Breach, London, New York, Paris, 1972), p. 21.

[12] Tjipto-Margo, B. and Evans, G. T., 1990, *J. Chem. Phys.*, **93**, 4254.

[13] Patey, G. N., Burnell, E. E., Snijders, J. G., and de Lange, C. A., 1983, *Chem. Phys. Lett.*, **99**, 271.

[14] van der Est, A. J., Burnell, E. E., and Lounila, J., 1988, *J. Chem. Soc., Faraday Trans. 2*, **84**, 1095.

[15] Burnell, E. E., van der Est, A. J., Patey, G. N., de Lange, C. A., and Snijders, J. G., 1987, *Bull. Magn. Reson.*, **9**, 4.

[16] A. J. van der Est, 1987, Ph.D. Thesis, University of British Columbia.

[17] Snijders, J. G., de Lange, C. A., and Burnell, E. E., 1982, *J. Chem. Phys.*, **77**, 5386.

[18] Snijders, J. G., de Lange, C. A., and Burnell, E. E., 1983, *J. Chem. Phys.*, **79**, 2964.

[19] Emsley, J. W., Hashim, R., and Luckhurst, G. R., 1983, *Molec. Phys.*, **49**, 1321.

[20] Luckhurst, G. R., Zannoni, C., Nordio, P. L., and Segre, U., 1975, *Molec. Phys.*, **30**, 1345.

[21] Counsell, C. J. R., Emsley, J. W., and Luckhurst, G. R., 1985, *Molec. Phys.*, **54**, 847.

[22] Emsley, J. W., Luckhurst, G. R., and Sachdev, H. S., 1989, *Molec. Phys.*, **67**, 151.

[23] Emsley, J. W., Luckhurst, G. R., and Sachdev, H. S., 1989, *Liq. Crystals*, **5**, 953.

[24] Emsley, J. W., Palke, W. E., and Shilstone, G. N., 1991, *Liq. Crystals*, **9**, 643.

[25] Emsley, J. W., Heeks, S. K., Horne, T. J., Dowells, M. H., Moon, A., Palke, W. E., Patel, S. U., Shilstone, G. N., and Smith, A., 1991, *Liq. Crystals*, **9**, 649.

[26] Emerson, A. P. J., Hashim, R., and Luckhurst, G. R., 1992, *Molec. Phys.*, **76**, 241.

[27] Photinos, D. J., Poon, C. D., Samulski, E. T., and Toriumi, H., 1992, *J. Phys. Chem.*, **96**, 8176.

[28] Photinos, D. J. and Samulski, E. T., 1993, *J. Chem. Phys.*, **98**, 10009.

[29] Terzis, A. F. and Photinos, D. J., 1994, *Molec. Phys.*, **83**, 847.

[30] Lounila, J. and Jokisaari, J., 1982, *Progr. NMR Spectroscopy*, **15**, 249.

[31] Barker, P. B., van der Est, A. J., Burnell, E. E., Patey, G. N., de Lange, C. A., and Snijders, J. G., 1984, *Chem. Phys. Lett.*, **107**, 426.

[32] Barnhoorn, J. B. S., de Lange, C. A., and Burnell, E. E., 1993, *Liq. Crystals*, **13**, 319.

[33] van der Est, A. J., Kok, M. Y., and Burnell, E. E., 1987, *Molec. Phys.*, **60**, 397.

[34] Zimmerman, D. S. and Burnell, E. E., 1990, *Molec. Phys.*, **69**, 1059.

[35] Zimmerman, D. S., Li, Y., and Burnell, E. E., 1991, *Mol. Cryst. Liq. Cryst.*, **203**, 61.

[36] Zimmerman, D. S. and Burnell, E. E., 1993, *Molec. Phys.*, **78**, 687.

[37] Ferrarini, A., Moro, G. J., Nordio, P. L., and Luckhurst, G. R., 1992, *Molec. Phys.*, **77**, 1.

[38] Wilson, M. R. and Allen, M. P., 1991, *Mol. Cryst. Liq. Cryst.*, **198**, 465.

[39] Wilson, M. R. and Allen, M. P., 1992, *Liq. Crystals*, **12**, 157.

[40] Burnell, E. E. and de Lange, C. A., 1980, *Chem. Phys. Lett.*, **76**, 268.

[41] Burnell, E. E. and de Lange, C. A., 1980, *J. Magn. Reson.*, **39**, 461.

[42] Burnell, E. E., de Lange, C. A., and Mouritsen, O. G., 1982, *J. Magn. Reson.*, **50**, 188.

[43] Gochin, M., Zimmerman, H., and Pines, A., 1987, *Chem. Phys. Letters*, **137**, 51.

[44] Gochin, M., Pines, A., Rosen, M. E., Rucker, S. P., and Schmidt, C., 1990, *Molec. Phys.*, **69**, 671.

[45] Rosen, M. E., Rucker, S. P., Schmidt, C., and Pines, A., 1993, *J. Phys. Chem.*, **97**, 3858.

[46] Janik, B., Samulski, E. T., and Toriumi, H., 1987, *J. Phys. Chem.*, **91**, 1842.

[47] Photinos, D. J., Samulski, E. T., and Toriumi, H., 1990, *J. Phys. Chem.*, **94**, 4688.

[48] Photinos, D. J., Samulski, E. T., and Toriumi, H., 1990, *J. Phys. Chem.*, **94**, 4694.

[49] Photinos, D. J., Poliks, B. J., Samulski, E. T., Terzis, A. F., and Toriumi, H., 1991, *Molec. Phys.*, **72**, 333.

[50] Aue, W. P., Bartholdi, E., and Ernst, R. R., 1976, *J. Chem. Phys.*, **64**, 2229.

[51] Weitekamp, D. P., 1983, *Adv. Magn. Reson.*, **11**, 111.

[52] Wokaun, A. and Ernst, R. R., 1977, *Chem. Phys. Lett.*, **52**, 407.

[53] Warren, W. S., Sinton, S., Weitekamp, D. P., and Pines, A., 1979, *Phys. Rev. Lett.*, **43**, 1791.

[54] Warren, W. S., Weitekamp, D. P., and Pines, A., 1980, *J. Chem. Phys.*, **73**, 2084.

[55] Warren, W. W. and Pines, A., 1981, *J. Chem. Phys.*, **74**, 2808.

[56] Yen, Y.-S. and Pines, A., 1983, *J. Chem. Phys.*, **78**, 3579.

[57] Weitekamp, D. P., Garbow, J. R., and Pines, A., 1982, *J. Magn. Reson.*, **46**, 529.

[58] Metropolis, N., Rosenbluth, A. W., Rosenbluth, M. N., Teller, A. M., and Teller, E., 1953, *J. Chem. Phys.*, **21**, 1087.

[59] Lebwohl, P. A. and Lasher, G., 1973, *Phys. Rev. A*, **7**, 426.

[60] Frenkel, D., 1987, *Molec. Phys.*, **60**, 1.

[61] Weis, J. J., Levesque, D., and Zarrogoicoechea, G. J., 1992, *Phys. Rev. Lett.*, **69**, 913.

[62] Weis, J. J., Levesque, D., and Zarrogoicoechea, G. J., 1993, *Molec. Phys.*, **80**, 1077.

[63] Levesque, D., Weis, J. J., and Zarrogoicoechea, G. J., 1993, *Phys. Rev. E*, **47**, 496.

[64] Li, K. Y., Zimmerman, D. S., and Burnell, E. E., 1993, *Molec. Phys.*, **78**, 673.

[65] Palke, W. E., Emsley, J. W., and Tildesley, D. J., 1994, *Molec. Phys.*, **82**, 177.

[66] Alejandre, J., Emsley, J. W., Tildesley, D. J., and Carlson, P., 1994, *J. Chem. Phys.*, **101**, 7027.

[67] Polson, J. M. and Burnell, E. E., 1994, *J. Magn. Reson. Series A*, **106**, 223.

[68] P. Diehl and C. L. Khetrapal, *NMR—Basic Principles and Progress*, Vol. 1, (Springer–Verlag, Berlin, 1969).

[69] J. W. Emsley and J. C. Lindon, *NMR Spectroscopy of Liquid Crystals*, (Pergamon, London, 1975).

[70] J. W. Emsley (Ed.), *Nuclear Magnetic Resonance of Liquid Crystals*, (Reidel, Holland, 1985).

[71] Drobny, G., Pines, A., Sinton, S., Weitekamp, D., and Wemmer, D., 1979, *Faraday Symp. Chem. Soc.*, **13**, 49.

[72] Sinton, S. and Pines, A., 1980, *Chem. Phys. Lett.*, **76**, 263.

[73] Warren, W. S. and Pines, A., 1981, *J. Am. Chem. Soc.*, **103**, 1613.

[74] Weitekamp, D. P., Garbow, J. R., and Pines, A., 1982, *J. Chem. Phys.*, **77**, 2870.

[75] Field, L. D., Pierens, G. K., Cross, K. J., and Terry, M. L., 1992, *J. Magn. Reson.*, **97**, 451.

[76] Rendell, J. C. T. and Burnell, E. E., 1995, *J. Magn. Reson. Series A*, **112**, 1.

[77] Yokozeki, A., Jr., C. F. W., and Bauer, S. H., 1974, *J. Am. Chem. Soc.*, **96**, 1026.

[78] Field, L. D. and Terry, M. L., 1986, *J. Magn. Reson.*, **69**, 176.

[79] Drobny, G., 1984, *Chem. Phys. Lett.*, **109**, 132.

[80] Olah, G. A. and Liang, G., 1977, *J. Am. Chem. Soc.*, **99**, 6045.

[81] P. Diehl, H. P. K. and Niederberger, W., 1971, *J. Magn. Reson.*, **4**, 352.

[82] P. Diehl, P. M. H. and Niederberger, W., 1971, *Mol. Phys.*, **20**, 139.

[83] Lucas, N. D. J., 1971, *Mol. Phys.*, **22**, 233.

[84] Lucas, N. D. J., 1972, *Mol. Phys.*, **23**, 835.

[85] Diehl, P. and Niederberger, W., 1973, *J. Magn. Reson.*, **9**, 495.

[86] S. J. Cyvin *Molecular Vibrations and Mean Square Amplitudes* (Elsevier, Amsterdam, 1968, Chap. 13.

[87] Hildebrant, R. L. and Weiser, J. D., 1971, *J. Chem. Phys.*, p. 4648.

[88] Polson, J. M. and Burnell, E. E., 1995, *J. Chem. Phys.*, **103**, 6891.

[89] P. J. Flory *Statistical Mechanics of Chain Molecules* (Wiley-Interscience, New York, 1969).

[90] Pratt, L. R. and Chandler, D., 1978, *J. Chem. Phys.*, **68**, 4202.

[91] Pratt, L. R. and Chandler, D., 1978, *J. Chem. Phys.*, **68**, 4213.

[92] Verma, A. L., Murphy, W. F., and Bernstein, H. J., 1974, *J. Chem. Phys.*, **60**, 1540.

[93] Durig, J. R. and Compton, D. A. C., 1979, *J. Phys. Chem.*, **83**, 265.

[94] Compton, D. A. C., Montero, S., and Murphy, W. F., 1980, *J. Phys. Chem.*, **84**, 3587.

[95] Heenan, R. K. and Bartell, L. S., 1983, *J. Chem. Phys.*, **78**, 1270.

[96] Wiberg, K. B. and Murcko, M. A., 1988, *J. Am. Chem. Soc.*, **110**, 8029.

[97] Gassler, G. and Huttner, W., 1990, *Z. Naturforsch*, **45a**, 113.

[98] Colombo, L. and Zerbi, G., 1980, *J. Chem. Phys.*, **73**, 2013.

[99] Kint, S., Scherer, J. R., and Snyder, R. G., 1980, *J. Chem. Phys.*, **73**, 1599.

[100] Cates, D. A. and MacPhail, A., 1991, *J. Phys. Chem.*, **95**, 2209.

[101] Ryckaert, J. P. and Bellemans, A., 1975, *Chem. Phys. Letters*, **30**, 123.

[102] Ryckaert, J. P. and Bellemans, A., 1978, *Discuss. Faraday Soc.*, **66**, 95.

[103] Rebertus, D. W., Berne, B. J., and Chandler, D., 1979, *J. Chem. Phys.*, **70**, 3395.

[104] Weber, T. A., 1978, *J. Chem. Phys.*, **69**, 2347.

[105] Jorgensen, W. L., 1981, *J. Am. Chem. Soc.*, **103**, 677.

[106] Jorgensen, W. L., 1982, *J. Chem. Phys.*, **77**, 5757.

[107] Jorgensen, W. L., 1983, *J. Phys. Chem.*, **87**, 5304.

[108] Edberg, R., Evans, D. J., and Morriss, G. P., 1986, *J. Chem. Phys.*, **84**, 6933.

[109] Wielopolski, P. A. and Smith, E. R., 1986, *J. Chem. Phys.*, **84**, 6940.

[110] Enciso, E., Alonso, J., Almarza, N. G., and Bermejo, F. J., 1989, *J. Chem. Phys.*, **90**, 413.

[111] Brown, D. and Clarke, J. H. R., 1990, *J. Chem. Phys.*, **92**, 3062.

[112] Almarza, Enciso, E., Alonso, J., Bermejo, F. J., and Alvarez, 1990, *Molec. Phys.*, **70**, 1.

[113] Tobias, D. J. and Brooks, C. L., 1990, *J. Chem. Phys.*, **92**, 2582.

[114] Ben-Shaul, A., Rabin, Y., and Gelbart, W. M., 1983, *J. Chem. Phys.*, **78**, 4303.

[115] Creamer, D. B., Pathria, R. K., and Rabin, Y., 1985, *J. Chem. Phys.*, **84**, 476.

[116] Gochin, M., Schenker, K. V., and Pines, A., 1986, *J. Am. Chem. Soc.*, **108**, 6813.

[117] Gochin, M., Hugi-Cleary, D., Zimmerman, H., and Pines, A., 1987, *Molec. Phys.*, **60**, 205.

[118] Photinos, D. J., Samulski, E. T., and Toriumi, H., 1992, *J. Phys. Chem.*, **96**, 6979.

[119] Snijders, J. G., de Lange, C. A., and Burnell, E. E., 1983, *Israel J. Chem.*, **23**, 269.

[120] Straley, J. P., 1974, *Phys. Rev. A*, **10**, 1881.

[121] Marčelja, S., 1974, *J. Chem. Phys.*, **60**, 3599.

[122] Bradford, W. F., Fitzwater, S., and Bartell, L. S., 1977, *J. Mol. Struct.*, **38**, 185.

[123] Aksnes, D. W. and Albriktsen, P., 1970, *Acta Chem. Scand.*, **24**, 3764.

[124] Adams, D. J., Luckhurst, G. R., and Phippen, R. W., 1987, *Molec. Phys.*, **61**, 1575.

[125] Luckhurst, G. R., Stephens, R. A., and Phippen, R. W., 1990, *Liq. Crystals*, **8**, 451.

[126] Luckhurst, G. R. and Simmonds, P. S. J., 1993, *Molec. Phys.*, **80**, 233.

[127] Frenkel, D. and Mulder, B. M., 1985, *Molec. Phys.*, **55**, 1171.

[128] Samborski, A., Evans, G. T., Mason, C. P., and Allen, M. P., 1994, *Molec. Phys.*, **81**, 263.

[129] Vieillard-Baron, J., 1972, *J. Chem. Phys.*, **56**, 4729.

[130] Leeuw, S. W., Perram, J. W., and Smith, E. R., 1980, *Proc. R. Soc. Lond. A.*, **373**, 27.

[131] Vrbancich, J. and Ritchie, G. L. D., 1980, *J. Chem. Soc. Farad. Trans. II*, **76**, 698.

[132] Shoemaker, R. L. and Flygare, W. H., 1969, *J. Chem. Phys.*, **51**, 2988.

[133] Battiglia, M. R., Buckingham, A. D., and Williams, J. H., 1981, *Chem. Phys. Lett.*, **78**, 421.

[134] Kukolich, S. G., Read, W. G., Shea, J. A., and Campbell, E. J., 1983, *J. Am. Chem. Soc.*, **105**, 6423.

[135] Amos, R. D. and Williams, J. H., 1979, *Chem. Phys. Lett.*, **66**, 471.

[136] Ayton, G. and Patey, G. N., 1995, *J. Chem. Phys.*, **102**, 9040.

[137] Tjipto-Margo, B. and Evans, G. T., 1991, *J. Chem. Phys.*, **94**, 4546.